2015

Optimization based control design techniques for distributed parameter systems

Manoj Kumar

Department: Mechanical and Aerospace Engineering

OPTIMIZATION BASED CONTROL DESIGN TECHNIQUES FOR DISTRIBUTED PARAMETER SYSTEMS

by

MANOJ KUMAR

A DISSERTATION

Presented to the Faculty of the Graduate School of the

MISSOURI UNIVERSITY OF SCIENCE AND TECHNOLOGY

In Partial Fulfillment of the Requirements for the Degree

DOCTOR OF PHILOSOPHY

in

AEROSPACE ENGINEERING

2015

Approved by

S. N. Balakrishnan, Advisor

Serhat Hosder

Robert G. Landers

Jagannathan Sarangapani

Abhijit Gosavi

ABSTRACT

The study presents optimization based control design techniques for the systems that are governed by partial differential equations. A control technique is developed for systems that are actuated at the boundary. The principles of dynamic inversion and constrained optimization theory are used to formulate a feedback controller. This control technique is demonstrated for heat equations and thermal convection loops. This technique is extended to address a practical issue of parameter uncertainty in a class of systems. An estimator is defined for unknown parameters in the system. The Lyapunov stability theory is used to derive an update law of these parameters. The estimator is used to design an adaptive controller for the system. A second control technique is presented for a class of second order systems that are actuated in-domain. The technique of proper orthogonal decomposition is used first to develop an approximate model. This model is then used to design optimal feedback controller. Approximate dynamic programming based neural network architecture is used to synthesize a sub-optimal controller. This control technique is demonstrated to stabilize the heave dynamics of a flexible aircraft wings. The third technique is focused on the optimal control of stationary thermally convected fluid flows from the numerical point of view. To overcome the computational requirement, optimization is carried out using reduced order model. The technique of proper orthogonal decomposition is used to develop reduced order model. An example of chemical vapor deposition reactor is considered to examine this control technique.

ACKNOWLEDGMENTS

I wish to express my sincere gratitude to my advisor, Dr. S. N. Balakrishnan, Professor, Department of Mechanical and Aerospace Engineering, for providing his valuable guidance, continued financial support, and encouragement towards my graduate studies. His advice towards the research work as well as towards teaching was always constructive.

I am grateful to my graduate committee for their assistance and valuable suggestions during various stages of my research. I am thankful to Dr. Serhat Hosder, Associate Professor, Department of Mechanical and Aerospace Engineering and Dr. Abhijit Gosavi, Associate Professor, Department of Engineering Management and System Engineering. Each provided their generous help within their respective research domain. I am also thankful to Dr. Jagannathan Sarangapani, Professor, Department of Electrical and Computer Engineering, for offering advance courses that made research more interesting and learning more fun. I would like to extend a special thanks to the Department of Mechanical and Aerospace Engineering for providing funding assistance throughout my research.

I am especially grateful to all my friends, particularly, Karthikeyan Rajagopal, and Dr. Ali Heydari, Assistant Professor, Mechanical Engineering, South Dakota School of Mines and Technology, for their generous input and suggestions during the course of studies.

Finally, I would like to thank my parents. My accomplishments would not have been possible without their blessings.

TABLE OF CONTENTS

Page

LIST OF ILLUSTRATIONS

1. INTRODUCTION

Consider a physical system that can be described by a finite number of state variables. A mathematical model of this system can be governed by a set of ordinary differential equations (ODEs). This model is, generally, called a lumped parameter model and can be written as

$$\frac{dx(t)}{dt} = f\left(x(t), u(t), t\right) \tag{1}$$

where $x(t) \in R^{n\times 1}$ is the state of the system, $u(t) \in R^{m\times 1}$ is the control input applied to the system, $f\left(\cdot\right)$ is a real valued function and t denotes the time. Here, both the state and the control are functions of time only. For example, the dynamics of a rigid mass in a pendulum can be described by lumped parameter model where $x(t)$ comprises of displacement and velocity of the mass at any time t.

There are systems for which lumped parameter models does not represent the system's behavior completely. Heat distribution on a plate, fluid flow in a channel, and convection in a reactor are few examples of that type of systems. A spatial variable must be taken into account in order to describe the system. These systems are defined by a set of partial differential equations (PDEs) and known as distributed parameter system (DPS) or infinite dimensional system. For example, let's consider a DPS defined in a spatial domain Ω

$$\frac{dx(y,t)}{dt} = g\left(x(y,t), \frac{\partial x(y,t)}{\partial y}, \frac{\partial^2 x(y,t)}{\partial y^2}, u(y,t), y, t\right) \tag{2}$$

with appropriate boundary conditions. Here, $x\left(y,t\right)$ and $u\left(y,t\right)$ are the state and the control, respectively, at a spatial location $y \in \Omega$ and time t. A one-dimensional heat distribution is an example of equation (2) where $x(y,t)$ represents the temperature

along the spatial variable y at any time t. Other examples of distributed parameter systems, not limited to equation (2), are fluid flow as described by Navier Stokes equations [1], flexible structure as described by Euler-beam equations [2], etc.

In general, all the physical systems are distributed in nature. A lumped parameter model is often considered to be satisfactory. However, such a model is not adequate while designing a feedback controller for underlying distributed parameter system. In these situations, one must consider the spatial distribution into account and analyze the system with PDEs. The control term in PDEs can be defined as, namely, in-domain control and boundary control. A system can be actuated using the both types of control action or either one of them. As the name suggests, the in-domain control acts inside the domain and the boundary control acts at the boundary. This dissertation presents control design methodologies for systems that are actuated in-domain and also for the systems in which control acts at the boundary.

1.1. LITERATURE SURVEY

The control design of distributed parameter systems has been an area of interest since early 1960. Many researches have presented different control design strategies in a gamut of research articles. Padhi and Ali offer a brief account of developments made in control design of distributed parameter systems in [3]. This paper discusses the development of control strategies from early developments (1960 – 1989) followed by the recent developments (1990 onwards). Various open problems are briefly discussed along with the possible future directions. This section briefly lists the development of control design techniques and various applications of distributed parameter systems.

In a broad sense, control design techniques for the distributed parameter systems can be categorized into one of the two approaches: ‘approximate-then-design (ATD)’ or ‘design-then-approximate (DTA)’.

The ATD scheme offers an interesting approach to solve the control design problem by approximating the original system to a lumped parameter model, possibly a reduced order model. Techniques such as the finite element method (FEM), the finite difference method (FDM), etc. can be used to obtain a lumped parameter model. The spatial domain is discretized and a solution is obtained at the discrete points in the case of FDM. The weighted residual approach is followed in the case of FEM to obtain an analogous lumped parameter model. The states of the model are defined in terms of coefficients of the predefined orthogonal basis functions (e.g., Legendre polynomials, Chebyshev polynomials, Fourier functions, etc.). This lumped model is then used to design the control action. However, the lumped parameter model, obtained from these techniques may not necessarily be a reduced order model. Therefore, any control synthesis may require solving a large number of equations; and hence become computationally expensive.

To circumvent this problem of resulting large number of equations and to obtain a reduced order model, the technique of proper orthogonal decomposition (POD), also known as Karhunen-Loeve expansion, has captured significant attention in the literature. Initially, the technique was proposed by Karhunen in [14] and by Loeve in [15]. Lumley [16] used this technique in the name of POD to model turbulent flows. In the POD technique, a finite number of ‘problem oriented’ orthonormal basis functions are designed. These basis functions are designed such that they approximately span the solution space of the original infinite dimensional system. These basis functions are further projected over the system’s equations to

obtain a low dimensional model with high accuracy. The technique gained more attention when the method of ‘snapshots’ was incorporated into the POD framework by Sirovich in [17]. The snapshot solutions are the representative solutions of the actual system. In order to obtain a set of snapshot solutions, the system is simulated for duration of time and state solutions are captured at different time intervals. An experimental solution can also be treated as a snapshot solution candidate.

The ATD philosophy is used at various places in the literature. Ravindran [18] describes the problem of obtaining POD basis functions as an eigen-value problem, and discusses the active control of fluid flow using the reduced order modeling. Singh et al. [19] discuss feedback linearizing control of unsteady flow past a circular cylinder where control action is achieved by a combination of suction, injection, and synthetic jets. Here, the control action is designed using POD technique based reduced order model. Ravindran discusses the optimal boundary feedback stabilization of fluid flows using model reduction in [20] where the controller is derived using linear quadratic regulator. Luo et al. [52] describe the application of POD to usual finite element formulation for two-dimensional solute transport problems. The objective is to reduce finite element formulation with lower dimensions and achieve high enough accuracy at the same time.

Atwell and King [21] apply POD to simulation and feedback control of the one-dimensional heat equation. Linear quadratic regulator problem and linear quadratic Gaussian problem are discussed in the paper. Camphouse [61] describes the POD technique to design the boundary control of 2D heat equations. Efe [62] discusses issues in the POD based modeling and boundary control of 2D heat flow.

References [22] - [27] present a novel technique to obtain a sub-optimal control solution for various PDE applications using proper orthogonal decomposition

(POD) and approximate dynamic programming (ADP). The POD technique is applied in order to obtain a finite dimensional model. This model is then used to obtain an ADP based suboptimal neuro-controller. Yadav, Padhi and Balakrishnan [22] develop surface temperature controller for high-speed aerospace vehicles. The design process is extended to develop an online robust neuro-controller to account for unmodeled dynamics and parametric uncertainties. In [23], Padhi and Balakrishnan describe the optimal control strategy of beaver population over a certain land area. Another article [24], from same authors, describes the synthesis of an optimal controller for a dispersion type tubular chemical reactor that is governed by two coupled nonlinear partial differential equations. This study can be used in synthesizing optimal control for a fairly general class of nonlinear distributed parameter systems. The paper [25] presents experimental implementation of a dual neural network based optimal controller for a heat diffusion system. Experimental results are demonstrated where objective is to attain a desired temperature profile over the spatial domain.

Kumar et al. [26] develop a sub-optimal control technique to control the heave dynamics of a flexible aircraft wing using continuous actuation. The discrete actuation and controller development is described in [27] for the same problem.

Suppose partial information (marred data) of the system is given to the user then how to restore the system or estimate the unknown data? Data gathered from remote-sensing satellites in the presence of cloud cover as a natural obstruction is an example of this scenario. Everson and Sirovich [53] address the problem of using Karhunen-Loeve transform with partial data. The objective is to recover the modal coefficients for gappy snapshot solutions using a set of empirical eigenfunctions. Willcox [55] addresses the issue of incomplete data set with the extension of POD method. The “gappy” POD method is described to handle unsteady flow

reconstruction problems. The paper [98] describes the aerodynamic data reconstruction using gappy POD method and discusses the airfoil shape optimization.

Model reduction has been studied with different perspectives in the literature. Moore [54] discusses the principal component analysis in linear systems to compute the singular value decomposition for analyzing signals. Kim [59] derives the Karhunen-Loeve procedure in the frequency domain as a tool for calculating eigenmodes of linear systems. The method is demonstrated for mechanical and fluid dynamic models. Willcox and Peraire [56] discuss the method of POD and concepts from balanced realization theory to perform a balanced reduction of a high-order linear system. The method is demonstrated for a linearized high order system that models unsteady motion of a two-dimensional airfoil.

Adaptive model reduction has emerged as an interesting concept where basis functions are computed recursively as more information of the system becomes available. Varshney, Pitchaiah and Armaou [57] describe a feedback control design of dissipative PDE systems using adaptive model reduction. Initially, an ensemble of eigenfunctions is constructed based on a relatively small number of snapshot solutions. The dominant eigenspace is recomputed with the addition of each snapshot with possible increase or decrease in its dimensionality. Pitchaiah and Armaou [58] address the problem of control design in the presence of measurement constraints where partial data is assumed to be measured. The study discusses the use of adaptive POD method using a snapshot reconstruction technique, and gappy adaptive POD methodology that constructs locally accurate low dimensional model.

The control design techniques based on DTA approach use the original system as defined by PDEs. The control is formulated analytically in this approach. A comprehensive treatment of optimal control development based on DTA philosophy

is presented by Curtain and Zwart in [4]. The control design approach is based on the infinite-dimensional operator theory rooted in the functional analysis. The approach is mainly confined to linear systems. The control is first formulated in the infinite-dimensional space and then approximated to a finite-dimensional space for implementation purpose.

Krstić and Smyshlyaev [5] present a text on the control design using backstepping transformation. This transformation is used for the linear partial differential equations and a boundary control is formulated as an analytic expression. The idea is to convert an unstable PDE to an exponential stable target system using the Volterra integral transformation; and control is computed as a solution of a certain well-posed PDE. While applying backstepping transformation in PDEs, one of the key issues is the choice of a target system. An appropriate target system is necessary to keep the nature of the transformed system.

Padhi and Balakrishnan [13] present two control design approaches for a class of first order distributed parameter systems. One approach can be applied to the systems when there is continuous actuation in the spatial domain. Principle of dynamic inversion with variational optimization theory is used to design this control action. The second approach combines the dynamic inversion technique with static optimization theory to design the control action at discrete points in the spatial domain.

Adaptive control design is desired when mathematical model of the system is not known accurately. Generally, uncertainty in the system dynamics exists due to inaccurate values of system's parameters. Smyshlyaev and Krstić [67] present three design methods, namely, the Lyapunov design, the passivity-based design, and the swapping design for adaptive control of PDE systems. Adaptive boundary control

design for unstable parabolic PDEs is discussed in a series of three companion papers [68] - [70]. He and Ge [71] present an adaptive boundary control design for a vibrating string under the influence of time-varying disturbance. The dynamics of vibrating string is governed by a nonhomogeneous hyperbolic PDE and two ODEs. By using the same string dynamics, the adaptive boundary control is developed for a flexible marine installation system in [72].

Boundary control problems in distributed parameter systems have been an area of growing interest in recent years. Researchers have presented control mythologies for theoretical as well as practical engineering problems. Krstić and Smyshlyaev [5] present a text on the boundary control of PDEs using backstepping design as mentioned previously. Liu and Krstić [6] discuss the problem of global exponential stabilization by boundary feedback for the Korteweg-de Vries-Burgers equation. Control law is derived with the stability proofs. In [7], Smyshlyaev and Krstić present the extension of backstepping method to plants with non-constant diffusivity/thermal conductivity and time-varying coefficients. The boundary stabilization problem is converted to a problem of solving a specific Klein-Gordon-type linear hyperbolic PDE. The paper [8] presents the first adaptive controllers for the reaction-advection-diffusion plants with spatially varying parameters that use only boundary actuation. The design of adaptive controllers is based on the Lyapunov method. The paper [9] presents backstepping boundary control designs for fluid systems. The controller formulation is discussed for the problems of vortex shedding around a cylindrical bluff body in the flow and also for the turbulent channel flow. The paper [10] discusses a stabilization problem of the Euler-Bernoulli beam. The beam is controlled at one end and has the sliding boundary condition at the opposite end. The controller is designed to achieve any prescribed decay rate of the closed loop system.

Ravindran [20] describes the optimal boundary control design using model reduction for the flow stabilization. Liu [60] study the problem of boundary control for two-dimension (2D) heat equations. Kumar and Balakrishnan [63] discuss the boundary control design for 2D heat equations based on DTA philosophy. The control is design for different boundary conditions using the principles of dynamic inversion and optimization theory. Ou et al. [64] demonstrates the setting up a suitable current spatial profile in tokamak plasmas. In the study, tokamak is a device of torus shape that uses the magnetic field to confine plasma at very high temperature. Gaye et al. [65] describes a sliding mode feedback control approach for the robust stabilization of the spatial distribution of current profile in tokamak plasmas. In [66], the author derives a nonlinear distributed parameter system model governing the motion of a cable with an attached payload immersed in the water. A feed-forward controller is designed based on the linearized system.

Delays are inevitable in the real systems. Sometimes even a small delay may be significant and make the system unstable. Delay can occur in the actuator's input and/or in the sensor's measurement as well. Krstić [41] provides a comprehensive text on delay compensation for nonlinear, adaptive and PDE systems. The text addresses various practical issues and proposes solutions using backstepping approach. Krstić and Bresch-Pietri [11] discuss a Lyapunov based adaptive control design that achieves global stability, without a requirement that the delay estimate be near the true delay value. Bekiaris-Liberis [42], in his PhD dissertation, presents procedures for the control and analysis of general nonlinear systems with delays and of nonlinear PDE systems. The paper [40] investigates the feedback control problem for the parabolic distributed parameter systems with or without time-delay. Nguyen [39] presents model predictive optimal control of time-delay distributed parameter systems

governed by first order, quasilinear hyperbolic PDEs. Zheng, Fu and Teng [43] discuss a linear distributed parameter bioprocess with boundary control input with time delay. The paper shows that the closed loop system generates a uniformly bounded C_0-semigroup of linear operators under a certain condition with respect to the feedback gain in the boundary feedback law.

An Aeroelastic study of a flight vehicle has been a subject of great interest and research. Its importance lies in the achieving better performance, safety operation (e.g., aileron reversal, flutter analysis) and related analysis in the field of aeronautics. Structural dynamics of an aircraft wing characterized by aeroelastic nature is modeled by partial differential equations. The paper [47] presents a nonlinear aeroelastic formulation of a coupled bending-torsion dynamics of a flexible wing structure that is fully coupled with an aircraft rigid body dynamics. A finite-element method is used to discretize the nonlinear aeroelastic equations of the coupled bending-torsion motion. An elastic shaped aircraft concept with aeroelastic modeling is described in [48] by Nguyen and Urnes. The aircraft model is based on the rigid body generic transport model originally developed at NASA Langley Research Center. The model computes both static and dynamic responses of the wing structures. Yucelen et al. [49] illustrate an application of derivative-free, output feedback adaptive control on an aeroelastic model of longitudinal dynamics for a generic transport model. A control oriented model for the longitudinal dynamics of a highly flexible flying wing is developed in [50] by Gibson, Annaswamy and Lavretsky. The comparative study between linear LQG/LTR and adaptive LQG/LTR controller was presented in this paper. John et al. [51] present a multiple input concurrent learning model reference adaptive control approach applied to longitudinal dynamics of the generic transport model aircraft. In

this study, a reduced order model of the short period flight dynamics coupled with structural bending and torsion is used.

Paranjape et al. [12] discuss PDE boundary control for flexible articulated wings on a robotic aircraft, where the output of interest is the net aerodynamic force or moment. Kumar et al. [26] describe a sub-optimal control technique based on POD and SNAC architecture for a class of second order systems. This technique is demonstrated to control the heave dynamics of a flexible aircraft wing. A beam-mass-beam model is defined where beam represents the wing and mass represents the fuselage. Here the control is defined as a continuous function over the beam. For practical implementation, a set of discrete actuators is defined over the beam and control action is designed in [27] using the same techniques of POD and SNAC.

The concepts of controllability and observability cannot be ignored while studying the infinite dimensional systems. It is intuitive to carry these concepts from the theory of finite dimensional systems to the infinite dimensional systems. The concept of stabilizability and detectability retain their full importance to a special subclass of the infinite dimensional systems. Fortunately, it is a very large subclass that is well represented in applications [4]. The situation with the properties of controllability and observability is very different. Most infinite dimensional systems can only achieve these properties in an approximate sense. The paper [28] reviews different observer design methods for first order and second order linear distributed parameter systems based on their infinite dimensional and finite dimensional descriptions. Engineers utilize the concepts of controllability and observability when actuators and sensors need to be placed in the spatial domain to achieve a desired objective. Misplaced actuators and sensors often lead to controllability and observability problems, and the desired system performance may not be achieved with

any choice of control law. The paper [29] discusses the optimal placement of control actuators and measurement sensors for transport-reaction processes. The optimal actuator and sensor location problem is formulated as the one of minimizing a meaningful cost functional that is solved by using standard unconstrained optimization techniques.

Alonso et al. [30] present a systematic approach to reconstruct the infinite dimensional field in distributed parameter systems using limited number of sensors. The POD technique, that captures the most relevant dynamic features of the solution, is employed with the solution of max-min optimization problem in this paper. The paper [31] develops a spatial H_2 norm based computational scheme for finding the optimal locations of sensors and actuators in controlled flexible structures. The proposed genetic algorithm is used to solve nonlinear optimization problem for this purpose. In the paper [34], H_∞ optimal actuator location problem is presented where actuators locations are chosen to minimize the effect of disturbances on the output. A derivative free optimization algorithm to calculate H_∞ optimal actuator locations is described in this study. Nestorovic and Trajkov [35] propose actuator and sensor placement optimization method, which is based on balanced reduced models. The optimization method relies on H_2 and H_∞ norms, as well as on controllability and observability Gramians. By assuming that a hierarchical structural exists between the actuators placement and controller design objective functions, the paper [36] solves a multiobjective design problem as a bi-level (leader and follower) Stackelberg game. The solution approach comprises of generic algorithms and sequential quadratic programming techniques and is applied to the design of a flexible truss structure.

With the recent developments in actuators and sensors technologies, the vibration control methods are in the attention. The paper [32] demonstrates an active

vibration control system of flexible structures by using piezoelectric sensors and actuators. Ji and Wang [33] develop an adaptive neural fuzzy controller for active vibration suppression in flexible structures. A recurrent identification network is developed to adaptively identify the system dynamics in this study. The paper [37] presents a strategy for active damping of cable structures, using active tendons. The control of the parametric vibration of passive cables due to deck vibration is demonstrated in this study. Another paper [38] describes the robust control technique to stabilize the cable system under the influence of external disturbances. An H_∞ feedback control is constructed with the partial observation of the state using an active tendon. The paper [73] develops the POD based control and demonstrates the experimental implementation to control the vibrations of transverse beam. In this study, linear quadratic Gaussian compensator control of transverse vibrations was implemented on an aluminum cantilevered beam in a smart structure paradigm.

Adaptive optics is one of the practical applications where the system dynamics is modeled by partial differential equations. Vogel and Yang [44] model a particular micro-electromechanical systems (MEMS) deformable mirror using a coupled system of nonlinear partial differential equations. A nonlinear constrained quadratic optimization problem is introduced in this paper for open-loop control of the MEMS mirrors. A model based feedforward control concept for fast set-point changes of large deformable mirrors is proposed in [45] by Rupple, Osten and Sawodny. In [46], performance enhancements for deformable membrane mirrors based on model-based feedforward control are presented. Due to lack of high speed internal position measurements of the membrane's location, feedback control of the distributed actuators cannot be implemented in the mirrors. It is shown that by using feedforward

control, the dominant dynamics of the membrane can still be controlled allowing for faster settling times and reduced membrane vibrations.

The problems of optimization related to shape, sizing, topology or control has been a part of attention in the field of distributed parameter systems. Shape optimization can be viewed as a part of structural optimization field. As the term indicates, optimization of the geometry is of primary interest. Jameson [95] presents the optimization concepts of control theory in the field of aerodynamic design. The paper demonstrates that control theory can be used to formulate computationally feasible procedures for aerodynamic designs. LeGresley and Alonso [97] present inviscid airfoil analysis and a design optimization method that uses reduced order models to reduce the cost of computation. Proper orthogonal decomposition technique is utilized to obtain the reduced order models in this study. Another paper [98] demonstrates the proper orthogonal decomposition technique with incomplete (gappy) data for field reconstruction and inverse airfoil design. Oyama, Nonomura and Fujii [99] propose a new approach to extract useful design information from the shape data of Pareto-optimal solution of an optimization problem in the study. The study [100] addresses the drag reduction goal for aircraft vehicle through three themes - innovative vehicle configurations via non planar wing optimization, a new concept of elastic wing shaping control, and a new aerodynamic control effector called a variable camber continuous trailing edge flap.

1.2. CONTRIBUTION

A control design technique, that is generic in its development, and computational efficient for implementation purpose, is always desired. First part of this dissertation presents a generic boundary control design methodology based on

design-then-approximate philosophy for nonlinear systems. This design follows the principles of dynamic inversion and optimization theory.

In real engineering systems, the accurate values of the system parameters are rarely known. These parameters define the characteristic property of the systems. Few examples of the parameters are such as: coefficient of conductivity in heat transfer applications, coefficient of viscosity in fluid flow applications, and coefficient of thermal expansion in convective flow problems. Implementation of any controller, as designed using the inaccurate value of the parameters, may leads to the system's instability. An adaptive control development is designed in second part of the dissertation that addresses the issue of parameter uncertainty.

Third part of this dissertation discusses the development of approximate-then-design philosophy based control design technique for a class of nonlinear systems. A reduced order model is developed by following the proper orthogonal decomposition technique with the weighted residuals. A sub-optimal controller is designed based on the reduced order model. Single network adaptive critic architecture is used for the controller synthesis.

In the last part, dissertation discusses an optimal control of stationary thermally convected fluid flow from numerical point of view. Traditionally, the optimization is carried out using finite difference, finite element or finite volume based discrete models that are usually of very high dimensions. These large dimension models require huge computations in solving the flow and in obtaining the optimal solution. A reduced order model based optimization procedure is examined to overcome the computational requirements where proper orthogonal decomposition technique is utilized to develop the reduced order model of low dimension.

Some portion of the dissertation is documented by the author in the papers [26], [27] and [63]. For a brief account of the development made here, reader may refer to these references.

1.3. ORGANIZATION OF THE DISSERTATION

This dissertation comprises of six sections. Section 1 introduces to the field of distributed parameter systems and their applications. Literature survey lists a gamut of design techniques in various problem domains.

Section 2 presents a boundary control design technique for nonlinear distributed parameter systems. A step wise procedure of controller formulation is described. The applicability of developed control is demonstrated for heat equations and thermal convection loops.

Section 3 introduces to a class of systems with parameter uncertainty. An adaptive controller development is discussed which also incorporates the idea of control design from Section 2. The developed controller is demonstrated for heat equations and thermal convection loops.

Section 4 describes the development of reduced order models for a class of systems. The POD technique for model reduction is introduced and a step wise procedure is discussed to obtain reduced order model by using Galerkin procedure. A sub-optimal control formulation based on neural network architecture is described for nonlinear systems. An aircraft flexible wing problem is considered to demonstrate the validity of developed controller.

Section 5 examined the reduced order modeling based optimization for stationary fluid flows. The flow is convection-driven. Reduced order models are analyzed to overcome the computation requirements while achieving the accuracy of

optimal solution. An example of high pressure chemical vapor deposition reactor is considered to discuss the optimization procedure.

Section 6 summarizes the developments made in this dissertation.

2. DYNAMIC INVERSION BASED BOUNDARY CONTROL OF DPS

In this section, a boundary control design methodology is developed based on the DTA philosophy. The methodology is inspired from the work by Padhi and Balakrishnan [13] where the principles of dynamic inversion and optimization theory were used to formulate an analytic expression of in-domain controller. Dynamic inversion [74], which is a special case of feedback linearization [76], has been successfully applied to many applications in which the system is defined by ODEs [77], [78]. The same principles are utilized here to design a state feedback boundary controller where optimization theory [75] facilitates in the formulation of a unique controller's expression. The main advantage of this methodology lies in its fairly general development that does not demand the knowledge of complex mathematical tools like infinite-dimensional operator theory and yet provides the closed form controller's expression. The designed controller is not computationally expensive and could be easily applied online.

Two examples are discussed to demonstrate the applicability and aspect of the methodology. Two-dimensional (2D) heat equations are first considered following with a model problem of a two dimensional cavity. Next, thermally convection loops are shown to be stabilized by the boundary control.

2.1. BOUNDARY CONTROL SYNTHESIS

2.1.1. System Description. Consider a system of partial differential equations as

$$x_t = f\left(x, x', x'', ..., y, t\right) \tag{3}$$

with appropriate boundary conditions. Here, $x(y,t)$ is the state of the system defined in a domain Ω. The state is a function of spatial variable $y \in \Omega$ and time t. The domain Ω is fixed and bounded by $\partial\Omega$. The function $f(\cdot)$ is a real valued function with same dimension as of the state. In the equation (3), x_t represents the time partial derivative and x' represents the spatial partial derivatives. The degree of spatial partial derivative is denotes by number of apostrophe $(')$.

The boundary control is an implicit function in the equation (3). It can be defined as Dirichlet, Neumann or Robin boundary condition. In this dissertation, we consider the Neumann boundary condition and represent it as the control, e.g., $u = \frac{\partial x(\partial\Omega,t)}{\partial \hat{n}}$. Here, u is the control at the boundary and $\hat{n}$ represents the normal unit vector at the boundary.

2.1.2. Controller Formulation. The objective of the control design is to actuate the system such that it tracks a target signal $x^*(\Omega,t)$. In order to achieve this objective, an output function $z(t)$ is defined as:

$$z(t) = \frac{1}{2}\int_{\Omega} \left\| x(\Omega,t) - x^*(\Omega,t) \right\|^2 d\Omega \tag{4}$$

It is important to note that $z \to 0$, means $x \to x^*$ point-wise. By following the principles of dynamic inversion [74], the control is designed to satisfy the following first order stable equation:

$$z_t + kz = 0 \tag{5}$$

In this equation, $k > 0$ is a user-defined parameter. An equation is derived by using (4) and (5), and written in a compact form as

$$\int_{\partial\Omega} g\left(x(s,t) - x^*(s,t)\right) u ds = \gamma \tag{6}$$

where the control term u will appear after carrying the integration in equation (5). The term $s \in \delta\Omega$ denotes the variable for integration. The function $\left|g\left(x\left(s,t\right)-x^{*}\left(s,t\right)\right)\right|>0$ if $\left|x\left(s,t\right)-x^{*}\left(s,t\right)\right|>0$ and $\left|g\left(x\left(s,t\right)-x^{*}\left(s,t\right)\right)\right|=0$ if $\left|x\left(s,t\right)-x^{*}\left(s,t\right)\right|=0, \quad \forall s \in \delta\Omega$. The term γ is a function of known values $\left(x, x^{*}, x', x^{*}', ..., k\right)$ and linearly proportional to the parameter k. Notice that the control term is inside the integral in the expression (6). This expression alone is insufficient in obtaining a unique value of control. To obtain a unique value, problem is designed within the framework of optimization theory as a control minimization problem with expression (6) acting as an equality constraint. Accordingly, a cost function $J\left(t\right)$ is defined as

$$J\left(t\right)=\frac{1}{2}\int_{\delta\Omega} r\left(s\right)\left[u\left(s,t\right)\right]^{2} ds \tag{7}$$

Here, $r\left(s\right)>0, \forall s \in \delta\Omega$ is the weighing function and chosen by the control designer. This weighing function provides the flexibility of putting relative importance of the control action at different spatial locations at the boundary. An augmented cost function $\overline{J}\left(t\right)$ is defined as

$$\overline{J}\left(t\right)=J\left(t\right)+\lambda\left[\int_{\delta\Omega} g\left(x\left(s,t\right)-x^{*}\left(s,t\right)\right)uds-\gamma\right] \tag{8}$$

where λ is a Lagrange multiplier. The control and the Lagrange multiplier are the unknown variables in the equation (8). Values of these variables are obtained by applying the necessary condition of optimality, i.e., by taking the first variation of $\overline{J}\left(t\right)$ and equating it to zero. As a result, the following control expression is obtained:

$$u(s,t)=\frac{\gamma g\left(x(s,t)-x^{*}(s,t)\right)}{r\int_{\delta\Omega}\frac{\left[g\left(x(s,t)-x^{*}(s,t)\right)\right]^{2}}{r}ds}\quad \forall s\in\delta\Omega \tag{9}$$

Comments:

1. The parameter k acts as the inverse of the time constant for the first order stable dynamics in (5). Hence, by increasing (decreasing) the value of k, a faster (slower) response can be obtained appropriately. This parameter also affects the amount of control action. The term γ indicates that the amount of control action is proportional to parameter k and, hence, inversely related to the time constant of the stable dynamics.

2. In the control expression (9), $\left|g\left(x(s,t)-x^{*}(s,t)\right)\right|=0$ as $x(s,t)\to x^{*}(s,t)\quad \forall s\in\delta\Omega$ and this creates a singular solution; however, the control value at the boundary goes to zero as $x(s,t)\to x^{*}(s,t)$. Let, D denotes the denominator in the expression (9). A tolerance value is set for D such that when $D<tol$ the corresponding control values are set to zero to avoid numerical problems.

2.2. HEAT EQUATIONS

2.2.1. Problem Description. The 2D heat equation on a unit square is defined as [79]

$$w_t=\varepsilon\left[w_{xx}(t,x,y)+w_{yy}(t,x,y)\right] \tag{10}$$

for time $t>0$ and spatial domain $(x,y)\in\Omega_1=\left([0,1]\times[0,1]\right)$, with the initial condition given as $w(0,x,y)=w_0(x,y)$. Here, w represents the temperature, and ε denotes the

thermal diffusivity. Subscripts are used to represent partial derivatives, i.e., $w_t \equiv \frac{\partial w}{\partial t}$, $w_{xx} \equiv \frac{\partial^2 w}{\partial x^2}$ and $w_{yy} \equiv \frac{\partial^2 w}{\partial y^2}$. The boundary conditions are given as

$$\begin{aligned} w_x(t,1,y) &= u_1(t,y) \\ w_y(t,x,1) &= u_2(t,x) \\ w_x(t,0,y) &= u_3(t,y) \\ w_y(t,x,0) &= u_4(t,x) \end{aligned} \tag{11}$$

Here, $u_1(t,y)$, $u_2(t,x)$, $u_3(t,y)$ and $u_4(t,x)$ are the controls acting on the boundary walls. In the study, the 2D heat equation is referred to as the system; the temperature and thermal diffusivity are referred to as the state and the parameter of the system, respectively. The objective of the boundary controls is to derive the system to a desired state as given by $w^*(x,y) \quad \forall (x,y) \in \Omega_1$.

2.2.2. Controller Development. By following the design procedure as discussed in Section 2.1.2, an output function $z(t)$ is defined as

$$z = \frac{1}{2} \iint_{0 \le y \le 1, 0 \le x \le 1} \left(w - w^*\right)^2 dxdy \tag{12}$$

Here, the temporal and the spatial variables are omitted in the formulation of control for brevity, i.e., $w \equiv w(x,y) \equiv w(t,x,y)$. The control is designed to satisfy the stable equation of z given as

$$z_t + k_1 z = 0 \tag{13}$$

In this equation, $k_1 > 0$ is a user-defined parameter. By substituting the expression (12) in (13) while also using the system dynamics (10), the following equation is obtained:

$$\begin{aligned}&\int_y \left(w-w^*\right)(1,y)\,w_x(1,y)\,dy+\int_x \left(w-w^*\right)(x,1)\,w_y(x,1)\,dx-\\&\int_y \left(w-w^*\right)(0,y)\,w_x(0,y)\,dy-\int_x \left(w-w^*\right)(x,0)\,w_y(x,0)\,dx=\gamma_1\end{aligned} \tag{14}$$

where

$$\gamma \triangleq \iint\left[\left(w_x-w_x^*\right)w_x+\left(w_y-w_y^*\right)w_y\right]dxdy+\frac{1}{\varepsilon}\iint\left(w-w^*\right)w_t^*dxdy-\frac{k_1}{\varepsilon}z \tag{15}$$

Here, the single integrals $\int_x(\cdot)dx$ and $\int_y(\cdot)\,dy$ are defined over the domains $x\in[0,1]$ and $y\in[0,1]$, respectively. Next, a cost function $J_1(t)$ is defined to find a unique solution of the control as

$$\begin{aligned}J_1=&\frac{1}{2}\int_y r_1(y)\left[u_1(y)\right]^2dy+\frac{1}{2}\int_x r_2(x)\left[u_2(x)\right]^2dx+\\&+\frac{1}{2}\int_y r_3(y)\left[u_3(y)\right]^2dy+\frac{1}{2}\int_x r_4(x)\left[u_4(x)\right]^2dx\end{aligned} \tag{16}$$

Here, $r_i>0$ for all i acts as the weighing profile for the control action u_i and can be chosen per design flexibility. By following the calculus of variation, an augmented cost function $\overline{J}_1(t)$ is defined using (16) and (14) as

$$\overline{J}_1=J_1+\lambda_1\left[\begin{aligned}&\int_y \left(w-w^*\right)(1,y)\,u_1(y)\,dy+\int_x \left(w-w^*\right)(x,1)\,u_2(x)\,dx-\\&-\int_y \left(w-w^*\right)(0,y)\,u_3(y)\,dy-\int_x \left(w-w^*\right)(x,0)\,u_4(x)\,dx-\gamma\end{aligned}\right] \tag{17}$$

where λ_1 is a Lagrange multiplier. By taking the first variation of $\overline{J}_1$ and equating it to zero, following expression is obtained for the boundary control

$$
\begin{aligned}
u_1(y) &= \frac{\gamma\left(w-w^*\right)(1,y)}{r_1(y)D_1} \\
u_2(x) &= \frac{\gamma\left(w-w^*\right)(x,1)}{r_2(x)D_1} \\
u_3(y) &= -\frac{\gamma\left(w-w^*\right)(0,y)}{r_3(y)D_1} \\
u_4(x) &= -\frac{\gamma\left(w-w^*\right)(x,0)}{r_4(x)D_1}
\end{aligned}
\tag{18}
$$

where

$$
D_1 \triangleq \left[\begin{aligned} &\int_y \frac{\left(w-w^*\right)^2(1,y)}{r_1(y)}dy + \int_x \frac{\left(w-w^*\right)^2(x,1)}{r_2(x)}dx + \\ &+\int_y \frac{\left(w-w^*\right)^2(0,y)}{r_3(y)}dy + \int_x \frac{\left(w-w^*\right)^2(x,0)}{r_4(x)}dx \end{aligned} \right] \tag{19}
$$

2.2.3. Results & Discussion. This section discusses the numerical results from representative simulations by using the control design developed in Section 2.2.2. These simulations were performed by discretizing the spatial domain, with equally spaced elements, with a distance of Δx along the x direction and Δy along the y direction. A total of $N_x \times N_y$ spatial elements were used along the x and y directions, respectively. The forward-in-time and central-in-space (FTCS) difference scheme [80] was used to simulate the system. Time step Δt was taken such that it satisfies the Von Neumann stability criterion [80]: $\Delta t \le \frac{(\Delta x)^2}{4\varepsilon}$. Satisfaction of this criterion ensures the numerical stability of the system's simulation. The simulation parameters are taken as: $\left(N_x \times N_y\right) = (50 \times 50)$, $\Delta t = 10^{-3}$ sec, $\varepsilon = 0.1$, $r_1(y) = r_3(y) = 1 \quad \forall y \in [0,1]$, $r_2(x) = r_4(x) = 1 \quad \forall x \in [0,1]$, $k_1 = 1$ and $tol = 10^{-10}$. The system was initialized with a non-zero surface profile given by

$$w(0,x,y)=\cos(\pi x)\cos(\pi y) \tag{20}$$

The boundary control (18) was applied to the system to achieve a desired profile given by $w^*(x,y)=1 \quad \forall(x,y)\in\Omega_1$. Figure 2.1(a)-(d) illustrates the state surface profile at time instants t = 0, 0.25, 0.5, and 2 seconds, respectively. In these figures, horizontal axes specify the surface's dimension and vertical axis specifies the magnitude of temperature over the surface. The system was stabilized to the desired level within 2 seconds by selecting the design parameter k_1 value as 1.

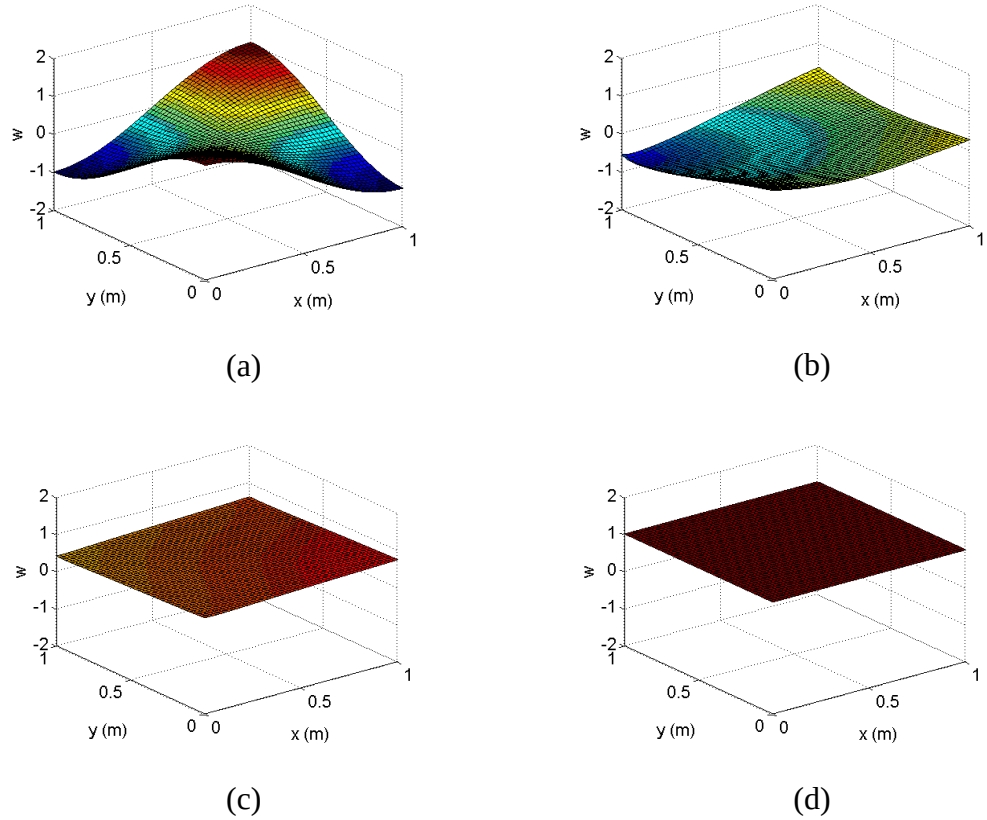

Figure 2.1. Temperature profile at (a) $t=0$, (b) $t=0.25$, (c) $t=0.5$, (d) $t=2$ seconds

Figure 2.2 illustrates the time history of the control profiles at each boundary wall. The horizontal axes specify the distance along the boundary wall and the time evolution. The vertical axis specifies the magnitude of the control profile on that boundary wall. It can be seen that all the control profiles approach zero as

$w(s) \to w^*(s)$. This behavior of the control can be understood from the heat equation (10). The spatial partial derivatives, as indicated on the right side of this equation, represent only the diffusion of heat over the surface. It is intuitive that once the control applied at the boundary drives the system to the reference level, system does not require any more heat energy and the system stays at that level with no more boundary control.

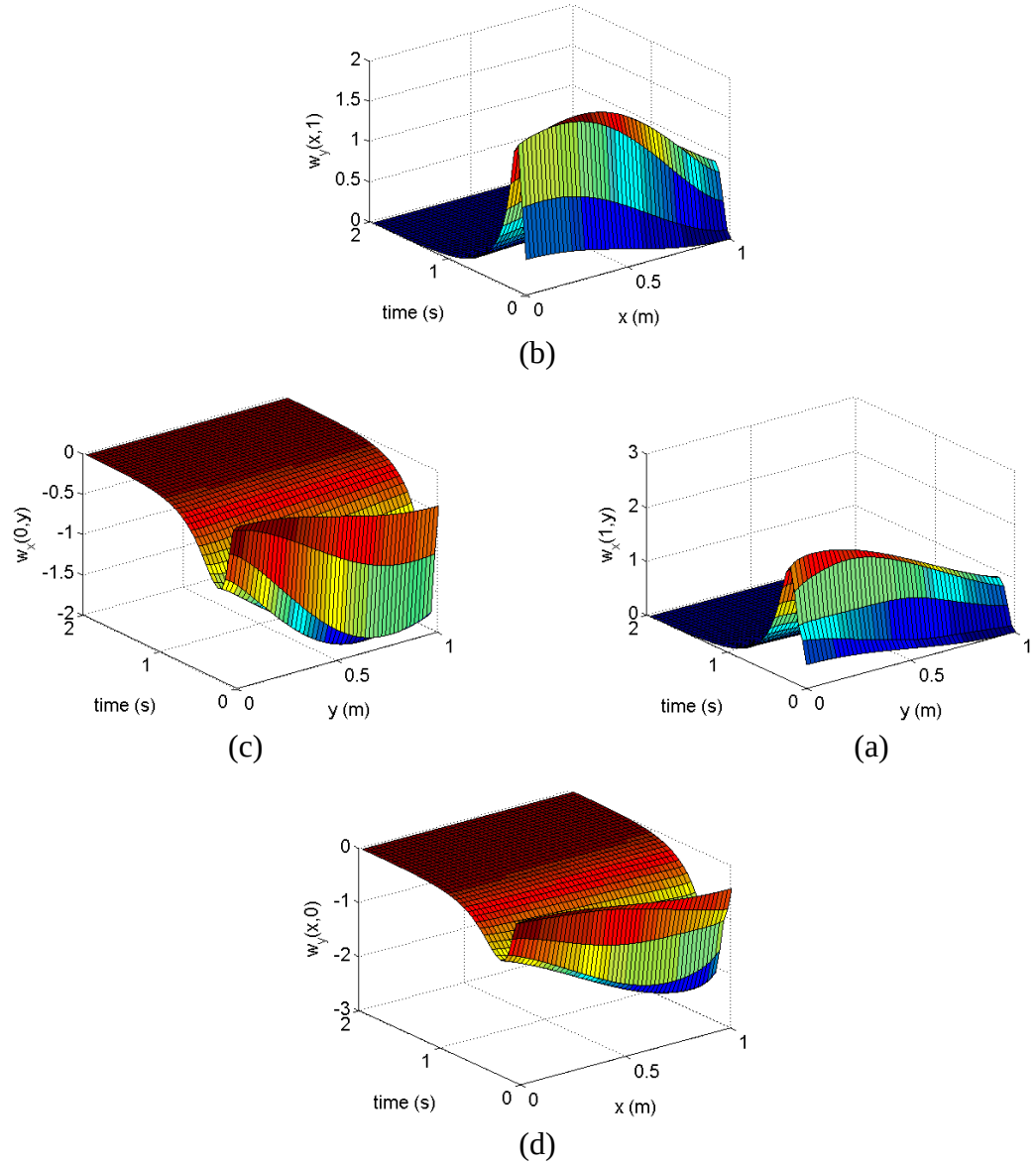

Figure 2.2. Time history of control profile at the boundary wall as specified by the co-ordinates (a) $(1, y)$ (b) $(x,1)$ (c) $(0, y)$ (d) $(x,0)$

To see the effect of singularity in the control expression (18), γ and D_1 are plotted with respect to time in Figure 2.3(a) and Figure 2.3(b), respectively. A snippet, that shows the plot on a smaller scale, is taken and attached to the same plot. In the Figure 2.3(b), term D_1 approaches the tolerance value of 10^{-10} near at $t = 3.4$ second. It was observed that numerator, which is $\gamma\left(w - w^*\right)$ at any boundary point, was lesser in magnitude as compared to the denominator after keeping the value of D_1 within the tolerance limit. This practical step avoids singularity in control values. If a tolerance limit is not set, the denominator may reach zero faster than the numerator and will result in a singular solution.

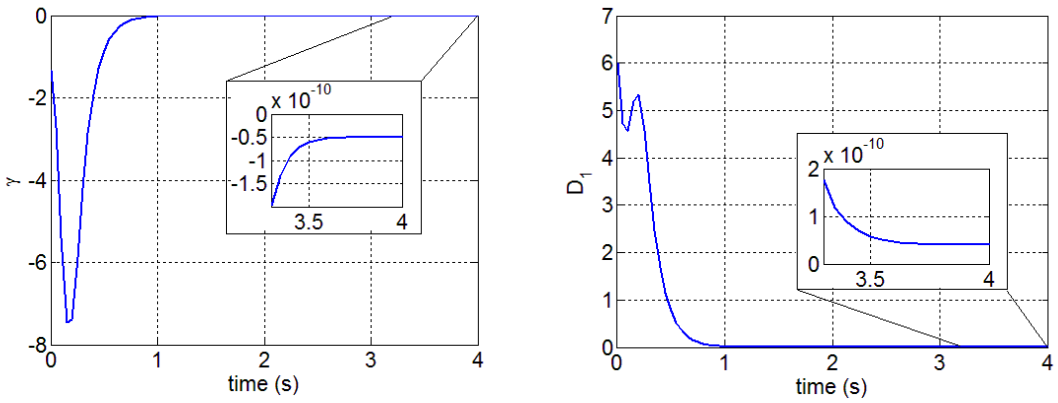

(a) (b)

Figure 2.3. Time history of (a) γ, and (b) denominator term D_1

2.3. 2D CAVITY PROBLEM

2.3.1. Problem Description. The control design technique, as described in Section 2.1.2, is applied to a 2D geometry of the kind seen in cavity noise reduction applications [61]. Figure 2.4(a) illustrates the geometry of the problem with spatial co-ordinates. In the Figure 2.4(a): $x_1 = 0$, $x_2 = 0.18$, $x_3 = 0.56$, $x_4 = 0.74$ and $y_1 = 0$, $y_2 = 0.18$, $y_3 = 0.36$, $y_4 = 0.74$. The problem domain Ω is defined by $\Omega = \Omega_1 \cup \Omega_2$,

where $\Omega_1 = \left([x_2, x_3]\times[y_1, y_2]\right)\cup\left([x_1, x_4]\times[y_3, y_4]\right)$ and $\Omega_2 = [x_2, x_3]\times[y_2, y_3]$. The cavity is described by the region Ω_2. The system dynamics is given by (10) on the domain $(x, y)\in\Omega$ for $t > 0$. The boundary conditions are given as follows

$$\begin{aligned} w_x(t, x_2, y) &= u_{c_1}(t, y) \quad at \quad \tau_1 \\ w_x(t, x_3, y) &= u_{c_2}(t, x) \quad at \quad \tau_2 \end{aligned} \tag{21}$$

and

$$w(t, x, y) = 0 \quad at \quad \tau_3 \tag{22}$$

where u_{c_1} and u_{c_2} are the Neumann boundary control. Boundaries τ_1, τ_2 are defined as: $\tau_1 = x_2\times[y_2, y_3]$, $\tau_2 = x_3\times[y_2, y_3]$. The rest of the boundary region is defined by τ_3. The objective is to drive the system to a desired temperature profile w^* with the following boundary conditions

$$\begin{aligned} w^*(x_2, y) &= 1 \quad at \quad \tau_1 \\ w^*(x_3, y) &= 1 \quad at \quad \tau_2 \end{aligned} \tag{23}$$

and

$$w^*(x, y) = 0 \quad at \quad \tau_3 \tag{24}$$

2.3.2. Controller Development. The controller is designed to satisfy the stable dynamics of z as given by (13). By using the boundary conditions (21) - (24), following equation is obtained:

$$\int_{\substack{y\in(y_2, y_3)\\ x=x_3}} \left(w - w^*\right)u_{c_2}\,dy - \int_{\substack{y\in(y_2, y_3)\\ x=x_2}} \left(w - w^*\right)u_{c_1}\,dy = \gamma_c \tag{25}$$

where

$$\gamma_c = \iint_{\Omega}\left[\left(w_x - w_x^*\right)w_x + \left(w_y - w_y^*\right)w_y\right]dxdy + \frac{1}{\varepsilon}\iint_{\Omega}\left(w - w^*\right)w_t^*\,dxdy - \frac{k_1}{\varepsilon}z \tag{26}$$

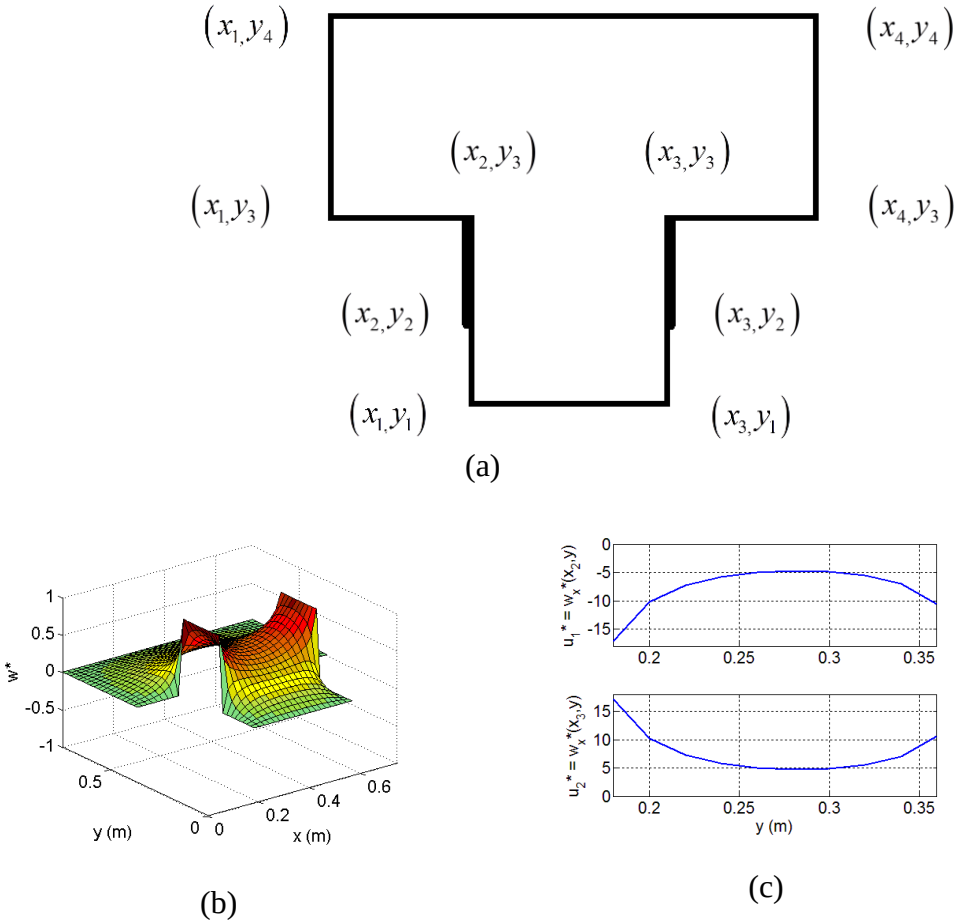

Figure 2.4. (a) geometry of a two dimensional cavity problem, (b) desired temperature profile, (c) desired control profile

To obtain a unique value of control from (25) and (26), a cost function, to be minimized, is defined as follows:

$$J_c = \frac{1}{2} \int_{\substack{y \in (y_2, y_3) \\ x = x_2}} r_{c_1} \left(u_{c_1} - u_{c_1}^* \right)^2 dy + \frac{1}{2} \int_{\substack{y \in (y_2, y_3) \\ x = x_3}} r_{c_2} \left(u_{c_2} - u_{c_2}^* \right)^2 dy \qquad (27)$$

Here, $u_{c_1}^*$ and $u_{c_2}^*$ are the desired control profiles corresponding to w^*. r_{c_1} and r_{c_2} are used defined control weighing profiles. The following control expression is obtained by using the procedure as described in Section 2.1.2.

$$
\begin{aligned}
u_{c_1} &= u_{c_1}^* - \frac{(\gamma_c - E_c)}{D_c r_{c_1}}\left(w - w^*\right) \quad at \quad \tau_1 \\
u_{c_2} &= u_{c_2}^* + \frac{(\gamma_c - E_c)}{D_c r_{c_2}}\left(w - w^*\right) \quad at \quad \tau_2
\end{aligned}
\tag{28}
$$

where

$$
\begin{aligned}
D_c &= \int_{\substack{y\in(y_2,y_3)\\ x=x_2}} \frac{\left(w-w^*\right)^2}{r_{c_1}} dy + \int_{\substack{y\in(y_2,y_3)\\ x=x_3}} \frac{\left(w-w^*\right)^2}{r_{c_2}} dy \\
E_c &= -\int_{\substack{y\in(y_2,y_3)\\ x=x_2}} \left(w-w^*\right) u_{c_1}^* dy + \int_{\substack{y\in(y_2,y_3)\\ x=x_3}} \left(w-w^*\right) u_{c_2}^* dy
\end{aligned}
\tag{29}
$$

2.3.3. Results & Discussion. Numerical simulations were carried out for this problem where the spatial domain was discretized by Δx in x direction and Δy in y direction. Simulation parameters are given as: $\Delta x = \Delta y = 0.02$, $\Delta t = 10^{-3}$, $\varepsilon = 0.1$, $r_{c_1}(y) = r_{c_2}(y) = 1 \quad \forall y \in [y_2, y_3]$ and $k_1 = 1/3$. Figure 2.4(b) shows the desired surface profile w^* and Figure 2.4(c) shows the desired control profiles $u_{c_1}^*$ and $u_{c_2}^*$, corresponding to w^*. It is easy to interpret the behavior of control on the boundary walls τ_1 and τ_2 due to symmetry of the problem. To satisfy the boundary conditions of the desired profiles (23) and (24) at steady state, it is necessary to maintain a positive heat flux at the boundaries τ_1 and τ_2. This positive heat flux was provided by $u_{c_1}^*$ and $u_{c_2}^*$ at their respective boundaries. Note that the negative values of $u_{c_1}^*$ at the boundary τ_1 represent positive heat flux.

The system was initialized with the zero temperature profile $w_0(x, y) = 0$ all over the domain. The control action, given by (28), was applied to the specified boundary walls. It was observed that the controller was able to derive the system to the desired temperature profile within 2 seconds. Figure 2.5(a) and Figure 2.5(b)

illustrate the magnitude of the temperature profile at $t = 0.25$ and $t = 2$ seconds, respectively. In these figures, horizontal axes specify the distance along the 2D geometry as shown in Figure 2.4(a). Figure 2.5(b) shows that the temperature profile that has reached to the desired level as shown in Figure 2.4(b).

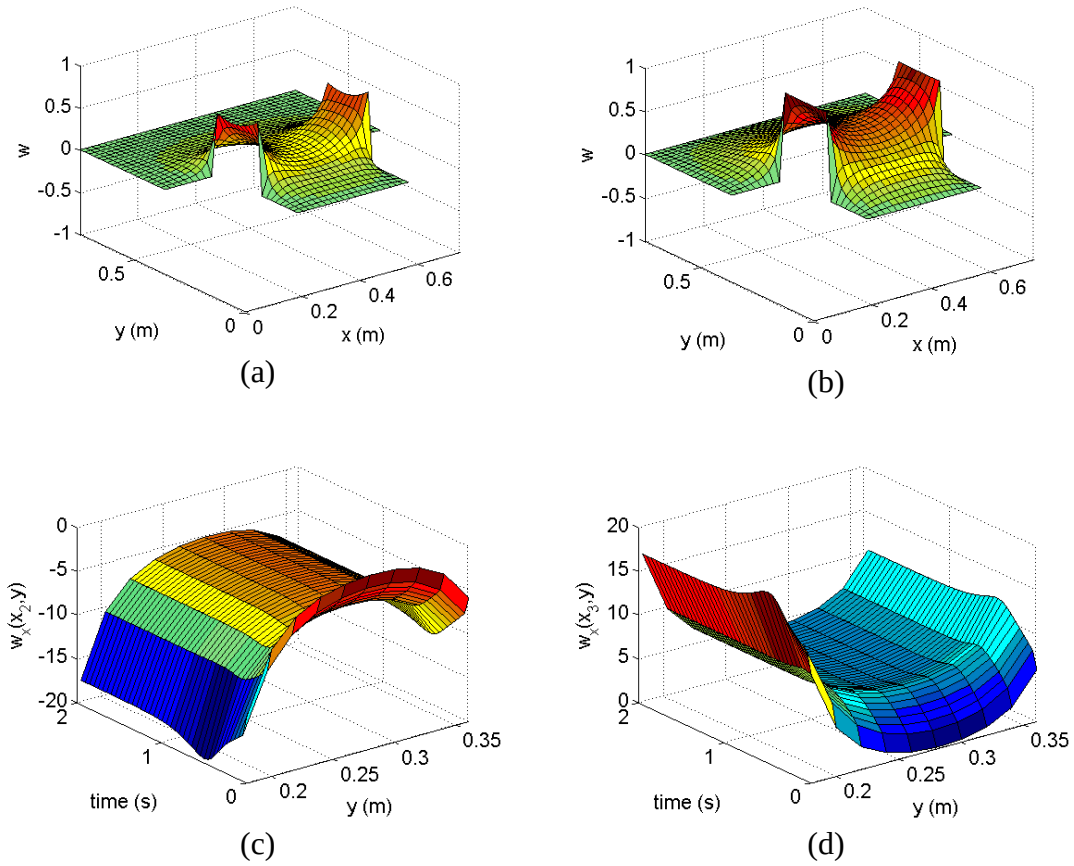

Figure 2.5. (a) and (b): temperature profile at $t = 0.25$ and $t = 2$, respectively; time history of control at (c) left boundary wall τ_1 (d) right boundary wall τ_2

In steady state, the non-zero control is necessary to maintain the system at the desired temperature profile. The nonlinear nature of the desired control profile, as shown in Figure 2.4(c), can be understood from the geometry of the problem. In order to satisfy the boundary conditions (23) and (24), it is required to have more heat flux near the end points, as compared to the central region of the boundary walls. Figure 2.5(c) and Figure 2.5(d) illustrates the time history of control profile at the boundary

walls τ_1 and τ_2, respectively. It can be observed that both control profiles approach their desired value as shown in Figure 2.4(c).

2.4. THERMAL CONVECTION LOOP

Thermal convection loop is a simplified model that represents a viable tool for studying the behavior of natural convection. The convection loops have been extensively studied (e.g., see [81] - [83]) and have been used in many applications such as solar heating and cooling systems, reactor cooling system, engine and computer cooling, etc. As the working principle of a convection loop is based on the natural convection, it provides a means for circulating the fluid without the use of pumps. A thermal convection loop is described here by a Newtonian viscous fluid contained in between two concentric cylinders standing in a vertical plain as shown in Figure 2.6. In this figure, R_1 and R_2 denote the inner and the outer radius of the cylinders, respectively. The process of heating the loop from below and cooling it from above creates a temperature gradient (opposite to gravity) that results in a change in the density of the fluid. The fluid with low temperature will be denser compared to the fluid with high temperature. This variation in density generates a buoyancy force that tends to move the fluid, i.e., fluid with high temperature tends to rise upwards and, conversely, fluid with low temperature tends to settle down. This motion is opposed by the force due to fluid's viscosity and thermal diffusivity. The fluid motion is created when the resistive force generated by these dissipative terms is overcome by the force due to buoyancy.

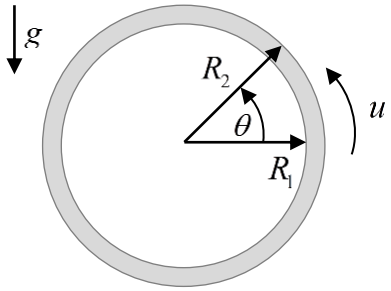

Figure 2.6. Geometry of the thermal convection loop

A feedback control needs to be applied when it is required to change the nature of the flow inside the loop. There are a few control design papers which have considered linear and nonlinear models of the loop dynamics. A PDE model of the loop was formulated by Burns, King and Rubio in [84] using the Boussinesq approximation. The loop was actuated by controlling the temperature at the outer radius. A linear approximation of the nonlinear model was used and a linear quadratic Gaussian (LQG) controller was designed based on the DTA scheme to achieve local stability. The controller was approximated to a finite-dimensional space by solving the associated riccati equation using finite element techniques. A nonlinear feedback controller based on ATD scheme was designed by Bošković and Krstić in [85]. The original nonlinear PDE model was first discretized in space using a finite difference method to obtain a high order system of coupled nonlinear ODEs. Two uncoupled systems were then formulated by using a backstepping transformation with Dirichlet boundary conditions. The loop was actuated by the velocity and the temperature, both controlled at the outer radius. Simulation results were presented for different sizes of spatial grid. The shortcoming of this technique is that the coordinate transformation does not hold in the limit when the discretized grid approaches the continuous domain. Moreover, one of the key issues is the choice of a target system while applying backstepping transformation in PDEs. An appropriate target system is

necessary to keep the parabolic character of the original system, i.e., keep the second spatial derivative in the transformed coordinates. A state feedback boundary control law was designed in [86] with a combination of singular perturbation theory and the backstepping method for infinite-dimensional linear systems. The nonlinear term in the loop dynamics was neglected while deriving the control law; and stability the system was proved using Lyapunov stability theory.

In this study, the convection loop is stabilized by applying boundary control (at the outer radius) where no approximation is used in constructing the controller. The following mathematical model [84] is used for the controller formulation and is written in cylindrical coordinates as

$$\begin{aligned} u_t(r,t) &= \frac{\gamma}{2\pi}\int_0^{2\pi} T\cos(\theta)\,d\theta + \nu\left(-\frac{u}{r^2}+\frac{u_r}{r}+u_{rr}\right) \\ T_t(r,\theta,t) &= -\frac{u}{r}T_\theta + \chi\left(\frac{T_{\theta\theta}}{r^2}+\frac{T_r}{r}+T_{rr}\right) \end{aligned} \tag{30}$$

with the boundary conditions $u(R_1,t)=u(R_2,t)=0$, $T(R_1,\theta,t)=KR_1\sin(\theta)$ and $T(R_2,\theta,t)=KR_2\sin(\theta)$. This model represents the coupled dynamics of the fluid motion; and the temperature at any point in the spatial domain is described by (radial, angular) position $(r,\theta)\in\Omega\equiv[R_1,R_2]\times[0,2\pi)$. The state of the thermal convection loop is described by the fluid velocity $u(r,t)$ and temperature $T(r,\theta,t)$ at any time $t\geq 0$. Subscripts with the state variables denote partial derivatives, i.e., $x_y \triangleq \partial x/\partial y$ and $x_{yy}\triangleq \partial^2 x/\partial y^2$. In the system of equations (30), $\gamma=|g|\beta$ where $|g|$ is the magnitude of acceleration due to gravity and β is the coefficient of thermal expansion. The coefficients ν and χ denote kinematic viscosity and thermal diffusivity, respectively.

In the model described above, the gap between the cylinders is assumed to be small, i.e., $R_2 - R_1 \ll R_1$ such that the fluid particle flows in circular streamlines at a fixed distance from the center of the cylinders. Therefore, the velocity depends only on the radial coordinate. Furthermore, fluid properties (β, v, χ) are assumed to be constant except for the density (Boussinesq approximation [84]).

2.4.1. Problem Statement. The no-motion steady state of the system described by (30) is of the form $(\bar{u}, \bar{T}) = (0, Kr\sin\theta)$, which is open loop unstable for sufficiently high values of K. A new variable $\tau = T - \bar{T} = T - Kr\sin\theta$ is introduced to shift the equilibrium to $(u, \tau) = (0,0)$. The system of equations (30) is then rewritten in terms of the new state variable as

$$\begin{aligned} u_t(r,t) &= \frac{\gamma}{2\pi}\int_0^{2\pi} \tau\cos(\theta)\,d\theta + v\left(-\frac{u}{r^2} + \frac{u_r}{r} + u_{rr}\right) \\ \tau_t(r,\theta,t) &= -Ku\cos(\theta) - \frac{u}{r}\tau_\theta + \chi\left(\frac{\tau_{\theta\theta}}{r^2} + \frac{\tau_r}{r} + \tau_{rr}\right) \end{aligned} \tag{31}$$

with the boundary conditions $u(R_1,t) = u(R_2,t) = 0$, $\tau(R_1,\theta,t) = 0$ and $\tau_r(R_2,\theta,t) = \Gamma(\theta,t)$. Here, $\Gamma(\theta,t)$ represents the heat flux at the outer radius of the loop and treated as the boundary control. From a physical point of view, total heat flux applied at the boundary of the convection loop will be $\Gamma(\theta,t) + K\sin\theta$. The objective is to stabilize the system in (31) using boundary control while satisfying rest of the boundary conditions. In this section, the thermal convection loop is regarded as the system, and fluid's coefficients are considered as the system's parameters.

2.4.2. Controller Development. This section describes the development of the proposed boundary control law by using the principles of dynamic inversion and

variational optimization. It is assumed that exact values of parameters (γ, v, χ) are known. First, an output function is defined as follows:

$$z(t) = \frac{p_1}{2}\int_{R_1}^{R_2} u^2(r,t)dr + \frac{p_2}{2}\int_{R_1}^{R_2}\int_{0}^{2\pi} \tau^2(r,\theta,t)\,d\theta dr \tag{32}$$

where $p_1, p_2 > 0$ are real numbers and act as weighing factors. A controller is designed to satisfy the following first order stable dynamics

$$z_t + k_2 z = 0 \tag{33}$$

here $k_2 > 0$ acts as a gain. By using the definition of z from (32) and the dynamics from (33), the following equation is obtained:

$$p_1\int_{R_1}^{R_2} u u_t dr + p_2\int_{R_1}^{R_2}\int_{0}^{2\pi} \tau\tau_t d\theta dr + k_2 z = 0 \tag{34}$$

Further, by substituting the expression of u_t and τ_t from the loop dynamics (31) in (34), we get

$$p_2\chi\int_{0}^{2\pi} \tau(R_2,\theta)\Gamma(\theta)\,d\theta + \Upsilon = 0 \tag{35}$$

where the term Υ is given by

$$\begin{aligned}\Upsilon = &\left(\frac{p_1\gamma}{2\pi} - p_2 K\right)\int_{R_1}^{R_2}\int_{0}^{2\pi} u\tau\cos(\theta)\,d\theta dr - p_1 v\int_{R_1}^{R_2}\left(\frac{u^2}{r^2} - \frac{uu_r}{r} + u_r^2\right)dr - \\ &- p_2\chi\int_{R_1}^{R_2}\int_{0}^{2\pi}\left(\frac{\tau_\theta^2}{r^2} - \frac{\tau\tau_r}{r} + \tau_r^2\right)d\theta dr + k_2 z\end{aligned} \tag{36}$$

In order to obtain unique value of control, a cost function is defined as

$$J_2(t) = \frac{1}{2}\int_{0}^{2\pi}\Gamma^2(\theta,t)\,d\theta \tag{37}$$

By following the principles of variational optimization as discussed in Section 2.1.2, the following control law is obtained:

$$\Gamma(\theta) = -\frac{\Upsilon}{p_2 \chi \int_0^{2\pi} \tau^2(R_2,\theta)\, d\theta}\, \tau(R_2,\theta) \tag{38}$$

Let, $D = p_2 \chi \int_0^{2\pi} \tau^2(R_2,\theta)\, d\theta$ denotes the denominator term. It may be noticed that both the numerator and the denominator in the this expression approach zero as $\tau(R_2,\theta) \to 0$. To avoid singular solutions, the control profile is set to zero when the absolute value of the denominator is less than a specified tolerance, i.e., $D < tol$.

2.4.3. Results & Discussion. The simulation parameters, taken from Burns et al. in [84], are $R_1 = 1.1975$ ft, $R_2 = 1.2959$ ft, $\beta = 8\times10^{-5}$/°F, $\chi = 1.514\times10^{-6}$ ft^2/sec and $\nu = 1.22\times10^{-5}$ ft^2/sec. The convection loop geometry was discretized into a grid of 50 by 90 points in the radial and the angular directions, respectively. The design parameters values were: $K = -0.03$, $p_1 = p_2 = 1$ and $k_2 = 10^{-3}$. All simulations were run with the initial state profile of the system as shown in Figure 2.7.

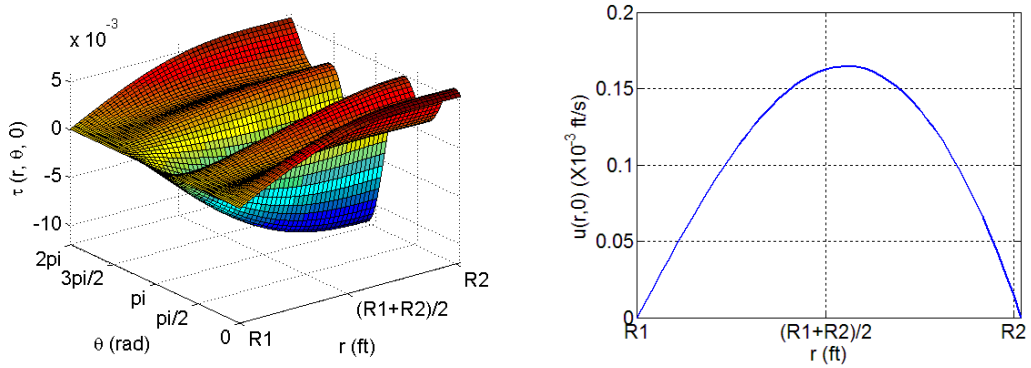

(a) (b)

Figure 2.7. Initial profile of the state variables (a) $\tau(r,\theta,0)$, and (b) $u(r,0)$

The system was first simulated without any application of boundary control. Evolution of $\tau(r,\theta,t)$ at the radial locations $r_i = R_1 + (R_2 - R_1)i/5$, for $(i = 3,5)$, are

shown in Figure 2.8 (a) and (b). The spatiotemporal profile of $u(r,t)$ is shown in Figure 2.8 (c).

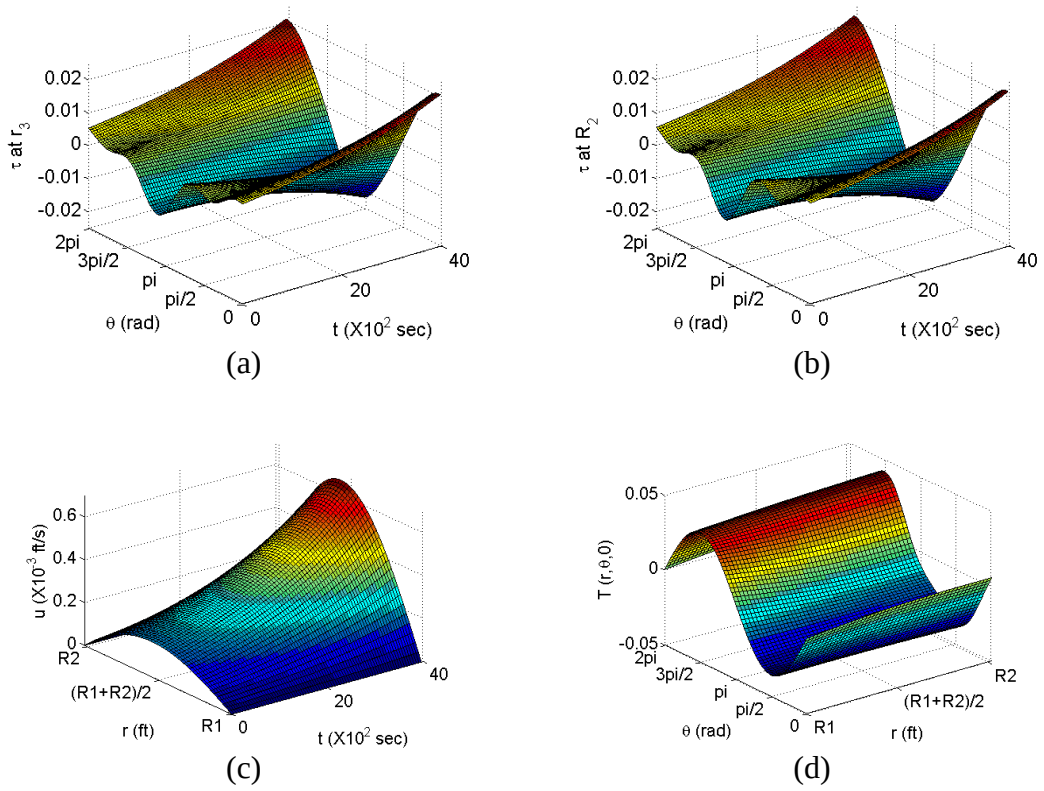

Figure 2.8. Time history of (a) $\tau(r_3,\theta,t)$, (b) $\tau(r_5,\theta,t)$ and (c) $u(r,t)$ in the case of uncontrolled loop, (d) Temperature $T(r,\theta,0)$ profile

From Figure 2.8 (a) and (b), it is clear that the system is unstable when initialized with a non- zero profile as shown in Figure 2.7. A physical interpretation of these results is as follows: The system was initialized with a temperature distribution with a relatively high value of τ near zero radian and a relatively low value at π radian. As the buoyancy force overcomes the dissipative force due to fluid viscosity and thermal diffusivity, fluid motion exhibits instability, i.e., the fluid in regions with high temperature starts rising upward and the fluid in the regions with low temperature starts settling down. This unstable motion can be observed in Figure 2.8 (c). Instability in the $\tau(r,\theta,t)$ state profile can be understood from the initial temperature

distribution $T(r,\theta,0)$. Figure 2.8 (d) shows the initial temperature distribution where $T(r,\theta,0)=\tau(r,\theta,0)+Kr\sin\theta$. Due to the flow in the positive direction, the fluid with low temperature starts to settle down at π radian and the fluid with high temperature flows upward at zero radian. This action lowers the temperature at π radian and increase the temperature at zero radian.

Next, the system was simulated with the application of boundary control. Time history of the control action is shown in Figure 2.9 (a). In the control profile, positive values of control means that heat is applied and negative values mean that heat is extracted, at the boundary. Initial state profile, as shown in Figure 2.7 (a), provides an idea of the nature of heat flux distribution that is required for the control action, i.e., heat should be added to the boundary points having negative values of $\tau(R_2,\theta,t)$ and, conversely, heat should be extracted from the boundary points having positive values of $\tau(R_2,\theta,t)$. Figure 2.9 (a) displays this nature of control profile. It can be observed that by applying this control action, the state profiles approach equilibrium as observed from Figure 2.9 (b) - (d). In investigating the control history, it was found that the absolute value of the numerator in the controller expression (38) was always lesser in magnitude as compared to the denominator D. This behavior was observed till 200×10^2 seconds where the denominator was still greater than the tolerance limit 10^{-30}. It is quite possible that the denominator may approach zero faster than the numerator for other values of design variables. To avoid any resulting singular solution, control values are set to zero as denominator goes below the specified tolerance.

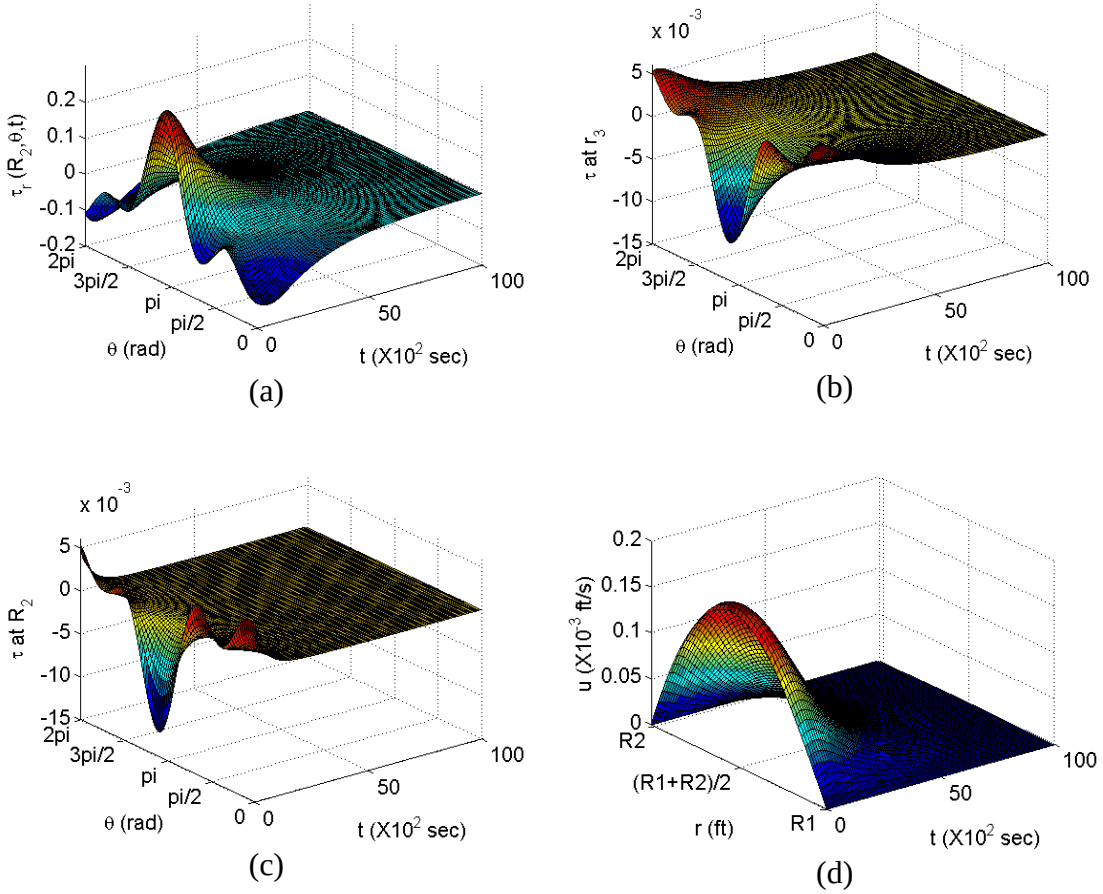

Figure 2.9. Time history of (a) the heat flux $\Gamma(\theta,t)$ at the outer radius, and (b) $\tau(r_3,\theta,t)$, (c) $\tau(r_5,\theta,t)$, (d) $u(r,t)$ in the case of controlled loop

To investigate the effect of gain k_2 on system stability, a simulation was run by taking half of its previous value i.e. $k_2 = 0.5\times10^{-3}$. This gain can be interpreted as the inverse of the time constant of the z dynamics. As the value of control $\Gamma(\theta,t)$ is directly proportional to k_2, it takes more time to stabilize the system with a low value of k_2. This stabilizing behavior of control can be observed in Figure 2.10 (a) which shows that the control profile reaches zero in nearly twice the time period as compared to the plot in Figure 2.9 (a). Figure 2.10 (b) shows the comparison in the magnitude of control effort at time $t = 0$ for different values of the gain parameter. The magnitude of control profile is more for the higher value of k_2.

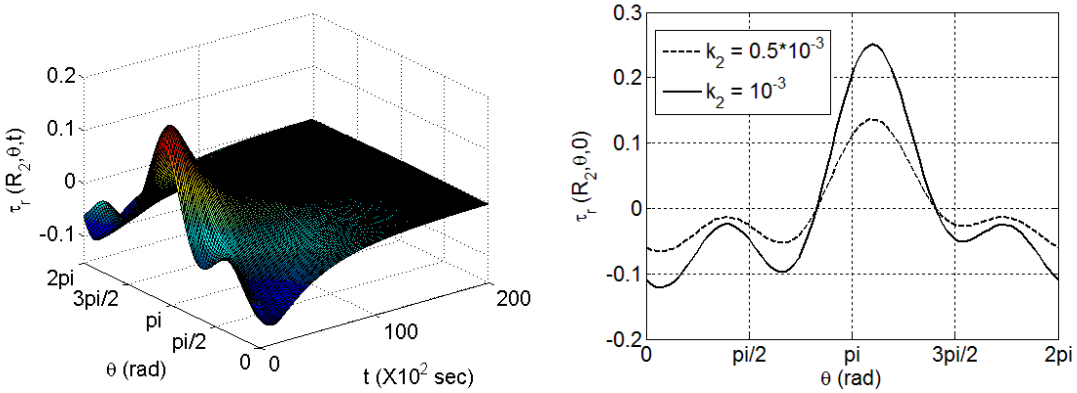

(a) (b)

Figure 2.10. (a) Time history of the heat flux $\Gamma(\theta,t)$ at the outer radius when $k_2 = 0.5\times10^{-3}$, (b) $\Gamma(\theta,0)$ profile for $k_2 = 0.5\times10^{-3}$ and $k_2 = 10^{-3}$

In summary, a control design technique for nonlinear systems was described in its generic form. By using the design procedure, controllers' expressions were formulated for heat equations and thermal convection loops. The results demonstrate that the design technique has an excellent promise, and due to its general formulation it can be applied to a variety of boundary control problems.

3. ADAPTIVE BOUNDARY CONTROL BASED ON LYAPUNOV STABILITY

It is not always possible to have an accurate mathematical model of engineering systems. An uncertainty in the system may exist either due to unmodeled dynamics or due to the system's parameters. Examples of systems' parameters are: coefficient of thermal diffusivity ε in the heat equation (10), coefficient of kinematic viscosity v in the fluid flow equation (30), etc. To address this practical issue of parameter uncertainty in the system, the control design methodology, as described in Section 2.1, is extended to formulate an adaptive controller.

In the process of designing an adaptive control law, an estimator is, generally, defined. In the present study, estimator has the similar mathematical structure as of the actual system except with the inaccurate values of system's parameters. By using the Lyapunov stability theory, an update law of these parameters is obtained such that estimator tracks the actual system. Once the tracking is established, an adaptive control law is formulated based on the estimator dynamics.

The applicability of this adaptive controller is demonstrated using the examples of heat equations and the thermally convected fluid flow as introduced in Section 2.

3.1. ADAPTIVE BOUNDARY CONTROL SYNTHESIS

3.1.1. System Description. Consider a system of partial differential equations as

$$x_t = F_0 + a_1 F_1 + a_2 F_2 + ... + a_n F_n \tag{39}$$

with appropriate boundary conditions. Here, the state $x(y,t)$ is a function of spatial variable $y \in \Omega$ and time t. In the equation (39), $F_i(x, x', x'', ..., y, t)$, $(i = 0,1,...n)$

are real valued functions. Here, x_t represents time partial derivative and x' represents spatial partial derivative. The degree of spatial partial derivative is denotes by number of apostrophe$(')$. It is assumed that the values of parameters $a_i \quad (i=1,2,...n)$ happen to be inside a lower and an upper bound as denoted by $\underline{a}_i$ and $\bar{a}_i$, respectively.

3.1.2. Controller Formulation. To design a feedback controller with uncertain values of parameters, an estimator is designed to track the system. It is important to note that the system state is available whereas the system parameters are unknown. The estimator serves two purposes here: (a) estimator is defined using inaccurate values of parameters; and it is used to derive an update law of the parameters, (b) estimator is used to formulate an adaptive control action. The estimator is assumed to be of the form

$$x_t = k_e\left(x - x\right) + F_0 + a_1F_1 + a_2F_2 + ... + a_nF_n \tag{40}$$

with the same boundary conditions as of the system. Here, $x(y,t)$ is the estimated state, $k_e < 0$ is a design matrix, $a_i(t) \quad (i=1,2,...,n)$ are the estimated values of unknown parameters a_i, respectively. The following error terms are defined as

$$\begin{aligned} e &= x - x \\ a_i &= a_i - a_i \end{aligned} \tag{41}$$

where e is the state estimation error and $a_i(t) \quad (i=1,2,...,n)$ are the parameter estimation errors. The state error dynamics can be written using (39), (40) and (41) as

$$e_t = k_e e + a_1F_1 + a_2F_2 + ... + a_nF_n \tag{42}$$

This error dynamics need to be stabilized to force the estimator to track the states of the actual system. By using the Lyapunov stability theory [87], a parameter

update law is derived to stabilize the error dynamics. Consider a candidate Lyapunov function V :

$$V = \frac{1}{2}\int_{\Omega} \|e\|^2 \, d\Omega + \frac{1}{2}\sum_{i=1}^{n} \frac{a_i^2}{f_i} > 0 \quad \forall \quad e \neq 0 \quad \& \quad a_i \neq 0 \tag{43}$$

Here, $f_i > 0 \quad (i = 1, 2, ..., n)$ are weighing factors for the parameter errors. The time derivative of V is written as

$$V_t = \int_{\Omega} e^T e_t d\Omega + \sum_{i=1}^{n} \frac{a_i a_{i_t}}{f_i} \tag{44}$$

By using the error dynamics (42), (44) becomes

$$V_t = \int_{\Omega} e^T k_e e d\Omega + \sum_{i=1}^{n} \frac{a_i}{f_i} \left(\int_{\Omega} f_i e^T F_i d\Omega + a_{i_t} \right) \tag{45}$$

The following parameter update law is given as

$$a_{i_t} = \begin{cases} 0, & if \quad a_i = \bar{a}_i \quad and \quad -\int_{\Omega} f_i e^T F_i \geq 0 \\ -\int_{\Omega} f_i e^T F_i, & if \quad a_i = \bar{a}_i \quad and \quad -\int_{\Omega} f_i e^T F_i < 0 \\ -\int_{\Omega} f_i e^T F_i, & if \quad \underline{a}_i < a_i < \bar{a}_i \\ -\int_{\Omega} f_i e^T F_i, & if \quad a_i = \underline{a}_i \quad and \quad -\int_{\Omega} f_i e^T F_i > 0 \\ 0, & if \quad a_i = \underline{a}_i \quad and \quad -\int_{\Omega} f_i e^T F_i \leq 0 \end{cases} \quad \forall \quad (i = 1, 2...n) \tag{46}$$

Consequently, (45) becomes

$$V_t = \begin{cases} \int_\Omega e^T k_e e d\Omega + \sum_{i=1}^{n} \frac{a_i}{f_i} \int_\Omega f_i e^T F_i d\Omega, & if \quad a_i = \bar{a}_i \quad and \quad -\int_\Omega f_i e^T F_i \geq 0 \\ \int_\Omega e^T k_e e d\Omega, & if \quad a_i = \bar{a}_i \quad and \quad -\int_\Omega f_i e^T F_i < 0 \\ \int_\Omega e^T k_e e d\Omega, & if \quad \underline{a}_i < a_i < \bar{a}_i \\ \int_\Omega e^T k_e e d\Omega, & if \quad a_i = \underline{a}_i \quad and \quad -\int_\Omega f_i e^T F_i > 0 \\ \int_\Omega e^T k_e e d\Omega + \sum_{i=1}^{n} \frac{a_i}{f_i} \int_\Omega f_i e^T F_i d\Omega, & if \quad a_i = \underline{a}_i \quad and \quad -\int_\Omega f_i e^T F_i \leq 0 \end{cases} \tag{47}$$

Since, $f_i > 0 \quad (i = 1, 2, ..., n)$, the following inequality is satisfied:

$$V_t \leq \int_\Omega e^T k_e e d\Omega \tag{48}$$

V_t is negative semi-definite, i.e., $V_t \leq 0$. This shows that estimation error in both the states and the parameters are bounded. Next, by assuming the bounded control action and using Barbalat's Lemma [87], it can be shown that $e \to 0$ as $t \to \infty$.

An adaptive controller is designed by following the procedure as described in Section 2.1.2. The difference from the previous design procedure is that here controller expression is derived using the estimator dynamics (40). A function $\hat{z}(t)$ is defined

$$\hat{z}(t) = \frac{1}{2} \int_\Omega \left\| x(\Omega, t) - x^*(\Omega, t) \right\|^2 d\Omega \tag{49}$$

with the following first order stable equation:

$$\hat{z}_t + k\hat{z} = 0 \tag{50}$$

Here, k has similar significance as k in Section 2.1.2. An equation is derived by using (49) and (50), and written in a compact form as

$$\int_{\partial\Omega} g\left(x(s,t) - x^*(s,t)\right) u ds = \gamma \tag{51}$$

In the equation (51), the function $\left|g\left(x(s,t)-x^*(s,t)\right)\right|>0$ if $\left|x(s,t)-x^*(s,t)\right|>0$ and $\left|g\left(x(s,t)-x^*(s,t)\right)\right|=0$ if $\left|x(s,t)-x^*(s,t)\right|=0, \quad \forall s\in\partial\Omega$. The term γ is a function of known values $\left(x, x, x^*, x', x', x^*', ..., k, a_1, ..., a_n\right)$ and linearly proportional to the parameter k. The controller is designed to (a) satisfy the stable dynamics given in (50) and (b) minimize the following cost function:

$$J(t)=\frac{1}{2}\int_{\partial\Omega}\hat{r}(s)\left[u(s,t)\right]^2 ds \tag{52}$$

Here, $\hat{r}(s)>0 \ \ \forall s\in\partial\Omega$ acts as the weighing profile for the control action $u(s,t)$ and can be chosen per design constraints. By using the calculus of variations [75], the following control expression is obtained:

$$u(s,t)=\frac{\gamma g\left(x(s,t)-x^*(s,t)\right)}{\hat{r}\int_{\partial\Omega}\frac{\left[g\left(x(s,t)-x^*(s,t)\right)\right]^2}{\hat{r}}ds} \quad \forall s\in\partial\Omega \tag{53}$$

3.2. HEAT EQUATIONS

In this section, adaptive control is formulated for the heat equation as described by (10) in the Section 2.2. Here, the unknown parameter is the coefficient of diffusivity ε that falls between a positive lower bound $\left(\underline{\varepsilon}\right)$ and an upper bound $\left(\bar{\varepsilon}\right)$.

3.2.1. Controller Development. To design a feedback controller with uncertain value of parameter, an estimator is designed to track the system's behavior. This estimator is assumed to be of the form

$$w_t = k_e\left(w - w\right) + \varepsilon\left[w_{xx} + w_{yy}\right] \tag{54}$$

where $k_e < 0$ is a design parameter and $\varepsilon(t)$ is the estimated value of the unknown parameter ε at time t. The boundary conditions are given as

$$\begin{aligned} w_x(t,1,y) &= w_x(t,1,y) \\ w_y(t,x,1) &= w_y(t,x,1) \\ w_x(t,0,y) &= w_x(t,0,y) \\ w_y(t,x,0) &= w_y(t,x,0) \end{aligned} \tag{55}$$

The state estimation error and the parameter estimation error are defined as $e = w - w$ and $\varepsilon = \varepsilon - \varepsilon$, respectively. By using these definitions, the state error dynamics is defined as

$$e_t = k_e e + \varepsilon\left[w_{xx}(t,x,y) + w_{yy}(t,x,y)\right] \tag{56}$$

A Lyapunov function is defined as

$$V = \frac{1}{2}\iint e^2 dxdy + \frac{1}{2f_\varepsilon}\varepsilon^2 \tag{57}$$

Here, $f_\varepsilon > 0$ is a real number. The following update law is given for the parameter $\varepsilon(t)$

$$\varepsilon_t = \begin{cases} 0, & if \quad \varepsilon = \bar{\varepsilon} \quad and \quad -f_\varepsilon E \geq 0 \\ -f_\varepsilon E, & if \quad \varepsilon = \bar{\varepsilon} \quad and \quad -f_\varepsilon E < 0 \\ -f_\varepsilon E, & if \quad \underline{\varepsilon} < \varepsilon < \bar{\varepsilon} \\ -f_\varepsilon E, & if \quad \varepsilon = \underline{\varepsilon} \quad and \quad -f_\varepsilon E > 0 \\ 0, & if \quad \varepsilon = \underline{\varepsilon} \quad and \quad -f_\varepsilon E \leq 0 \end{cases} \tag{58}$$

such that the inequality $V_t \leq k_e \iint e^2 dxdy \leq 0$ is satisfied. Note that the double integral is defined over the domain $(x,y) \in \left([0,1]\times[0,1]\right)$ in this section.

Next, an output function is defined as: $\hat{z}(t) = \frac{1}{2}\iint \left(w - w^*\right)^2 dxdy$. An adaptive controller is formulated to satisfy the stable dynamics $\hat{z}_t + k_1 \hat{z} = 0$ and to minimize the following cost function:

$$J = \frac{1}{2}\int_y \hat{r}_1(y)\left[u_1(y)\right]^2 dy + \frac{1}{2}\int_x \hat{r}_2(x)\left[u_2(x)\right]^2 dx + \\ + \frac{1}{2}\int_y \hat{r}_3(y)\left[u_3(y)\right]^2 dy + \frac{1}{2}\int_x \hat{r}_4(x)\left[u_4(x)\right]^2 dx \tag{59}$$

By using the calculus of variations [75], the following control expressions are obtained

$$u_1(y) = \frac{\gamma\left(w - w^*\right)(1, y)}{\hat{r}_1(y) D}$$
$$u_2(x) = \frac{\gamma\left(w - w^*\right)(x, 1)}{\hat{r}_2(x) D}$$
$$u_3(y) = -\frac{\gamma\left(w - w^*\right)(0, y)}{\hat{r}_3(y) D} \tag{60}$$
$$u_4(x) = -\frac{\gamma\left(w - w^*\right)(x, 0)}{\hat{r}_4(x) D}$$

where

$$\gamma \triangleq \iint \left[\left(w_x - w_x^*\right) w_x + \left(w_y - w_y^*\right) w_y\right] dxdy - \\ - \frac{k_e}{\varepsilon}\iint \left(w - w^*\right)\left(w - w\right) dxdy + \frac{1}{\varepsilon}\iint \left(w - w^*\right) w_t^* dxdy - \frac{k_1}{\varepsilon}\hat{z} \tag{61}$$

and

$$D \triangleq \left[\begin{array}{l} \int_y \frac{\left(w-w^*\right)^2(1,y)}{\hat{r}_1(y)}dy + \int_x \frac{\left(w-w^*\right)^2(x,1)}{\hat{r}_2(x)}dx + \\ + \int_y \frac{\left(w-w^*\right)^2(0,y)}{\hat{r}_3(y)}dy + \int_x \frac{\left(w-w^*\right)^2(x,0)}{\hat{r}_4(x)}dx \end{array} \right] \tag{62}$$

3.2.2. Results & Discussion. The system was simulated by applying the adaptive control law given by (60). The objective was to drive the system to the following desired surface profile: $w^*(x,y)=1 \quad \forall (x,y)\in([0,1]\times[0,1])$. The simulation parameters were taken as: $\hat{r}_1(y)=\hat{r}_3(y)=1 \quad \forall y\in[0,1]$, $\hat{r}_2(y)=\hat{r}_4(y)=1 \quad \forall x\in[0,1]$, $(\underline{\varepsilon},\bar{\varepsilon})=(10^{-2},0.2)$, $k_1=0.2$, $k_e=-0.2$, $f_\varepsilon=0.078$.

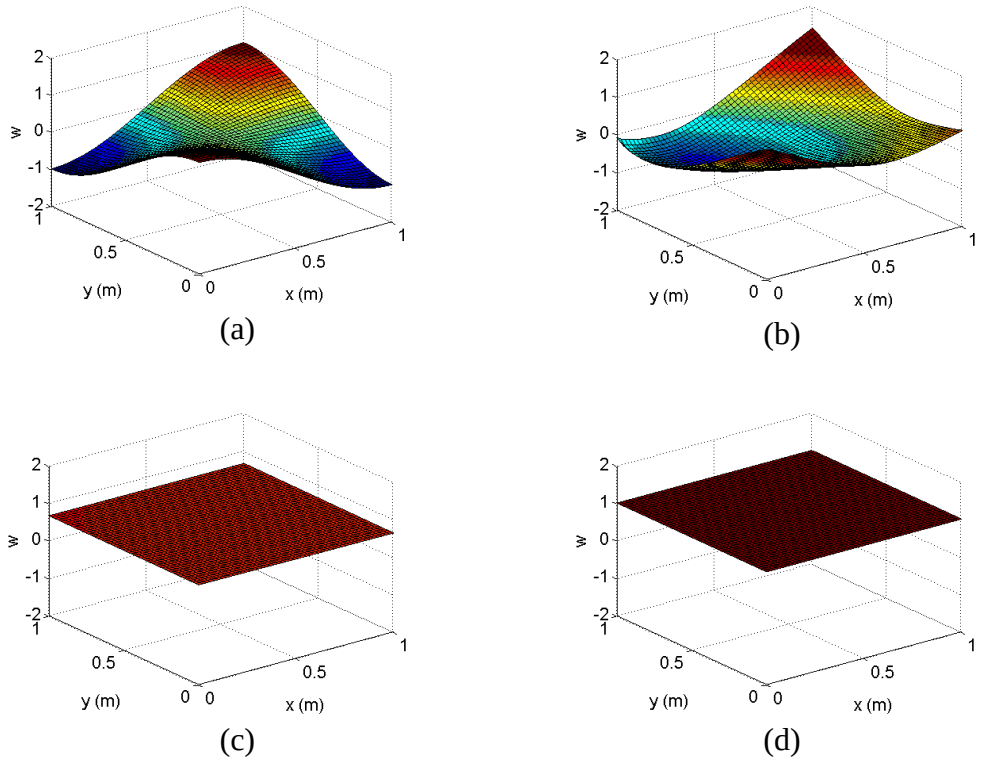

Figure 3.1. State profile at (a) $t=0$, (b) $t=0.2$, (c) $t=1$, (d) $t=30$

The estimator's state was initialized with a zero surface profile $w(0,x,y)=0$; and the parameter ε was initialized with the lower bound. Figure 3.1 shows the surface

profile of actual system at the time instants $t = 0,\ 0.2,\ 1$ and 30 second. It can be observed that the controller is able to drive the system to the desired surface profile in 30 seconds.

The variables k_e and f_ε play an important role in the estimation of the parameter ε. The variable k_e provides robustness to the estimated state error dynamics (56). Its significance lies in the fact that it stabilizes the error dynamics quickly (slowly) for a higher (lower) value and, vice-versa. Values of the variables k_e and f_ε should be tuned appropriately such that the estimation error in both the state and the parameter approaches zero about the same time for several cases. Interested readers may refer [88] to study the role of these variables on the stability of the estimator dynamics.

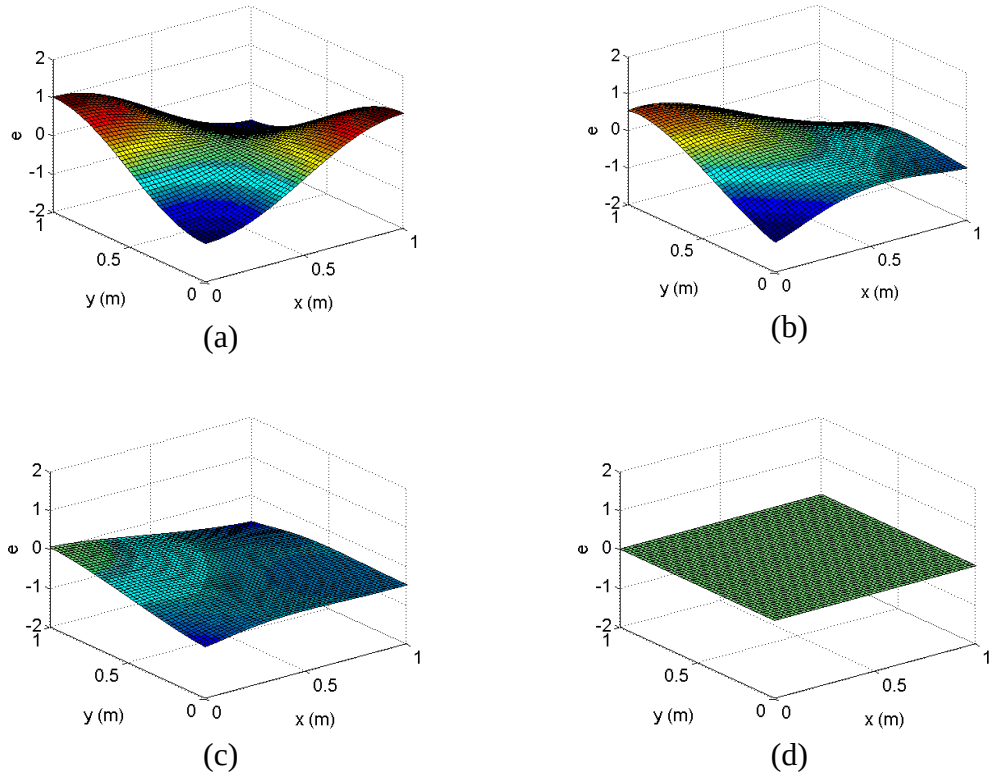

Figure 3.2. State estimation error profile at (a) $t = 0$, (b) $t = 0.2$, (c) $t = 1$, (d) $t = 30$

Figure 3.2 illustrates the estimation error at time instants $t = 0,\ 0.2,\ 1$ and 30 second. The error profile approaches zero in 30 seconds. Figure 3.3 illustrates the time history of parameter's estimated value. The evolution of the parameter depends on the role played by the state error profile and spatial derivatives in the parameter's update law. It was observed that the estimated value remains in the bounds and the actual value is estimated very well within 30 seconds.

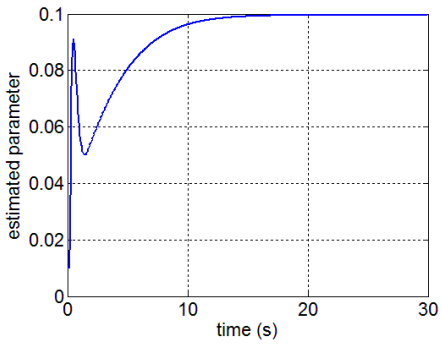

Figure 3.3. Time history of estimated parameter ε

The transient behavior of the control action can be observed in Figure 3.4 from time $t = 0$ to 1 second. During this time period, control (heat flux) at the boundaries causes the system to achieve nearly a flat surface profile. This transition requires maximum amount of heat flux at the boundary as compared to the rest of the time period. It was observed that it takes significant amount of time to reach to the target profile after $t = 1$ second. Transient performance of this process can be made faster by taking a higher value of k_1. Note that the term $\frac{k_1}{\varepsilon}\hat{z}$, in the γ expression (61), dominates the other terms as the system's state reaches a nearly flat surface profile. The system was simulated for $k_1 = 0.5$. To compare the results obtained with $k_1 = 0.2$, control action at the boundary wall co-ordinates $(1, y)$ is plotted in Figure

3.5. Figure 3.5 (a) and (b) illustrate the control profile for $k_1 = 0.2$ from $t = 0$ to1 second and $t = 1$ to 30 seconds, respectively.

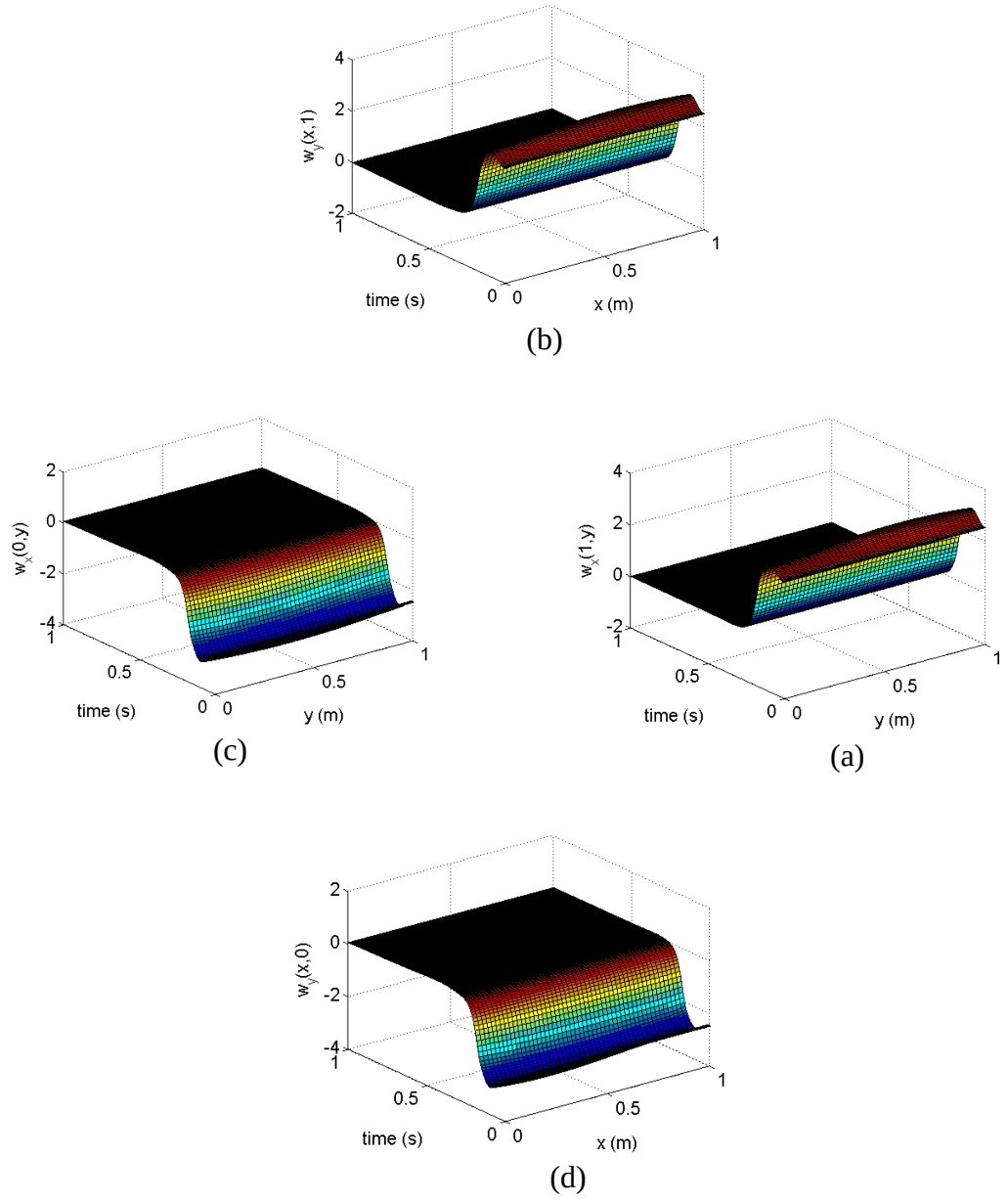

Figure 3.4. Time history of control profile at the boundary wall as specified by the co-ordinates (a) $(1, y)$ (b) $(x,1)$ (c) $(0, y)$ (d) $(x,0)$, from time $t = 0$ to 1 second

Figure 3.5 (c) and (d) illustrate the control profile for $k_1 = 0.5$ from $t = 0$ to1 second and $t = 1$ to 20 seconds, respectively. The time history of the control action is shown in these separate figures for each value of k_1 to show the relative magnitude of the

control effort. To compare the effect of k_1 in the control profile, relatively high value of control action can be observed in Figure 3.5 (c) as compared to in Figure 3.5 (a). Moreover, the system approaches the target profile and control approaches zero in 20 seconds for $k_1 = 0.5$ as shown in Figure 3.5 (d).

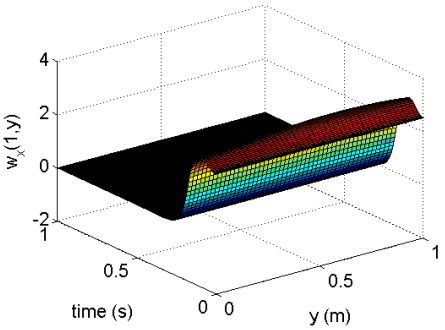

(a) from time $t = 0$ to 1 second

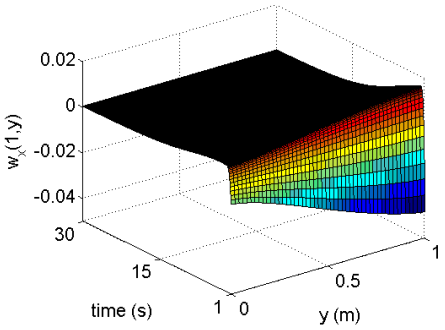

(b) from time $t = 1$ to 30 second

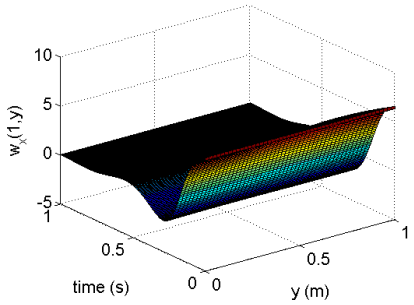

(c) from time $t = 0$ to 1 second

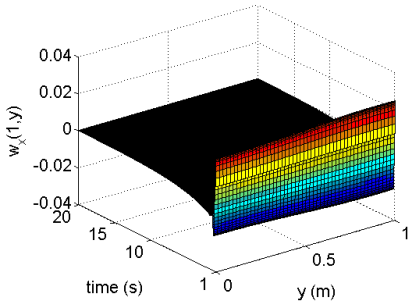

(d) from time $t = 1$ to 20 second

Figure 3.5. Time history of boundary control profile at the right boundary wall (a) and (b): for $k_1 = 0.2$, (c) and (d): for $k_1 = 0.5$

3.3. THERMAL CONVECTION LOOP

This section discusses the development of an adaptive control law for thermal convection loop dynamics as described by (31). Here, the values of parameters (γ, ν, χ) are not known accurately. We assume that the value of each parameter is bounded below and above. The pairs $(\underline{\gamma}, \overline{\gamma}), (\underline{\nu}, \overline{\nu})$ and $(\underline{\chi}, \overline{\chi})$ denote the (lower, upper) bounds of γ, ν and χ, respectively.

3.3.1. Controller Development. An estimator is defined by the following dynamics

$$\begin{aligned} u_t(r,t) &= k_u\left(u-u\right)+\frac{\gamma}{2\pi}\int_0^{2\pi}\tau\cos(\theta)\,d\theta+\hat{v}\left(-\frac{u}{r^2}+\frac{u_r}{r}+u_{rr}\right) \\ \hat{\tau}_t(r,\theta,t) &= k_\tau\left(\hat{\tau}-\tau\right)-Ku\cos(\theta)-\frac{u}{r}\tau_\theta+\chi\left(\frac{\tau_{\theta\theta}}{r^2}+\frac{\tau_r}{r}+\tau_{rr}\right) \end{aligned} \tag{63}$$

with boundary conditions $u(R_1,t)=u(R_2,t)=0$, $\hat{\tau}(R_1,\theta,t)=0$ and $\hat{\tau}_r(R_2,\theta,t)=\Gamma(\theta,t)$. In (63), $u(r,t)$ and $\hat{\tau}(r,\theta,t)$ are the estimated states of $u(r,t)$ and $\tau(r,\theta,t)$, respectively. k_u and k_τ are the design parameters; and $\gamma(t),\hat{v}(t),\chi(t)$ are the estimated values of γ,v,χ, respectively. The state estimation errors in u and τ are defined as

$$e_u \triangleq u-u;\quad e_\tau \triangleq \hat{\tau}-\tau \tag{64}$$

The parameter estimation errors in γ,v,χ are defined as

$$\gamma \triangleq \gamma-\gamma;\quad \tilde{v} \triangleq \hat{v}-v;\quad \chi \triangleq \chi-\chi \tag{65}$$

By using the definitions (64), (65) and the dynamics in (31) and (63), the error dynamics are derived as

$$\begin{aligned} e_{u_t}(r,t) &= k_u e_u+\frac{\gamma}{2\pi}\int_0^{2\pi}\tau\cos(\theta)\,d\theta+\tilde{v}\left(-\frac{u}{r^2}+\frac{u_r}{r}+u_{rr}\right) \\ e_{\tau_t}(r,\theta,t) &= k_\tau e_\tau+\chi\left(\frac{\tau_{\theta\theta}}{r^2}+\frac{\tau_r}{r}+\tau_{rr}\right) \end{aligned} \tag{66}$$

By using Lyapunov stability theory, a parameter update law is obtained such that the estimator stability can be proved in a global sense. Consider a candidate Lyapunov function V as

$$V\left(e_u,e_\tau,\gamma,\tilde{v},\chi\right)=\frac{1}{2}\int_{R_1}^{R_2}e_u^2\,dr+\frac{1}{2}\int_{R_1}^{R_2}\int_0^{2\pi}e_\tau^2\,d\theta dr+\frac{1}{2f_\gamma}\gamma^2+\frac{1}{2f_v}\tilde{v}^2+\frac{1}{2f_\chi}\chi^2 \tag{67}$$

where $f_\gamma, f_\nu, f_\chi > 0$. Let $(x_1, x_2, x_3) \equiv (\gamma, \nu, \chi)$, $X_1 = -\frac{f_\gamma}{2\pi}\int_{R_1}^{R_2}\int_0^{2\pi} e_u \tau \cos(\theta)\, d\theta dr$,

$X_2 = -f_\nu \int_{R_1}^{R_2} e_u \left(-\frac{u}{r^2} + \frac{u_r}{r} + u_{rr}\right) dr$ and $X_3 = -f_\chi \int_{R_1}^{R_2}\int_0^{2\pi} e_\tau \left(\frac{\tau_{\theta\theta}}{r^2} + \frac{\tau_r}{r} + \tau_{rr}\right) d\theta dr$, the following update law is then given for each parameter $(i = 1,2,3)$:

$$x_{i_t} = \begin{cases} 0, & if \quad x_i = \bar{x}_i \quad and \quad X_i \geq 0 \\ X_i, & if \quad x_i = \bar{x}_i \quad and \quad X_i < 0 \\ X_i, & if \quad \underline{x}_i < x_i < \bar{x}_i \\ X_i, & if \quad x_i = \underline{x}_i \quad and \quad X_i > 0 \\ 0, & if \quad x_i = \underline{x}_i \quad and \quad X_i \leq 0 \end{cases} \tag{68}$$

For the given update law (68) of each parameter, the following inequality is satisfied for the time derivative of Lyapunov function

$$V_t \leq k_u \int_{R_1}^{R_2} e_u^2 dr + k_\tau \int_{R_1}^{R_2}\int_0^{2\pi} e_\tau^2 d\theta dr \tag{69}$$

If $k_u < 0$ and $k_\tau < 0$, V_t is negative semi-definite, i.e., $V_t \leq 0$. This shows that estimation errors in both the states and the parameters are bounded. Next, by applying Barbalat's Lemma [87], it can be shown that $e_u \to 0$ and $e_\tau \to 0$ as $t \to \infty$. Next, an output function $\hat{z}(t)$ is defined as

$$\hat{z}(t) = \frac{p_1}{2}\int_{R_1}^{R_2} u^2(r,t) dr + \frac{p_2}{2}\int_{R_1}^{R_2}\int_0^{2\pi} \hat{\tau}^2(r,\theta,t)\, d\theta dr \tag{70}$$

where $p_1, p_2 > 0$ are real numbers and act as weighing factors. The control is formulated to satisfy the following stable dynamics: $\hat{z}_t + k_2 \hat{z} = 0$ and to minimize the following cost function: $J(t) = \frac{1}{2}\int_0^{2\pi} \Gamma^2(\theta,t)\, d\theta$. By following the principles of variational calculus, control expression is derived and given as

$$\Gamma(\theta) = -\frac{\Upsilon}{p_2 \chi \int_0^{2\pi} \hat{\tau}^2 (R_2, \theta) d\theta} \hat{\tau}(R_2, \theta) \tag{71}$$

where

$$\begin{aligned}
\Upsilon = {} & k_u p_1 \int_{R_1}^{R_2} u e_u dr + p_1 \frac{\gamma}{2\pi} \int_{R_1}^{R_2} \int_0^{2\pi} u\tau \cos\theta d\theta dr - \\
& - p_1 \hat{\nu} \int_{R_1}^{R_2} \left(\frac{uu}{r^2} - \frac{u}{r} + u_r \right) dr + k_\tau p_2 \int_{R_1}^{R_2} \int_0^{2\pi} \hat{\tau} e_\tau d\theta dr - \\
& - p_2 \int_{R_1}^{R_2} \int_0^{2\pi} \left(Ku\hat{\tau} \cos\theta + \frac{u}{r} \hat{\tau}\tau_\theta + \frac{\chi}{r^2} \hat{\tau}_\theta \tau_\theta + \frac{\chi \hat{\tau} \tau_r}{r} + \chi \hat{\tau}_r \tau_r \right) d\theta dr + k_2 \hat{z}
\end{aligned} \tag{72}$$

3.3.2. Results & Discussion. The unstable loop dynamics with parameter uncertainties was stabilized by the application of adaptive control given by (71). The upper bounds of parameters were set at twice their true values and lower bounds at one-tenth of their true values. To show the effects of uncertainties on the system, the system was first simulated with the boundary control given by (38). This control action was computed by assuming the upper bound of each system parameter as its actual value. Figure 3.6 (a) and Figure 3.6 (b) show the evolution of $\tau(R_2, \theta, t)$ and $u(r,t)$, respectively. Although the control attempts to stabilize the system as shown in Figure 3.6 (c), the system does not reach equilibrium due to insufficient amount of control effort.

Next, the adaptive boundary control was applied to the same convection loop system. The estimated values of the parameters γ, $\hat{\nu}$ and χ were initialized with their respective upper bound and the estimator states were initialized with the zero profile given as $u(r,0) = 0 \quad \forall \quad r \in [R_1, R_2]$ and $\hat{\tau}(r,\theta,0) = 0 \quad \forall \quad (r,\theta) \in [R_1, R_2] \times [0, 2\pi)$. The design variables were chosen as: $k_u = -0.5$, $k_\tau = -0.1$, $f_\gamma = 5.5 \times 10^3$, $f_\nu = 15$,

$f_\chi = 10^{-3}$. Variables k_u and k_τ provide robustness to the estimator dynamics; the variables f_γ, f_v and f_χ serve as learning rates in the parameters' update law (68). Values of these variables should be tuned appropriately such that the estimation errors in both the states and the parameters approach zero about the same time for several test cases. Significance of k_u and k_τ lie in the fact that high values of these variables stabilize the state error dynamics quickly and, conversely, low values slowly.

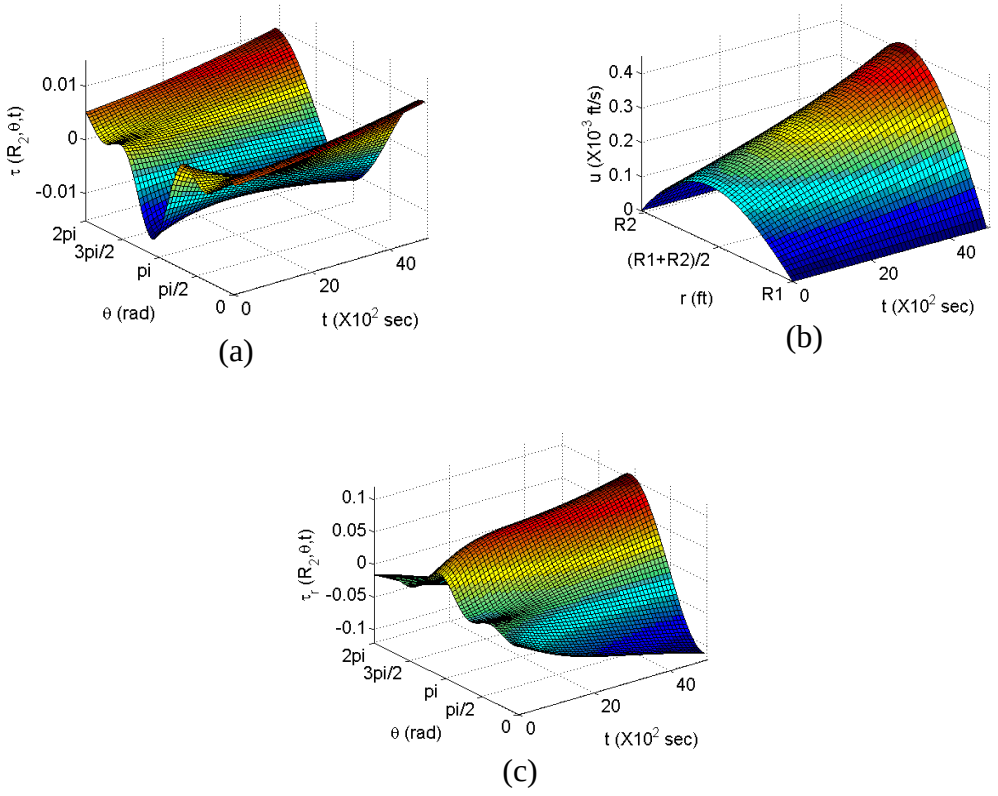

Figure 3.6. Time history of (a) $\tau(R_2,\theta,t)$, and (b) $u(r,t)$ with the application of (c) the non-adaptive control $\Gamma(\theta,t)$ the presence of parameter uncertainty

To test the effectiveness of the parameter estimation algorithm, a percentage relative error is first defined for each parameter as $e_\gamma = 100\times\frac{\gamma}{\gamma}$, $e_v = 100\times\frac{\tilde{v}}{v}$ and $e_\chi = 100\times\frac{\chi}{\chi}$. The evolution of each parameter occurs according to its update law as

given by (68). Figure 3.7 (a) shows the time history of state estimation error e_u . This error approaches zero within 1000 seconds. Figure 3.7 (b) and Figure 3.7 (c) show the parameter estimation errors e_γ and e_v, respectively, with time. A reason of achieving the accurate estimation of parameters is due to oscillations. The system is excited so that the parameters affecting the excited modes are estimated very well. To understand this mathematically, readers may refer to persistency of excitation condition described in reference [87] (chapter 6).

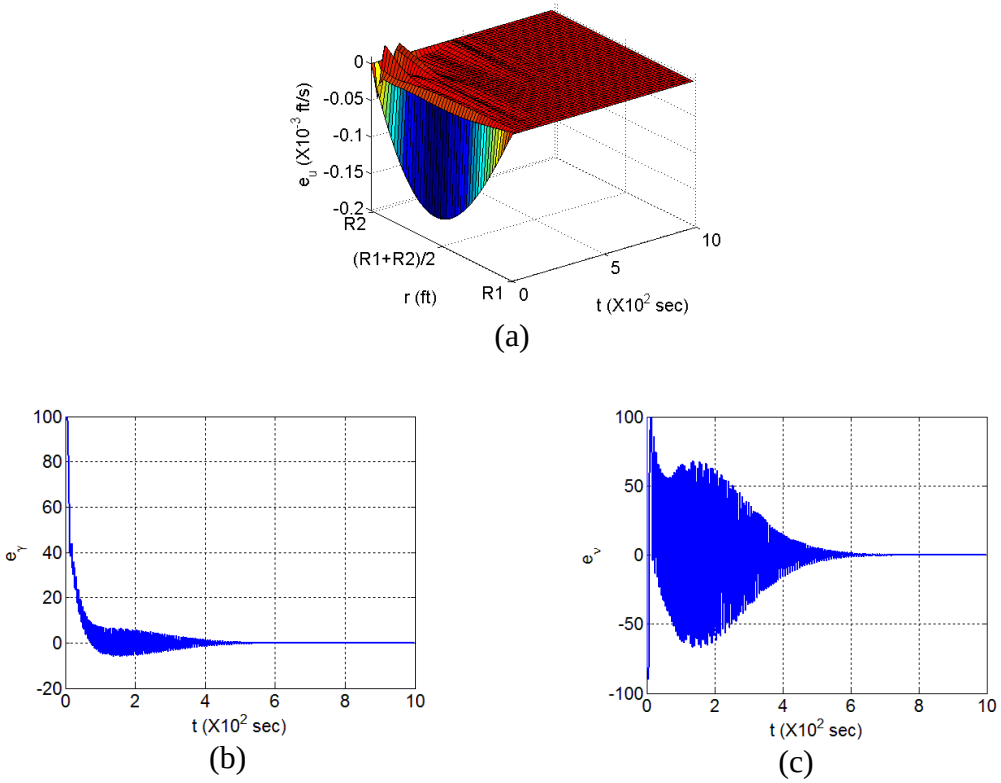

Figure 3.7. Time history of (a) the state estimation error $e_u(r,t)$, and the percentage relative errors (b) e_γ and (c) e_v

Figure 3.8 (a) shows the state estimation error e_τ history which approaches zero within 200 seconds. Figure 3.8 (b) shows the percentage relative error e_χ. It is clear that the parameter χ was estimated well within 200 seconds. It is observed from

Figure 3.8 (b) that there is no change in the estimated value $\hat{\chi}$ during the initial 60 seconds. This effect is reflected in the error e_τ dynamics as shown in Figure 3.8 (a).

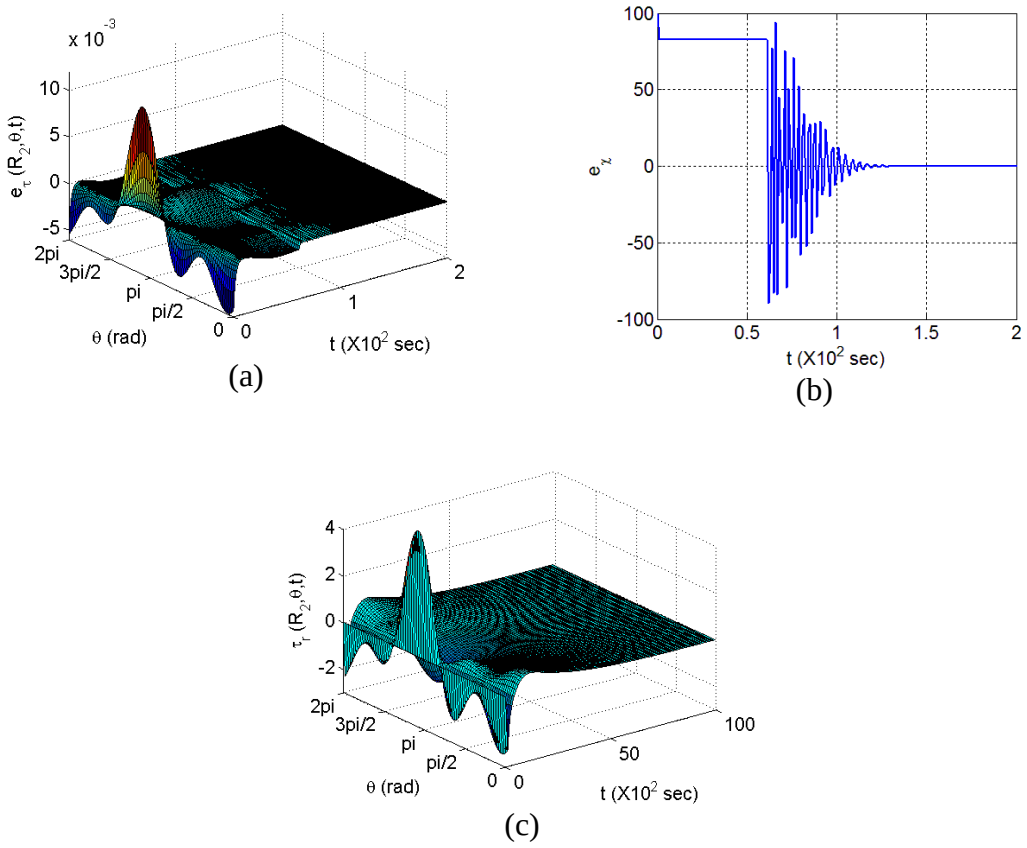

Figure 3.8. Time history of (a) the state estimation error $e_\tau(r,\theta,t)$, (b) the percentage relative error e_χ , and (c) adaptive boundary control $\Gamma(\theta,t)$

Figure 3.8 (c) shows the time history of the adaptive boundary control. At time $t=0$, the value of control is zero as the estimator dynamics is initialized with the zero profile. As the estimation errors in the states and the parameter go to zero, the adaptive control behaves same as the non-adaptive control with accurate information of parameters, as expected.

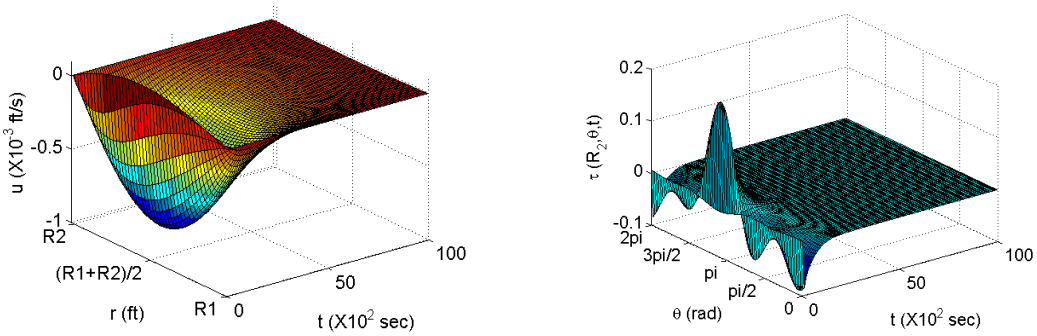

(a) (b)

Figure 3.9. Time history of (a) $u(r,t)$ and (b) $\tau(R_2,\theta,t)$

Figure 3.9 shows the evolution of the actual states $u(r,t)$ and $\tau(R_2,\theta,t)$ after the application of the adaptive control. It is clear that by the application of control, the convection loop system has been stabilized.

4. REDURED ORDER MODELING BASED OPTIMAL CONTROL DESIGN

This section describes a control design methodology based on approximate-then-design (ATD) philosophy. The original system (distributed parameter system) is first approximated to a finite-dimensional reduced order model. This model is then used to synthesize the control action. This control methodology is described for a class of second order distributed parameter systems. The technique of proper orthogonal decomposition (POD) is used here to obtain a reduced order model. This model is then used to design a sub-optimal control action by using approximate dynamic programming (ADP) formulations [89].

Dynamic programming offers the most comprehensive solution approach for nonlinear optimal control formulation. However, the associated Hamilton-Jacobi-Bellman equation demands excessive amount of computation to obtain the optimal control. ADP overcomes this computation complexity by accessing the function approximation capabilities of neural networks. Moreover, the solution can be implemented online, since the control computation requires minimal calculations. The solution to the ADP formulation is obtained through a dual neural network approach called adaptive critics (AC). Heuristic dynamic programming (HDP) and dual heuristic programming (DHP) are two classes of adaptive critics. In HDP, one of the networks, namely, action network represents the mapping between the state and control variables while the second network, called critic network, represents the mapping between state and the cost function to be minimized. In the DHP class, the action network has the same representation whereas the critic network maps the states to the co-states. A single network adaptive critic (SNAC) [90] was developed to eliminate the need for the second network in the adaptive critic architecture. This

resulted in considerable decrease in the offline training effort and simplification in the online implementation with less computation resources and storage.

In this section, the POD technique and approximate dynamic programming are combined to develop a generic control design approach for a class of nonlinear DPS. System with continuous and discrete control actuation over the domain is studied. This approach is applied to control the heave dynamics of an aircraft flexible wing model. This application comes under the field of aeroelastic studies, which deals with the interaction of structural, inertial and aerodynamic forces.

4.1. PROBLEM DESCRIPTION

The PDE describing a 2nd order system dynamics with appropriate boundary conditions is given as

$$\begin{aligned} \dot{x}_1 &= f_1\left(x, x', x'', \ldots\right) \\ \dot{x}_2 &= f_2\left(x, x', x'', \ldots\right) + g\left(x, x', x'', \ldots\right)u \end{aligned} \tag{73}$$

where the dynamics is defined in a one-dimensional spatial domain Ω. The state $x(t,y) = \left[x_1(t,y), x_2(t,y)\right]^T$ is a continuous function of time and spatial variable $y \in \Omega$. In (73), $\dot{x}_i$ represents the partial derivative with respect to time and x' represents the spatial partial derivative. The degree of spatial partial derivative is denotes by number of apostrophe $(')$. Functions $f_1(\cdot)$, $f_2(\cdot)$ and $g(\cdot)$ are real valued. It is assumed that $\left|g(\cdot)\right| > 0 \quad \forall t, y$. In the case of continuous actuation, control $u(t,y)$ is defined as

$$u(t,y) \equiv u_c(t,y) \tag{74}$$

where $u_c(t,y)$ is continuous function of time t and spatial variable y. In the case of discrete actuation, control $u(t,y)$ is defined as

$$u(t,y)=\sum_{m=1}^{M}\nu(t,y).\delta(y-y_m) \tag{75}$$

here $\nu(t,y)$ is a continuous function both in time t and space y. The function $\delta(\cdot)$ is defined such that the following is satisfied

$$\int_{y_0}^{y_f}\nu(t,y).\delta(y-y_m)\,dy=\nu(t,y_m) \tag{76}$$

The objective is to find the optimal control $u(t,y)$, that minimizes the following quadratic cost function

$$J=\frac{1}{2}\int_{t=t_o}^{t\to\infty}\int_{y=y_o}^{y=y_f}\left[x^T qx+ru^2\right]dy\,dt \tag{77}$$

where $q\in R^{2\times 2}$ is a weighting matrix on the state variables, and $r\in R$ is a weighing factor on the control variable. t_o is the initial time. y_o and y_f are the boundary points.

4.2. REDUCED ORDER APPROXIMATION

4.2.1. POD Technique. This section discusses the development of a low order finite dimensional model for the control synthesis. The very first step is to generate the snap-shot solutions [17]. In practice, system is excited using several control input and solution is captured at different time instants. Padhi [91] discusses snapshot solution generation by initializing the system with state profile with L_2 norm bound. These snapshot solutions are used to obtain a set of orthonormal basis functions. Ravindran describes the problem of obtaining these basis functions in [18].

This problem is discussed here in brief. Let, $S=\{U_i : 1 \le i \le N\}$ be a set of snap shot solutions defined in $L^2(\Omega)$. $L^2(\Omega)$ is an inner product space with the following property

$$(a,b)=\int_{\Omega} a^T b\,dy \tag{78}$$

with a and b as defined on L^2. Superscript T represents the transpose of vector and dy is the element of integration in (78). A basis function $\Phi \in L^2(\Omega)$ is defined by linear combination of snap shots as

$$\Phi=\sum_{i=1}^{N} w_i U_i \tag{79}$$

where $w_i \quad (i=1,2,...,N)$ are constants. The function Φ is desired to maximize the following energy function

$$E=\frac{1}{N}\sum_{i=1}^{N}\frac{\left|(U_i,\Phi)\right|^2}{(\Phi,\Phi)} \tag{80}$$

The problem of maximizing this function is casted into finding eigenvalue of the following eigenvalue problem:

$$CW=\lambda W \tag{81}$$

where $C_{ij}=\frac{1}{N}\int_{\Omega} U_i(y)U_j(y)\,dy$ and $W=[w_1,w_2,...,w_N]^T$ is the eigenvector corresponding to eigenvalue λ. To obtain orthonormal basis functions, each eigenvector is normalized with corresponding eigenvalue as $W^TW=\frac{1}{N\lambda}$. Generally, few eigenvalues captures the maximum amount of energy as represented by the function in (80). Eigenvalues are arranged in descending order as

$$\lambda_1 \ge \lambda_2 \ge ... \ge \lambda_N \ge 0$$

Let, $\overline{N}$ be such that $\sum_{i=1}^{\overline{N}} \lambda_i \cong \sum_{i=1}^{N} \lambda_i$. Usually, it turns out that $\overline{N} \ll N$. Let, $W_i = \left[w_{i_1}, w_{i_2}, ..., w_{i_N} \right]^T$ be the eigenvector corresponding to the eigenvalue $\lambda_i \quad \left(i = 1, 2, ..., \overline{N} \right)$. These eigenvectors are normalized such that $W_i^T W_i = \frac{1}{N\lambda_i}$. Then, basis functions are constructed as

$$\Phi_i(y) = \sum_{j=1}^{N} w_{i_j} U_j(y) \quad \left(i = 1, 2, ..., \overline{N} \right) \tag{82}$$

where w_{i_j} is the j^{th} element of i^{th} eigenvector.

4.2.2. Lumped Parameter System. The reduction of infinite-dimensional problem to a finite set of ordinary differential equations and the related cost function are explained in this section. The states of the system can be represented using the basis functions obtained from the POD technique. For the system described in (73), the states x_1 and x_2 are represented using independent basis functions as

$$\begin{aligned} x_1(t,y) &= \sum_{i=1}^{\overline{N}_1} x_{1_i}(t) \Phi_{1_i}(y) \\ x_2(t,y) &= \sum_{i=1}^{\overline{N}_2} x_{2_i}(t) \Phi_{2_i}(y) \end{aligned} \tag{83}$$

where $x_{1_i}(t)$ and $x_{2_i}(t)$ are auxiliary states, and $\Phi_{1_i}(y)$ and $\Phi_{2_i}(y)$ are basis functions for states $x_1(t,y)$ and $x_2(t,y)$. $\overline{N}_1$ and $\overline{N}_2$ are the number of eigenvalues to capture the energy corresponding to the states $x_1(t,y)$ and $x_2(t,y)$. Orthonormal property of basis functions can be utilized to obtain the auxiliary states at any time as

$$\begin{aligned} x_{1_i}(t) &= \int_{\Omega} x_1(t,y) \Phi_{1_i}(y) dy \\ x_{2_i}(t) &= \int_{\Omega} x_2(t,y) \Phi_{2_i}(y) dy \end{aligned} \tag{84}$$

It is assumed that a state feedback controller spans a subspace of the state variables. Hence, the basis functions for the states are assumed to be capable of spanning the controller as well. The continuous control profile $u_c(t,y)$ can be expressed as

$$u_c(t,y) = \sum_{i=1}^{\bar{N}_1} u_{1_i}(t)\Phi_{1_i}(y) + \sum_{i=1}^{\bar{N}_2} u_{2_i}(t)\Phi_{2_i}(y) \tag{85}$$

where $u_{1_i}(t)$ and $u_{2_i}(t)$ are auxiliary control variables. The control profile $\nu(t,y)$ in the discrete actuation case can also be represented in this manner. We keep the representation for $\nu(t,y)$ same as (85). For convenience, we define

$$\begin{aligned} X_1 &\triangleq \left[x_{1_1}, \ldots, x_{1_{\bar{N}_1}} \right]^T, \quad X_2 \triangleq \left[x_{2_1}, \ldots, x_{2_{\bar{N}_2}} \right]^T \\ U_1 &\triangleq \left[u_{1_1}, \ldots, u_{1_{\bar{N}_1}} \right]^T, \quad U_2 \triangleq \left[u_{2_1}, \ldots, u_{2_{\bar{N}_2}} \right]^T \end{aligned} \tag{86}$$

Next, Galerkin procedure [2] is applied to obtain a reduced order model of the system (73). The evolution equation of $x_1(t,y)$ is multiplied by $\Phi_{1_j}(y)$ for $j = 1,2,...,\bar{N}_1$ and integrated over the system domain Ω as

$$\int_\Omega \left(\dot{x}_1 = f_1(x, x', x'', ...) \right) \Phi_{1_j} dy \tag{87}$$

Similarly, the evolution equation of $x_2(t,y)$ is multiplied by $\Phi_{2_j}(y)$ for $j = 1,2,...,\bar{N}_2$ and integrated over the system domain Ω as

$$\int_\Omega \left(\dot{x}_2 = f_2(x, x', x'', ...) + g(x, x', x'', ...)u \right) \Phi_{2_j} dy \tag{88}$$

The partial derivatives are relaxed while integrating by parts in (87) and (88), and a weak form of these equations is obtained. Boundary conditions are satisfied in the weak form. By using the definition (83) and orthonormal property of basis functions, (87) and (88) becomes:

$$\frac{dx_{1_j}}{dt} = f_{1_j}\left(X_1, X_2\right), \quad j = 1,2,...,\overline{N}_1$$
$$\frac{dx_{2_j}}{dt} = f_{2_j}\left(X_1, X_2\right) + g_j\left(X_1, X_2\right)\left[U_1, U_2\right], \quad j = 1,2,...,\overline{N}_2 \tag{89}$$

where

$$f_{1_j}\left(X_1, X_2\right) = \int_{\Omega} f_1\left(x, x', x'', \ldots\right)\Phi_{1_j}\, dy$$
$$f_{2_j}\left(X_1, X_2\right) = \int_{\Omega} f_2\left(x, x', x'', \ldots\right)\Phi_{2_j}\, dy \tag{90}$$
$$g_j\left(X_1, X_2\right)\left[U_1, U_2\right] = \int_{\Omega} g\left(x, x', x'', \ldots\right) u\, \Phi_{2_j}\, dy$$

The spatial dependence is cancelled and the approximate system is represented in the form of auxiliary state and auxiliary control variables. It is important to notice that the difference in the approximate systems of continuous and discrete actuation case will be reflected in $g_j\left(X_1, X_2\right)$.

The cost function in (77) can be represented in terms of auxiliary state and auxiliary control variables. By using the definition (83), the term $\int_{y_o}^{y_f}\left(x^T q x\right) dy$ can be written as

$$\int_{y_o}^{y_f}\left(x^T q x\right) dy = \left[X_1^{\,T}, X_2^{\,T}\right] Q \left[X_1^{\,T}, X_2^{\,T}\right]^T \tag{91}$$

and the term $\int_{y_o}^{y_f}\left(ru^2\right) dy$ can be written as

$$\int_{y_o}^{y_f}\left(ru^2\right) dy = \left[U_1^{\,T}, U_2^{\,T}\right] R \left[U_1^{\,T}, U_2^{\,T}\right]^T \tag{92}$$

where

$$q = \begin{bmatrix} q_{11} & q_{12} \\ q_{21} & q_{22} \end{bmatrix}_{2\times 2}, Q = \left[Q_{ab}\right]_{\overline{N}\times\overline{N}}, \; R = r\left[R_{ab}\right]_{\overline{N}\times\overline{N}}, \overline{N} = \overline{N}_1 + \overline{N}_2, \quad a, b = 1,2 \tag{93}$$

and

$$Q_{ab_{ij}} = q_{ab}\int_{\Omega}\Phi_{a_i}(y)\Phi_{b_j}(y)dy \tag{94}$$

For continuous actuation case,

$$R_{ab_{ij}} = \int_{\Omega}\Phi_{a_i}(y)\Phi_{b_j}(y)dy \tag{95}$$

and for discrete actuation case,

$$R_{ab_{ij}} = \sum_{m=1}^{M}\Phi_{a_i}(y_m)\Phi_{b_j}(y_m) \tag{96}$$

Thus the cost function in (77) can be written as

$$J = \frac{1}{2}\int_{t=t_o}^{t\to\infty}\left(\left[X_1^T, X_2^T\right]Q\left[X_1^T, X_2^T\right]^T + \left[U_1^T, U_2^T\right]R\left[U_1^T, U_2^T\right]^T\right)dt \tag{97}$$

4.3. OPTIMAL CONTROL FORMULATION

This section briefly discusses the optimal control synthesis for lumped parameter model in the framework of approximate dynamic programming. This study uses the single network adaptive critic architecture to design the optimal control. The problem is formulated in discrete domain to derive the optimality condition. Readers can refer to [90] for a detailed discussion. Consider a system given by

$$X_{k+1} = F_k\left(X_k, U_k\right) \tag{98}$$

where $X_k \in R^{n\times 1}$ and $U_k \in R^{m\times 1}$ represents the state and the control, respectively, at time step k. The objective is to obtain a control U_k that minimizes the following cost function

$$J = \sum_{k=1}^{N-1}\Psi_k\left(X_k, U_k\right) \tag{99}$$

where Ψ_k represents a nonlinear utility function from the time step k to $k+1$. Note that N represents the number of discrete time steps here. The expression (99) represents the cost function for an infinite horizon problem as $N \to \infty$. The cost-to-go at the time step k can be written as

$$J_k = \sum_{i=k}^{N-1} \Psi_i \left(X_i, U_i \right) \tag{100}$$

such that J_k and J_{k+1} can be expressed in a single expression

$$J_k = \Psi_k + J_{k+1} \tag{101}$$

The costate vector λ_k at the time step k is defined by

$$\lambda_k \triangleq \frac{\partial J_k}{\partial X_k} \tag{102}$$

The relation between λ_k and λ_{k+1}, also called as costate propagation equation, can be derived by incorporating the definition (102) in the expression (101) as

$$\lambda_k = \left(\frac{\partial \Psi_k}{\partial X_k} \right) + \left(\frac{\partial X_{k+1}}{\partial X_k} \right)^T \lambda_{k+1} \tag{103}$$

Necessary condition for optimality is given as

$$\frac{\partial J_k}{\partial U_k} = 0 \tag{104}$$

The optimal control equation is obtained by using (102) and (104) in (101) as

$$\left(\frac{\partial \Psi_k}{\partial U_k} \right) + \left(\frac{\partial X_{k+1}}{\partial U_k} \right)^T \lambda_{k+1} = 0 \tag{105}$$

The core of the SNAC controller synthesis lies in the offline iterative training of the critic network. The schematic of neural network training is shown in Figure 4.1. At any iteration i, the critic neural network NN_i is a mapping of state X_k (at time step k) as an input and costate λ_{k+1}^a (at time step $k+1$) as an output. The control U_k,

at any iteration, is obtained using X_k and λ_{k+1}^a from the equation (105) This control is required to obtain the state at the next time step, i.e., X_{k+1}. The costate λ_{k+2}^a is then computed from the critic network NN_i. This costate provides the target costate λ_{k+1}^t by using the costate equation (103). This target value is used to update the critic network. A tolerance value ε is set to check the convergence of the network at any iteration, i.e., if $\frac{\lambda_{k+1}^t - \lambda_{k+1}^a}{\lambda_{k+1}^t} < \epsilon$, then the network is said to be converged.

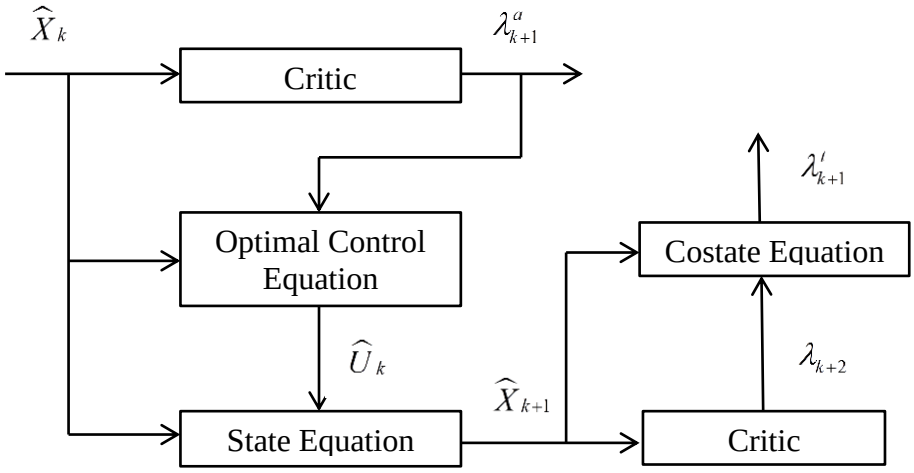

Figure 4.1. Schematic of neural network training

After the offline training of critic network, controller can be implemented online with few computations. Figure 4.2 shows the block diagram of control solution implementation. A feedback $x(t, y)$ is taken at any time t and corresponding auxiliary state $X(t)$ is obtained using the expression (84). The auxiliary control $U(t)$, as obtained from trained SNAC network, is used to compute the distributed control profile $u(t, y)$ from (85). This control is then applied to the actual system.

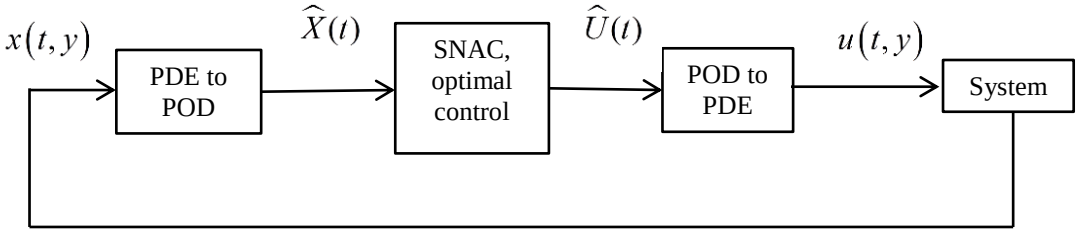

Figure 4.2. Implementation of control solution

4.4. AIRCRAFT FLEXIBLE WING PROBLEM

In this study, a flexible wing aircraft model is represented by using two Euler-Bernoulli beams connected to a rigid mass, namely, beam-mass-beam (BMB) system. A schematic of the BMB system is shown in Figure 4.3. The BMB system primarily represents the heave dynamics of an aircraft model, which is initially assumed to be in a level flight with its wings straight and the lift force balancing the weight. Any perturbation in the wing's shape causes a change in the local angle-of-attack distribution over the wing and this in turn leads to perturbation in lift distribution. The objective is to achieve a level flight condition using the control action.

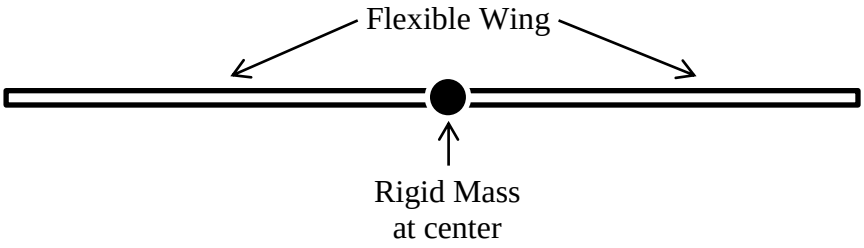

Figure 4.3. Aircraft flexible wing model (BMB system)

4.4.1. Problem Description. The dynamics of the left beam $\left(0 \le y \le \frac{l}{2}\right)$ and the right beam $\left(\frac{l}{2} < y \le l\right)$ of the BMB system is given by the following equations

$$\rho a \frac{\partial^2 w_L(t,y)}{\partial t^2} + EI \frac{\partial^4 w_L(t,y)}{\partial y^4} + \gamma_1 \frac{\partial w_L(t,y)}{\partial t} + \\ + \gamma_2 I \frac{\partial^5 w_L(t,y)}{\partial t \partial y^4} = -\frac{\Delta L(t,y)}{\frac{l}{2}} + b_L(y) u_L(t,y) \tag{106}$$

and

$$\rho a \frac{\partial^2 w_R(t,y)}{\partial t^2} + EI \frac{\partial^4 w_R(t,y)}{\partial y^4} + \gamma_1 \frac{\partial w_R(t,y)}{\partial t} + \\ + \gamma_2 I \frac{\partial^5 w_R(t,y)}{\partial t \partial y^4} = -\frac{\Delta L(t,y)}{\frac{l}{2}} + b_R(y) u_R(t,y) \tag{107}$$

for time $t > 0$. Here, l is the total length of the beam system (assuming the beams are symmetrical). $u_L(u_R)$ and $w_L(w_R)$ are the control function and displacement of the left (right) beam from their level condition, respectively. Level condition is defined by the displacement and the rate of displacement being zero for all $y \in l$. b_L and b_R are the control input function for the left and the right beam, respectively. The system is subjected to a set of boundary conditions

$$EI \frac{\partial^2 w_L(t,0)}{\partial y^2} + \gamma_2 I \frac{\partial^3 w_L(t,0)}{\partial t \partial y^2} = 0 \tag{108}$$

$$EI \frac{\partial^3 w_L(t,0)}{\partial y^3} + \gamma_2 I \frac{\partial^4 w_L(t,0)}{\partial t \partial y^3} = 0 \tag{109}$$

$$EI \frac{\partial^2 w_R(t,l)}{\partial y^2} + \gamma_2 I \frac{\partial^3 w_R(t,l)}{\partial t \partial y^2} = 0 \tag{110}$$

$$EI \frac{\partial^3 w_R(t,l)}{\partial y^3} + \gamma_2 I \frac{\partial^4 w_R(t,l)}{\partial t \partial y^3} = 0 \tag{111}$$

$$w_L\left(t, \frac{l}{2}\right) = w_R\left(t, \frac{l}{2}\right) \tag{112}$$

$$\frac{\partial w_L\left(t,\frac{l}{2}\right)}{\partial y}=\frac{\partial w_R\left(t,\frac{l}{2}\right)}{\partial y} \tag{113}$$

$$EI\frac{\partial^3 w_L\left(t,\frac{l}{2}\right)}{\partial y^3}+\gamma_2 I\frac{\partial^4 w_L\left(t,\frac{l}{2}\right)}{\partial t\partial y^3}-EI\frac{\partial^3 w_R\left(t,\frac{l}{2}\right)}{\partial y^3}- -\gamma_2 I\frac{\partial^4 w_R\left(t,\frac{l}{2}\right)}{\partial t\partial y^3}=m\frac{\partial^2 w_L\left(t,\frac{l}{2}\right)}{\partial t^2} \tag{114}$$

$$EI\frac{\partial^2 w_L\left(t,\frac{l}{2}\right)}{\partial y^2}+\gamma_2 I\frac{\partial^3 w_L\left(t,\frac{l}{2}\right)}{\partial t\partial y^2}-EI\frac{\partial^2 w_R\left(t,\frac{l}{2}\right)}{\partial y^2}- -\gamma_2 I\frac{\partial^3 w_R\left(t,\frac{l}{2}\right)}{\partial t\partial y^2}=I_Z\frac{\partial^3 w_R\left(t,\frac{l}{2}\right)}{\partial t^2\partial y} \tag{115}$$

and the initial condition

$$\begin{aligned} w_L(0,y)&=f_L(y), \qquad \frac{\partial w_L}{\partial t}(0,y)=g_L(y)\\ w_R(0,y)&=f_R(y) \qquad \frac{\partial w_R}{\partial t}(0,y)=g_R(y)\end{aligned} \tag{116}$$

Here, f_L, f_R, g_L, g_R are continuous bounded functions. E is the Young's modulus, I is the area moment of inertia of the beam, ρ is the density of the beam material, a is the cross-sectional area of the beam, I_Z is the mass moment of inertial of the rigid mass, γ_1 is the coefficient of viscous damping, γ_2 is the coefficient of Kelvin-Voigt damping, m is the mass of rigid connection between the beams.

A physical interpretation of the boundary conditions is given as follow. Constraints (108) and (109) specifies that the left end of the BMB system is free from any external moment and force, respectively. Similar interpretation can be made for the right end from (110) and (111). Constraints (112) and (113) specify the continuity in the beam displacement and its partial derivative, respectively at the center of the

BMB system. Constraints (114) and (115) represents the translational and rotational motion of the mass at the center.

The objective is to obtain control to minimize a quadratic cost function given as

$$J = \frac{1}{2}\int_{t=0}^{t\to\infty}\int_{y=0}^{y=l}\left[x^T q x + r u^2\right] dy\, dt \tag{117}$$

4.4.2. Lumped Parameter Model. A lumped parameter model is first obtained by projecting a set of POD basis functions over the system equations (106) and (107) while satisfying the boundary conditions (108) - (115). A SNAC based controller is then developed by using the lumped parameter model. In this study, symmetric solutions are simulated for simplicity by assuming $b_L(y) = b_R(y) = b$. Let,

$$\begin{aligned} x_1(t,y) &\triangleq w_L(t,y) \\ x_2(t,y) &\triangleq \frac{\partial w_L(t,y)}{\partial t} \end{aligned} \tag{118}$$

where x_1 represents the beam displacement and x_2 represents the rate of the beam displacement. By using the definition (118), the BMB system (106) can be expressed in the form of (73) as

$$f_1 \equiv x_2(t,y) \tag{119}$$

$$f_2 \equiv -\frac{EI}{\rho a}\frac{\partial^4 x_1(t,y)}{\partial y^4} - \frac{\gamma_1}{\rho a}x_2(t,y) - \frac{\gamma_2 I}{\rho a}\frac{\partial^4 x_2(t,y)}{\partial y^4} - \frac{\Delta L(t,y)}{\frac{l\rho a}{2}} \tag{120}$$

and $g = \frac{b(y)}{\rho a}$. $\Delta L(t,y)$ is the change in lift distribution from the level position and written as

$$\Delta L(t,y) = \frac{1}{2}\rho_a V_o^2 c C_{l_\alpha}\Delta\alpha \tag{121}$$

where ρ_a is density of air at sea level, V_o is the airspeed, c is the chord length, C_{l_α} is the lift-curve slope, and the change in the angle-of-attack $\Delta\alpha$ is defined as $\Delta\alpha = \sin^{-1}\left(\frac{x_2}{V_0}\right)$. A third-order approximation of the sine inverse function is considered in this study and written as $\Delta\alpha \approx \frac{x_2}{V} + \frac{1}{6}\left(\frac{x_2}{V_0}\right)^3$.

Let, $\Phi_{1_j}(y)$ for $j = 1, 2, ..., \overline{N}_1$ and $\Phi_{2_j}(y)$ for $j = 1, 2, ..., \overline{N}_2$ be the POD basis functions for the wing displacement and the rate of wing displacement, respectively. The auxiliary states and the control vectors in the lumped parameter model are defined by the expression (86). The functions as shown in (90) for lumped parameter model of this problem are written as

$$f_{1_j}\left(X_1, X_2\right) = \sum_{i=1}^{\overline{N}_2}\left(\int_0^{l/2}\Phi_{2_i}\Phi_{1_j}\,dy\right)x_i, \quad j = 1, 2, ..., \overline{N}_1 \tag{122}$$

$$\begin{aligned} f_{2_j}\left(X_1, X_2\right) = &-\frac{EI}{\rho a}\sum_{i=1}^{\overline{N}_1}\left(\int_0^{\frac{l}{2}}\Phi_{1_i}^2\Phi_{2_j}^2\,dy\right)x_{1_i} - \frac{\gamma_2 I}{\rho a}\sum_{i=1}^{\overline{N}_2}\left(\int_0^{\frac{l}{2}}\Phi_{2_i}^2\Phi_{2_j}^2\,dy\right)x_{2_i} - \\ &-\int_0^{\frac{l}{2}}\frac{\Delta L(t,y)}{\frac{l\rho a}{2}}\Phi_{2_j}\,dy - \frac{\gamma_1}{\rho a}x_{2_j} + \frac{1}{\rho a}\left[\left(EI\frac{\partial^2 x_1}{\partial y^2} + \gamma_2 I\frac{\partial^2 x_2}{\partial y^2}\right)\Phi_{2_j}^2\right]\Bigg|_{y=\frac{l}{2}} - \\ &-\frac{1}{\rho a}\left[\left(EI\frac{\partial^3 x_1}{\partial y^3} + \gamma_2 I\frac{\partial^3 x_2}{\partial y^3}\right)\Phi_{2_j}\right]\Bigg|_{y=\frac{l}{2}} \end{aligned} \tag{123}$$

While these functions remain same for the continuous as well as the discrete actuation case. The expression for $g_j\left(X_1, X_2\right)\left[U_1, U_2\right]$ is different where

$$g_j\left(X_1, X_2\right)\left[U_1, U_2\right] = \frac{1}{\rho a}\sum_{i=1}^{\overline{N}_1}\left(\int_0^{\frac{l}{2}} b(y)\Phi_{1_i}\Phi_{2_j}dy\right)u_{1_i} + \\ + \frac{1}{\rho a}\sum_{i=1}^{\overline{N}_2}\left(\int_0^{\frac{l}{2}} b(y)\Phi_{2_i}\Phi_{2_j}dy\right)u_{2_i} \tag{124}$$

is the expression for continuous case and for discrete case, this expression is given as

$$g_j\left(X_1, X_2\right)\left[U_1, U_2\right] = \frac{1}{\rho a}\sum_{i=1}^{\overline{N}_1}\left(\sum_{m=1}^{M} b(y_m)\Phi_{1_i}(y_m)\Phi_{2_j}(y_m)\right)u_{1_i} + \\ + \frac{1}{\rho a}\sum_{i=1}^{\overline{N}_2}\left(\sum_{m=1}^{M} b(y_m)\Phi_{2_i}(y_m)\Phi_{2_j}(y_m)\right)u_{2_i} \tag{125}$$

4.4.3. SNAC based Controller. After obtaining the lumped parameter model in the form of (89), optimal control is synthesized using the SNAC architecture. The state vector X and the control vector U, as shown in (98), are defined as $X = \begin{bmatrix} X_1 \\ X_2 \end{bmatrix}$ and $U = \begin{bmatrix} U_1 \\ U_2 \end{bmatrix}$. The cost function is defined in the form of (97). Note that the cost function has different R matrix for the continuous and the discrete actuation cases. The expression for R matrix is given by (95) and (96) in the continuous and the discrete actuation case, respectively.

In SNAC architecture, neural network captures the relationship between the state X at time step k and the costate λ at time step $k+1$. The dimension of the costate vector is same as that of the state vector. For this problem, the neural network is split internally into $\left(\overline{N}_1 + \overline{N}_2\right)$ sub-networks, assuming one network for each channel of the costate vector. The input to each sub-network, however, is the entire state vector X. This is done to speed up the training process since cross coupling of

neural network weights for different components of the output vector are absent in such a framework.

First step of training procedure is state generation for neural network training. Note that the auxiliary states can be computed from $x(t, y)$ using the expression (84). Many state profiles $x(t, y)$, from a set of snap shot solutions, can be used to construct the lumped parameter states, which can subsequently be used for training the networks. This process, however, would slow down the training significantly due to requirement of large number of state profiles. Therefore, an alternative method is followed. All the snapshots are used to get the minimum and maximum value for the auxiliary states. Let, Let $\hat{X}_{\min}$ and $\hat{X}_{\max}$ denote the vectors of minimum and maximum of $\hat{X}$, respectively. In each iteration of SNAC networks training, a set of random states are generated within the range of $\left[\hat{X}_{\min}, \hat{X}_{\max}\right]$. Training is performed until all sub-networks converges to a given value of tolerance ε. A convex combination $\left[\beta\lambda_{k+1}^{t} + (1-\beta)\lambda_{k+1}^{a}\right]$ is taken as the target output for faster convergence of the neural networks, where $0 < \beta \leq 1$ is the learning rate for the neural networks training.

4.4.4. Simulation Study. Simulation study for the flexible wing problem was carried out with the following parameters' values: length of the BMB system $l = 10\,\text{m}$, $\rho = 980\,\text{kg/m}^3$, $a = 0.0735\,\text{m}^2$, $E = 2\times10^6\,\text{N/m}^2$, $I = 1.734\times10^{-7}\,\text{m}^4$, $\gamma_1 = 0.025\,\text{kg/m-sec}$, $\gamma_2 = 10^4\,\text{kg/m}^5\text{-sec}$, $m = 5\,\text{kg}$, $I_z = 10^{-3}\,\text{kg-m}^2$, $\rho_a = 1.225\,\text{kg/m}^3$, $V_0 = 50\,\text{m/sec}$, $c = 1.47\,\text{m}$, $C_{l_\alpha} = 5.73\,/\text{rad}$.

The first step was to generate POD basis functions for the BMB system. The system was simulated for just 2 seconds by initializing it with sinusoidal state profiles

and control profiles. At every one tenth of a second, a snap shot solution was captured. A snap shot contains the beam displacement and the rate of the beam displacement profile. A total of 3840 snap shot solutions were captured and stored. The POD technique is applied next and orthonormal basis functions were generated for the beam displacement and the rate of the beam displacement. Figure 4.4 illustrates the percentage of energy, as given by the expression (80), in all the beam displacement snap shot solutions as captured by the number of eigenvalues. It was observed that $\overline{N}_1 = 10$ eigenvalues are sufficient to capture 99.99% of energy. Similar observation was made for the rate of the beam displacement solutions where $\overline{N}_2 = 10$ eigenvalues were sufficient to capture 99% of energy.

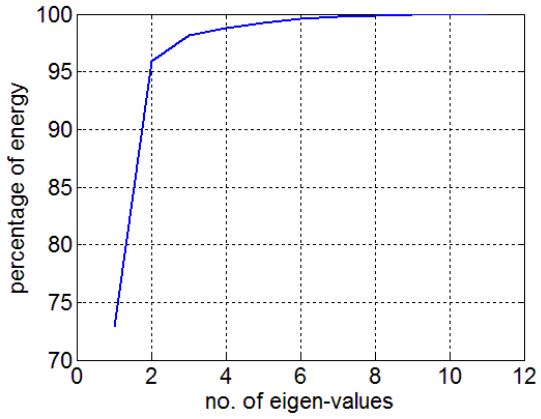

Figure 4.4. Percentage of energy I stored in all the beam displacement snap shot solutions as captured by number of eigenvalues

Figure 4.5 illustrates the ten POD basis functions for the beam displacement. First basis function $\Phi_{1_1}(y)$ captures near 73% energy of all the beam displacement snap shot solution as shown in Figure 4.4. First and second basis function together capture near 96% of energy likewise. The POD basis functions were projected over the system equation (106) and a nonlinear lumped parameter model were obtained for

both the continuous actuation and the discrete actuation case in the form of (89). In both the lumped parameter models, $X \in R^{20\times1}$ and $U \in R^{20\times1}$.

In the process of optimal control design, cost function parameters were taken different for continuous and discrete actuation case. The state penalizing matrix $q = \begin{bmatrix} 10^3 & 0 \\ 0 & 10^2 \end{bmatrix}$ was same in both the cases whereas control penalizing term $r = 1$ for continuous actuation case and $r = 0.01$ for discrete actuation case was taken. In the SNAC architecture, 20 sub-networks were trained where input to every network was state vector X and output of i^{th} network was the i^{th} element of costate vector $\lambda \in R^{20\times1}$. A linear-in-parameter neural network structure was used for every costate output. The following functions were used in the linear-in-parameter neural network: $\left[X_{1_1}, \ldots, X_{1_{10}}, X_{2_1}, \ldots, X_{2_{10}}, \left(X_{2_1}\right)^2, \left(X_{2_1}\right)^3, \left(X_{2_1}\right)^4, X_{1_1} X_{2_1} \right]^T_{24\times1}$. Initialization of neural network weights plays a crucial role in the convergence of networks, especially for a nonlinear lumped parameter model. A linear approximation of the nonlinear model was developed in the form: $\frac{dX}{dt} = AX + BU$ where $A \in R^{20\times20}$ represents the system matrix and $B \in R^{20\times20}$ represents the control matrix. In SNAC, the critic network maps the relation $\lambda_{k+1} = \left(I + PBR^{-1}B^T\right)^{-1} PAX_k$ (see ref. [75]) from state X_k at time step k to the costate λ_{k+1} at time step $k+1$. All the sub-networks in the critic network were pre-trained using this relation.

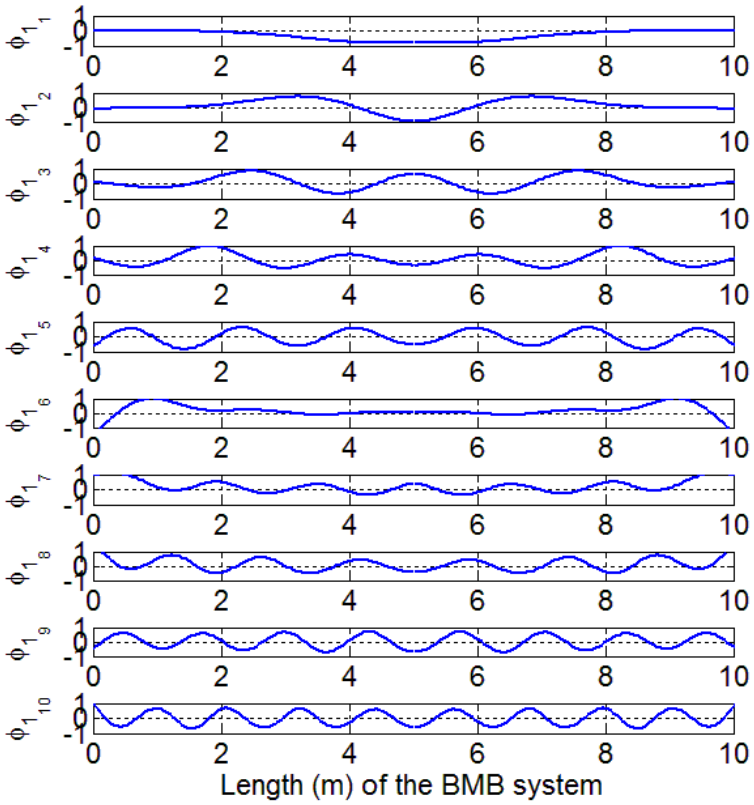

Figure 4.5. Ten POD basis functions for the beam displacement

The networks' training was carried over 500 random states, in a range of $\left[\hat{X}_{\min}, \hat{X}_{\max}\right]$, at every iteration. The learning rate of value $\beta = 0.5$ was used for smooth convergence of all the networks. The significance of learning rate is that the low value (near zero) of β makes the convergence slower and high value (near one) makes the convergence faster but may results in divergence. A tolerance value of $\varepsilon = 10^{-10}$ was set for every sub-network as a convergence criteria. The same network architecture and parameters were used in SNAC training for both the lumped parameter models of the continuous and the discrete actuation case. Figure 4.6 shows the results of SNAC training for lumped parameter model of the continuous actuation case. Figure 4.6 (a) illustrates the second norm of the relative error $\frac{\lambda_{k+1}^{t} - \lambda_{k+1}^{a}}{\lambda_{k+1}^{t}}$ of all

the sub-networks with respect to the iterations. Figure 4.6 (b) illustrates the convergence history of all the sub-networks' weights.

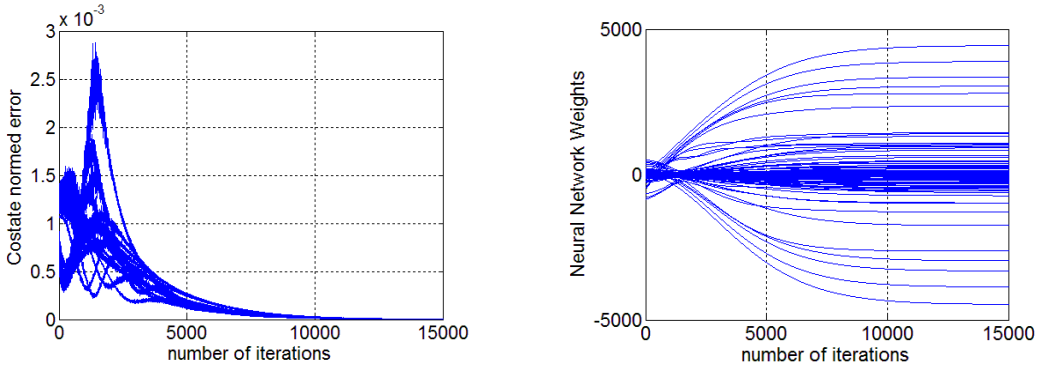

(a) (b)

Figure 4.6. SNAC training: (a) costate normed error, (b) networks' weights, with respect to iterations

4.4.4.1. Results of continuous actuation case. The BMB system was simulated by perturbing it from level flight condition. A sudden gust (for example) was assumed to cause the wing to deform from its straight position. The desired (equilibrium) states of the system were taken as zero. The initial state profile was assumed as

$$x_1(0,y) = 0.01\sin^5\left(\frac{\pi y}{l}\right)$$
$$x_2(0,y) = -0.1\sin^5\left(\frac{\pi y}{l}\right) \quad (126)$$

Figure 4.7 illustrates the results from the SNAC controller implementation. It can be observed that the control action is able to bring the beam system to the desired equilibrium state, i.e., both the beam displacement and the rate of the beam displacement profiles go to zero. Analysis of the validity of POD approximation of the underlying PDE system is carried out by comparing the actual state profiles to approximated profiles (generated by using the expression (83)).

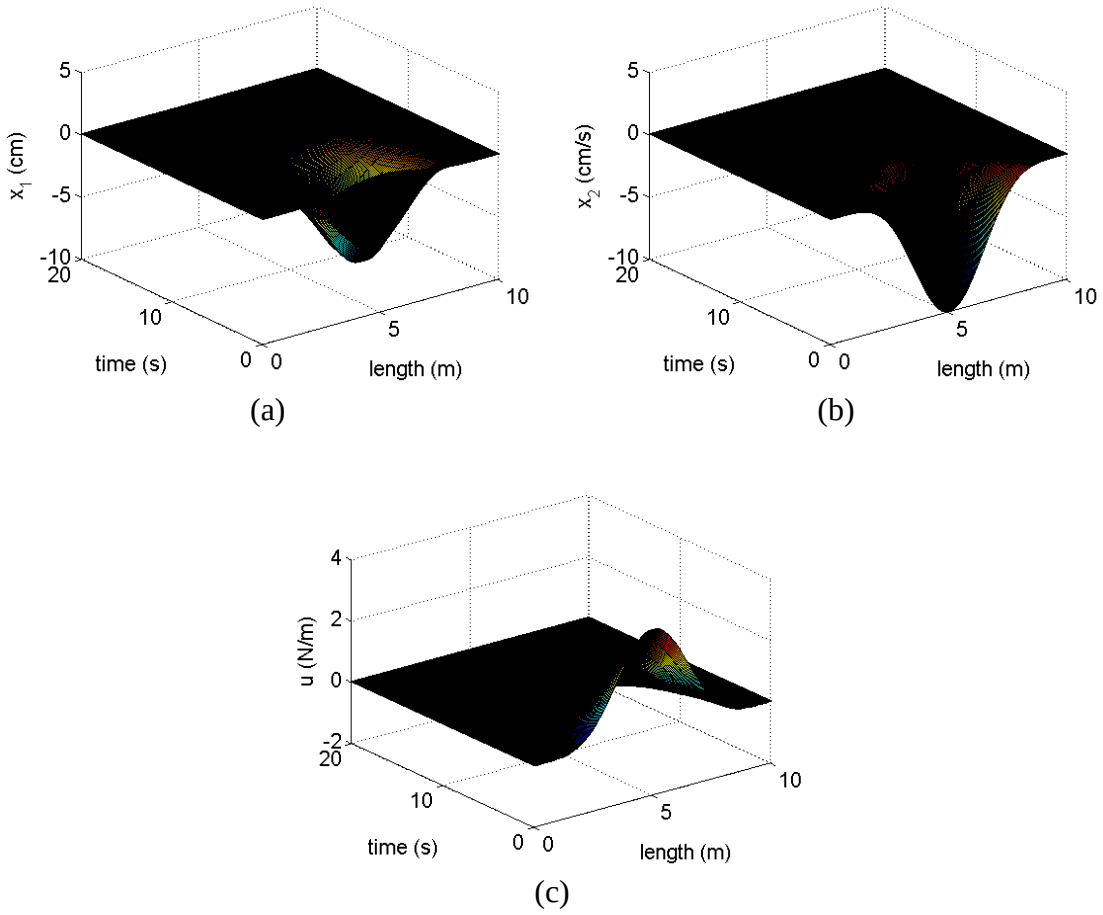

Figure 4.7. Time history of (a) the beam displacement, (b) the rate of the beam displacement, (c) continuous control action

Figure 4.8 shows that basis functions are able to capture the state profile quite well at the different time instants. Note that the SNAC controller is developed based on the approximate profile in the lumped parameter model. Due to a close approximation, as shown in Figure 4.8, control actions designed using a lumped parameter system are effective in controlling the actual BMB system.

In order to show the versatility of the control design approach, system was simulated using a different initial condition. These simulation results shown in Figure 4.9 clearly indicate that the system is stabilized. Figure 4.9 (a) and (b) show the states' trajectories with respect to time. Figure 4.9 (c) shows the stabilizing feedback control action which is able to direct the system towards desired equilibrium condition.

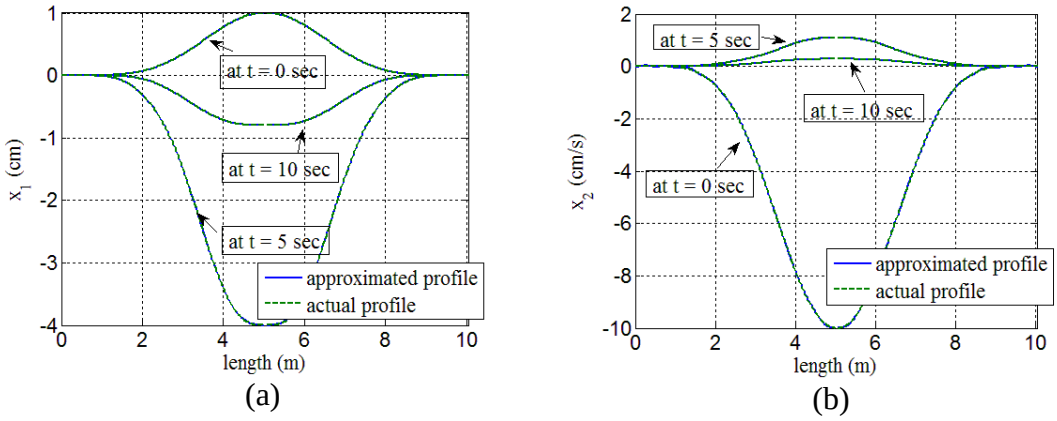

Figure 4.8. Comparison of actual profile and approximate profile for (a) the beam displacement, (b) the rate of the beam displacement at different time instants

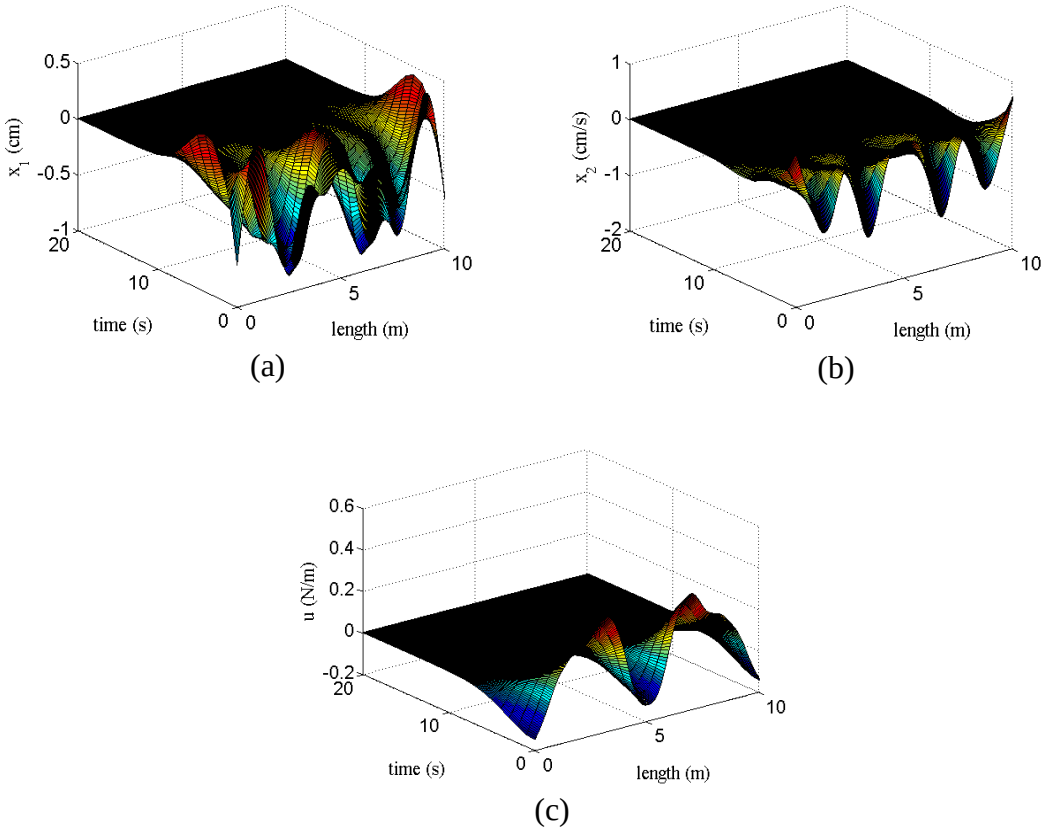

Figure 4.9. Time history of (a) the beam displacement, (b) the rate of the beam displacement, (c) control action, for different initial condition

4.4.4.2. Results of discrete actuation case. The BMB system was actuated by equally spaced 24 discrete actuators on each of the beam. The system was first

simulated with the initial states given by (126). Figure 4.10 (a) illustrates the time history of the beam displacement and Figure 4.10 (b) illustrates the time history of the rate of the beam displacement. It can be observed that the system is regulated towards the level condition by the application of discrete actuators as shown in Figure 4.10 (c). By comparing the control action as shown in Figure 4.7 (c) and Figure 4.10 (c), it was observed that discrete control effort, to drive the BMB system to the level position in nearly 20 seconds, was more as compared in the continuous actuation case. This performance the BMB system was achieved by taking the control penalty in the cost function for discrete actuation case as $r = 0.01$.

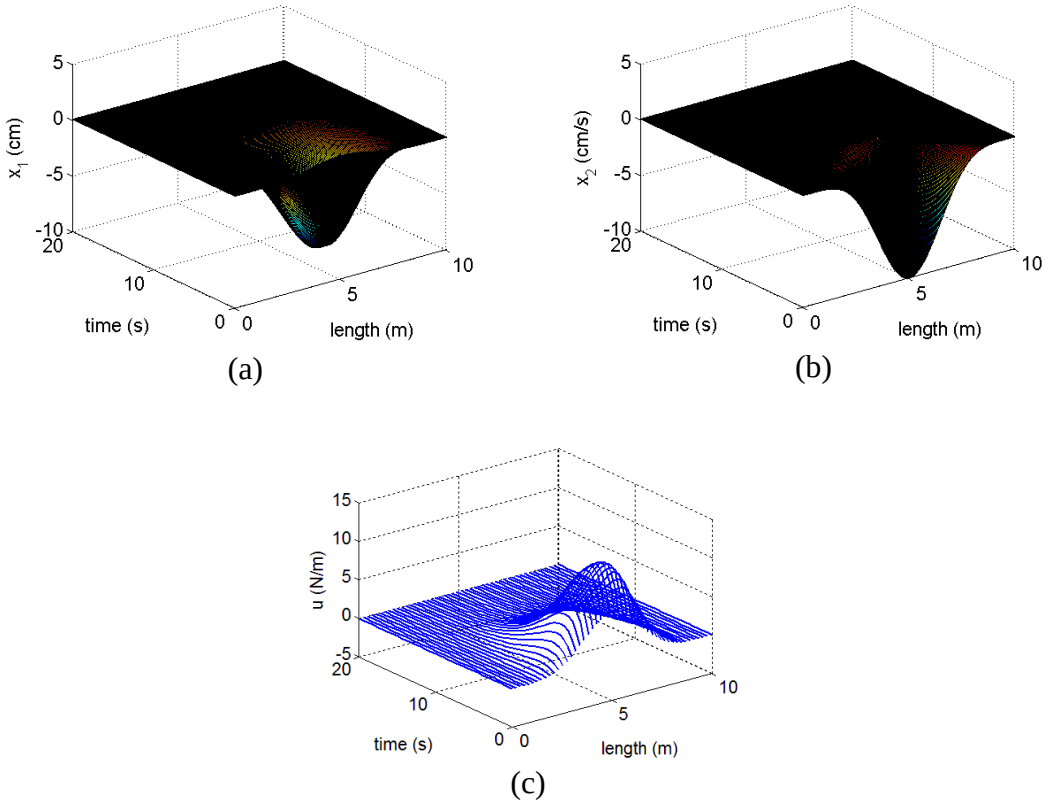

Figure 4.10. Time history of (a) the beam displacement, (b) the rate of the beam displacement, (c) discrete control action

Figure 4.11 illustrates the simulation results when the BMB system was initialized with a different initial condition. The control action is able to drive the system to its level position. The accuracy of the lumped parameter model was

validated while simulating the BMB system under this stabilizing control action. The actual state profiles were compared, at different time instants, to the approximate profile generated using the expression (83).

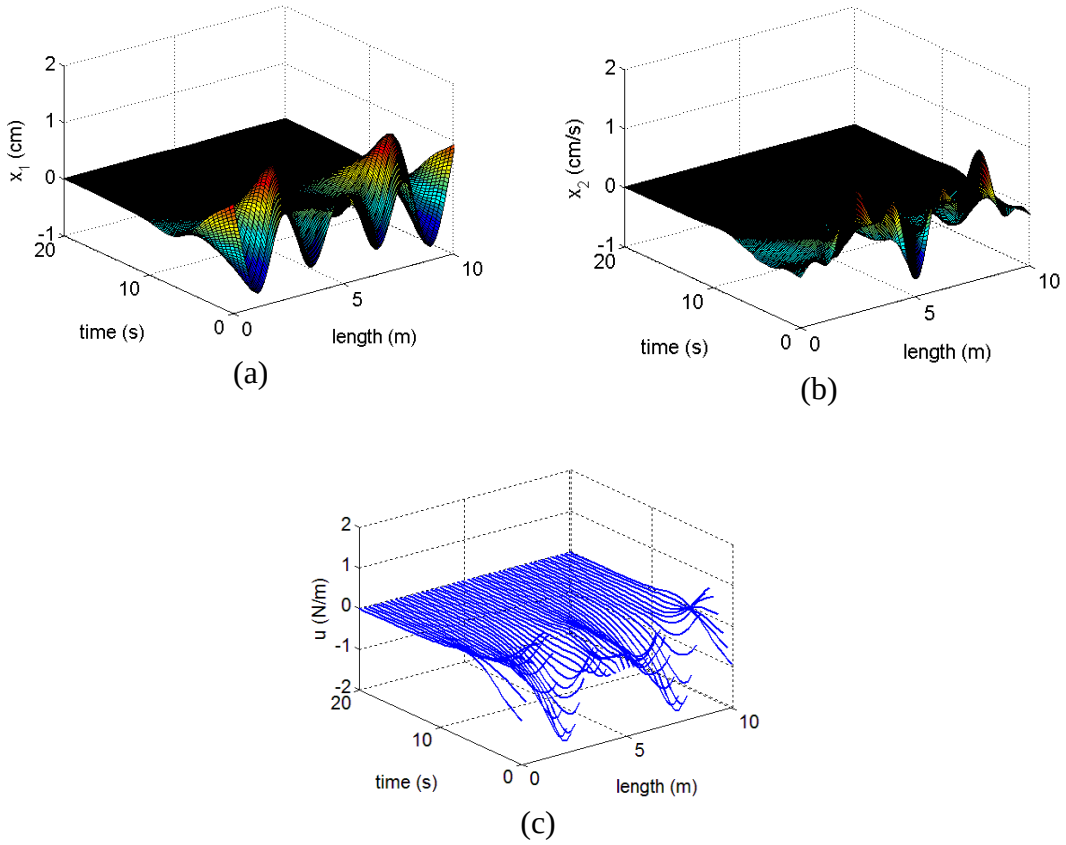

Figure 4.11. Time history of (a) the beam displacement, (b) the rate of the beam displacement, (c) discrete control action, for different initial condition

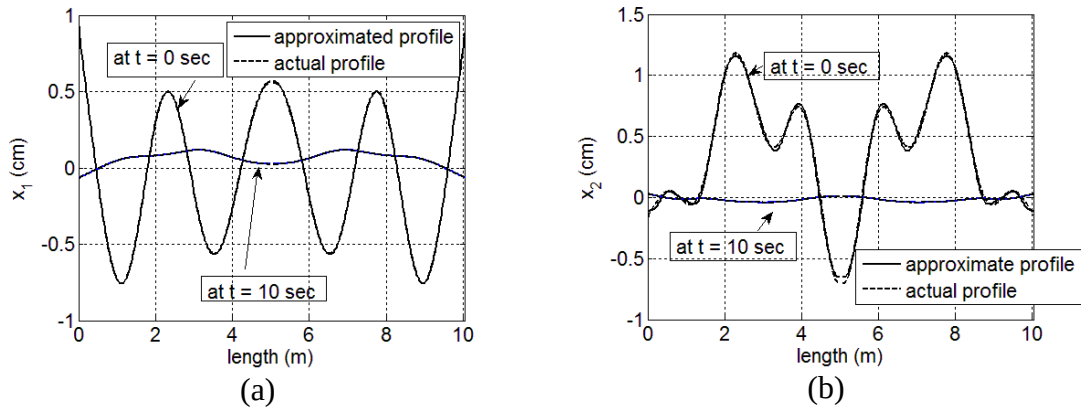

Figure 4.12. Comparison of actual profile and approximate profile for (a) the beam displacement, (b) the rate of the beam displacement at different time instants

Figure 4.12 (a) illustrates that the basis functions are able to capture the beam displacement profile at different time instants. Similar behavior can be observed in the rate of the displacement profile in Figure 4.12 (b). Due to the closeness (accuracy) of the approximations, control action was effective to the actual system and was able to regulate the system.

4.4.4.3. Comments.

1. Same POD basis functions were used to generate a lumped parameter model for the BMB system in the continuous as well as the discrete actuation case.

2. It is crucial to generate sufficient snap shot solutions that cover the domain of the solutions where optimal trajectories lie.

3. The BMB system is analyzed with the left beam equation (106) and the right beam equation (107) while satisfying constraints (112) - (115) at the middle point. The POD basis functions were generated separately for the left beam and the right beam. Due to this reason, the continuity constraints (112) and (113) are not guaranteed to satisfy. Therefore, only symmetrical solutions were simulated in this study. In order to analyze the unsymmetrical solutions, it is important to consider the BMB system as ‘one’ system instead of ‘left and right’ beam. The continuity constraints (112) and (113) will be satisfied inherently in this manner.

4. A controller, other than SNAC based, can be very well used here. Comparing to the controller based on state dependent riccati equation (SDRE) [92], feedback linearization and sliding mode [76] require online design as per the feedback whereas SNAC based controller is trained offline and can be implemented online with few computations. Further, it requires storing only the neural network weights that takes minimal memory space.

5. REDUCED ORDER MODELING BASED OPTIMIZATION

Optimization procedures in the distributed parameter systems require a huge computational memory and data storage. For underlying spatial domain, finite difference, finite element, finite volume methods are generally applied to obtain a finite dimensional model (e.g., see [93] and [101] - [104]). In order to obtain accurate model of the system, these methods lead to large number of equations. In other words, the finite dimensional model contains large number of unknown variables. These equations serve as the constraint while optimizing a defined cost function.

The study described here attempts to overcome the problem of computational requirements while achieving the accuracy of the optimal solution. A reduced order modeling procedure is described using the technique of proper orthogonal decomposition with weighted residuals. Section 4 presents the use of the POD technique for developing an approximate model of a dynamic system. Here, the POD technique is utilized to obtain an approximation of steady state partial differential equations.

The control of viscous flow is crucial for many scientific applications such as in chemical reaction, combustion, crystal growth process, etc. In this study, the optimization method is demonstrated to minimize the vorticity in viscous incompressible thermally convected flows by using boundary control in the form of heat flux. A numerical example of a high pressure chemical vapor deposition (CVD) reactor is discussed in which the objective is to minimize the recirculations in the flow.

5.1. PROBLEM DESCRIPTION

The steady state equations of a thermally convected fluid flow are given in a bounded domain Ω as [93]

$$0 = \mu\left(\frac{\partial^2 u}{\partial x^2} + \frac{\partial^2 u}{\partial y^2}\right) - \rho_0\left(u\frac{\partial u}{\partial x} + v\frac{\partial u}{\partial y}\right) - \frac{\partial p}{\partial x} \tag{127}$$

$$0 = \mu\left(\frac{\partial^2 v}{\partial x^2} + \frac{\partial^2 v}{\partial y^2}\right) - \rho_0\left(u\frac{\partial v}{\partial x} + v\frac{\partial v}{\partial y}\right) - \frac{\partial p}{\partial y} + g\rho_0\left(1 - \beta\left(T - T_0\right)\right) \tag{128}$$

$$0 = \kappa\left(\frac{\partial^2 T}{\partial x^2} + \frac{\partial^2 T}{\partial y^2}\right) - \rho_0 c_p\left(u\frac{\partial T}{\partial x} + v\frac{\partial T}{\partial y}\right) \tag{129}$$

$$\frac{\partial u}{\partial x} + \frac{\partial v}{\partial y} = 0 \tag{130}$$

where u and v represent horizontal and vertical component of the fluid velocity, respectively. T represents the temperature and p represents the pressure. g is the acceleration of gravity. x and y represent the spatial variable in horizontal and vertical direction, respectively. The viscosity μ, heat conductivity κ, thermal expansion coefficient β, and specific heat at constant pressure c_p are constant parameters. By assuming a length scale l, a velocity scale U, and a temperature scale $T_1 - T_0$ in the flow, nondimensional parameters of the flow are defined as: Reynolds number $\mathrm{Re} = \rho_0 U l / \mu$, Prandtl number $\mathrm{Pr} = \mu c_p / k$, and Grashof number $Gr = \beta l^3 \rho_0^2 g\left(T_1 - T_0\right) / \mu^2$. By taking the following transformation: $x \leftarrow x / l$, $y \leftarrow y / l$, $u \leftarrow u / U$, $v \leftarrow v / U$, $T \leftarrow \left(T - T_0\right) / \left(T_1 - T_0\right)$, $p \leftarrow \left(p + gy\right) / \rho_0 U^2$, the flow equations (127) - (130) are derived in nondimensional form and given as

$$0 = \frac{1}{R_e}\left(\frac{\partial^2 u}{\partial x^2} + \frac{\partial^2 u}{\partial y^2}\right) - u\frac{\partial u}{\partial x} - v\frac{\partial u}{\partial y} - \frac{\partial p}{\partial x} \tag{131}$$

$$0 = \frac{1}{R_e}\left(\frac{\partial^2 v}{\partial x^2} + \frac{\partial^2 v}{\partial y^2}\right) - u\frac{\partial v}{\partial x} - v\frac{\partial v}{\partial y} - \frac{\partial p}{\partial y} + \frac{G_r}{R_e^2}T \tag{132}$$

$$0 = \frac{1}{R_e P_r}\left(\frac{\partial^2 T}{\partial x^2} + \frac{\partial^2 T}{\partial y^2}\right) - u\frac{\partial T}{\partial x} - v\frac{\partial T}{\partial y} \tag{133}$$

$$\frac{\partial u}{\partial x} + \frac{\partial v}{\partial y} = 0 \tag{134}$$

A cost function is given as

$$J = \frac{1}{2}\int_{\Omega}\left(\frac{\partial v}{dx} - \frac{\partial u}{dy}\right)^2 d\Omega + \frac{\delta_h}{2}\int_{\Gamma_1} h^2 d\Gamma_1 \tag{135}$$

where $\left(\frac{\partial v}{dx} - \frac{\partial u}{dy}\right)$ is the vorticity at any point (x, y) in the domain Ω, h is the control at some boundary Γ_1 and δ_h is a control penalizing parameter. The objective is to minimize the cost function J while satisfying the constraints (131) - (134) and appropriate boundary conditions.

5.1.1. Numerical Example: CVD Reactor. This example describes the control problem of transport process in a chemical vapor deposition (CVD) reactor [93], [94]. CVD reactors are used in applications that involve the deposition of layer of material onto a surface. The geometry of a typical vertical reactor, as shown in Figure 5.1 is a classical configuration for the growth of the semiconductor compound. The formation of compound takes place by a chemical reaction between reactant gases, introduced at Inlet Γ_i, and substrate, kept at Γ_2, at very high temperature. The relatively high temperature creates density variation and the resulting flow is affected by buoyancy driven convection. In order to have uniform growth rate of the compound, it is essential to have the fluid flow without recirculation. The objective here is to minimize the vorticity by controlling the heat flux at the side walls Γ_1.

The geometry of the prototype reactor is illustrated in Figure 5.1 with an inlet Γ_i and two outlets Γ_o. The width of inlet and outlet is $1/3$. The height of the inlet port Γ_s is $1/3$.

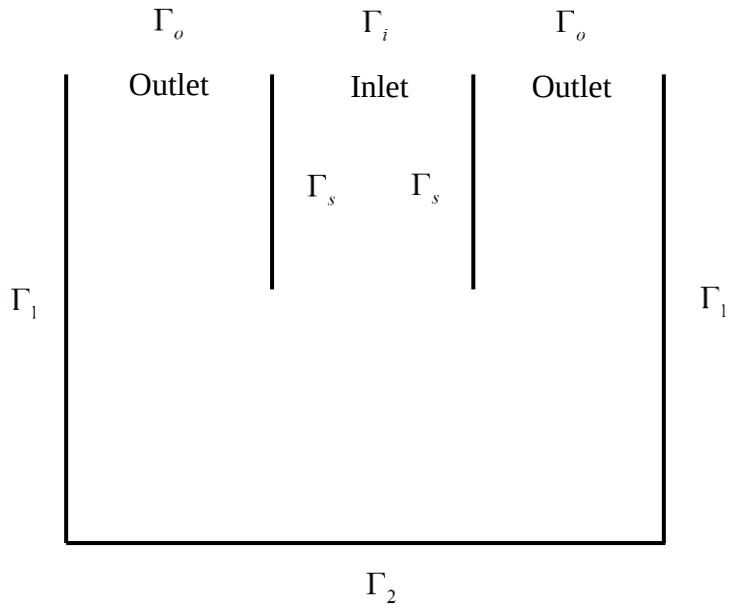

Figure 5.1. Geometry of the reactor with boundary walls

Flow variables at the boundaries are given as

$$\begin{aligned}
&\Gamma_i: \quad u=0, \quad \frac{\partial p}{\partial y}=\frac{8}{\mathrm{Re}}, \quad T=0\\
&\Gamma_o: \quad \frac{\partial u}{\partial y}=\frac{\partial v}{\partial y}=0, \quad \frac{\partial T}{\partial y}=0\\
&\Gamma_2: \quad u=0, \quad v=0, \quad T=1\\
&\Gamma_1: \quad u=0, \quad v=0, \quad \frac{\partial T}{\partial x}=(h-T)\\
&\Gamma_s: \quad u=0, \quad v=0, \quad T=0
\end{aligned} \tag{136}$$

The boundary constraints (136) need to be satisfied in order to obtain a meaningful flow inside the reactor.

5.1.2. CFD Solution. The steady state solution of the equations (131) - (134) while satisfying (136) is obtained using finite difference approach. The square geometry of CVD reactor is discretized with equal number of nodal points in

horizontal and vertical directions. The values of flow variables are computed at these nodal points. Central difference scheme [80] is used to evaluate the spatial partial derivative at any nodal point in the domain. Conservative form of the Navier-Stokes equations is used in order to avoid any numerical instability. By using the continuity equation, the equations in conservative form are derived as

$$0 = \frac{1}{R_e}\left(\frac{\partial^2 u}{\partial x^2} + \frac{\partial^2 u}{\partial y^2}\right) - \frac{\partial u^2}{\partial x} - \frac{\partial uv}{\partial y} - \frac{\partial p}{\partial x} \tag{137}$$

$$0 = \frac{1}{R_e}\left(\frac{\partial^2 v}{\partial x^2} + \frac{\partial^2 v}{\partial y^2}\right) - \frac{\partial uv}{\partial x} - \frac{\partial v^2}{\partial y} - \frac{\partial p}{\partial y} + \frac{G_r}{R_e^2}T \tag{138}$$

$$0 = \frac{1}{R_e P_r}\left(\frac{\partial^2 T}{\partial x^2} + \frac{\partial^2 T}{\partial y^2}\right) - \frac{\partial Tu}{\partial x} - \frac{\partial Tv}{\partial y} \tag{139}$$

A Poisson equation is derived for pressure using equations (134), (137) and (138) as

$$\frac{\partial^2 p}{\partial x^2} + \frac{\partial^2 p}{\partial y^2} = -\left(\frac{\partial^2 u}{\partial x^2}\right)^2 - \left(\frac{\partial^2 v}{\partial y^2}\right)^2 - 2\frac{\partial^2 (uv)}{\partial x \partial y} + \frac{G_r}{R_e^2}\frac{\partial T}{\partial y} \tag{140}$$

This equation (140) satisfies the continuity equation and it is used in computing a steady state flow. The control is parameterized using ‘sufficient’ Fourier basis functions as

$$h = \sum_{i=1}^{N_h} d_i \Phi_i^h \tag{141}$$

The parameterization is done to obtain the optimal solution with respect to small number of control variables $D = \left[d_1, d_2, ..., d_{N_h}\right]$. Otherwise, optimal value of control action need to be evaluated at each nodal point of the boundary Γ_1.

A steady state solution is desired for the equations (137) - (140) while satisfying given constraints (136) and control h at the boundary Γ_1. Finite difference iterative scheme is used for that purpose. The iterative method is initialized with no

flow in the domain. In the central finite difference discretization, the flow variable terms at every nodal point are extracted (from the second derivative) to the left hand side of the equation (137) - (139). These terms are computed as values at the next iteration. Poisson equation (140) is solved for pressure separately by the matrix method [105]. Let $R^{eq}\left(u^*, v^*, T^*, p^*\right) = 0$ represents the system of equations (137) - (140) where u^*, v^*, T^* and p^* be the steady state solution. The residual at any iteration k is defined by $R^{eq}\left(u^k, v^k, T^k, p^k\right)$. The iterative procedure is stopped when the residual satisfies the tolerance criterion: $\left|R^{eq}\left(u^k, v^k, T^k, p^k\right)\right| < \varepsilon$.

5.2. OPTIMIZATION SCHEME

The author follows the optimization scheme, adjoint method, as described by Jameson in [96]. The adjoint method is an iterative method where control solution is updated at every iteration till the solution converges to a local optimal value. The method can be initialized with several initial conditions in order to find the global optimal value.

Let, $R^{eq} = 0$ represents the set of steady state system's equations, z denotes the state vector and D denotes the control. Then, the adjoint equation is given by [96]

$$\left[\frac{\partial R^{eq}}{\partial z}\right]^T \Psi = \frac{\partial J}{\partial z} \tag{142}$$

where Ψ denotes the Lagrange multiplier. This multiplier is used to update the control with a learning rate λ as

$$\delta D = -\lambda\left(\left[\frac{\partial J}{\partial D}\right]^T - \Psi^T\left[\frac{\partial R^{eq}}{\partial D}\right]^T\right) \tag{143}$$

The advantage of using adjoint method is that it yields the gradient (change in control) with respect to arbitrary number of design variables with the cost of a single flow (steady state equations) and adoint solution (equation (142)) at every iteration. When the relative cost error at any iteration goes below a tolerance value, i.e., $\left|\frac{\delta J^k}{J^k}\right| < \varepsilon$, then iterative method is stopped. This stopping condition is taken as the convergence criteria for the adjoint method in this study.

5.3. REDUCED ORDER MODELING

The POD technique is used first to obtain a set of the 'problem oriented' basis functions. These basis functions are projected over the system equations using the Galerkin procedure [2]. As a result, a set of algebraic equations are obtained. These equations represent the reduced order model of the steady state Navier-Stokes equations.

First, a series of steady state solutions of u, v, T and p are obtained by introducing several boundary control action. Using the snapshot method [18], POD basis are computed for the state variables. The state approximations are given as

$$u \cong \sum_{i=1}^{N_{uv}} a_i \Phi_i^u, \quad v \cong \sum_{i=1}^{N_{uv}} a_i \Phi_i^v, \quad T \cong T_{av} + \sum_{i=1}^{N_T} b_i \Phi_i^T, \quad p \cong \sum_{i=1}^{N_p} c_i \Phi_i^p \tag{144}$$

where $\left(\Phi_i^u, \Phi_i^v\right)$ for $\left(i = 1, 2, ..., N_{uv}\right)$, Φ_i^T for $\left(i = 1, 2, ..., N_T\right)$ and Φ_i^p for $\left(i = 1, 2, ..., N_p\right)$ denote the basis functions to approximate the state variables (u, v), T and p, respectively. a_i, b_i and c_i act as the auxiliary state variable in the reduced order model. Note that homogeneous boundary conditions are satisfied in the generation of POD basis functions. Temperature profile has inhomogeneous boundary condition $T = 1$ at Γ_2. In order to satisfy this boundary condition, T_{av} is computed by

taking average of all the temperature snap shots and the POD technique is applied on the rest.

The basis functions are projected over the equations (137) - (140) while using the representations in (144), and a set of algebraic equations is obtained as

$$0 = F\left(A, B, C\right) \tag{145}$$

where $A = \left[a_1, a_2, ..., a_{N_{uv}}\right]^T$, $B = \left[b_1, b_2, ..., b_{N_T}\right]^T$ and $C = \left[c_1, c_2, ..., c_{N_p}\right]^T$. The function $F\left(\cdot\right) \in R^{\left(N_{uv}+N_T+N_p\right)\times 1}$ represents a set of nonlinear algebraic equations. The number of equations are equal to number of unknown state variables A, B and C. The quadratic nonlinearity in the function $F\left(\cdot\right)$ arises due to nonlinear terms in the equations (137) - (140).

The cost function (135) can be represented in terms of state and control variables as

$$J = \frac{1}{2} A^T Q A + \frac{1}{2} D^T R D \tag{146}$$

where Q and R are matrices such that $Q_{i,j} = \int_{\Omega} \left(\frac{\partial \Phi_i^v}{\partial x} - \frac{\partial \Phi_i^u}{\partial y} \right) \left(\frac{\partial \Phi_j^v}{\partial x} - \frac{\partial \Phi_j^u}{\partial y} \right) dxdy$ for $i, j = 1, 2, ..., N_{uv}$ and $R_{i,j} = \delta_h \int_{\Gamma_1} \Phi_i^h \Phi_j^h dy$ for $i, j = 1, 2, ..., N_h$.

5.3.1. Why Using a Reduced Order Model. The motivation behind this study is to overcome the computational requirements of optimization based on the actual system. The philosophy of using a surrogate model is that less number of unknown variables in the optimization problem requires less computation as compared to large number of unknown variables.

Let's consider that spatial domain is discretized into $(N_x \times N_y)$ nodal elements in horizontal and vertical directions. The unknown variables to obtain the optimal

solution in present problem becomes $(4\times N_x \times N_y)$ as flow variables u, v, T, and p are defined at each nodal point. In a reduced order model, only a few POD basis functions are sufficient to represent a set of snapshot solutions. Generally the number of POD basis function or number of unknown variables in the reduced order model are significantly less as compared to the number of nodal points in the spatial domain. This is the main advantage using a reduced order model when computing an optimal solution based on this model.

5.3.2. Result & Discussion. The spatial domain of the reactor was discretized into (28×28) nodal points. The control was parameterized with 5 Fourier basis functions: $\Phi^h = \left[1, \sqrt{2}\sin(2\pi y), \sqrt{2}\cos(2\pi y), \sqrt{2}\sin(4\pi y), \sqrt{2}\cos(4\pi y)\right]$ for $0 \le y \le 1$.

5.3.2.1. Optimization based on actual system. The adjoint method was first run using the finite difference model of the actual system. The tolerance $\varepsilon = 10^{-5}$ was selected to stop the iterations when computing the steady state solution. The tolerance value of 10^{-3} was selected as the convergence criteria in the adjoin method. The control variables were initialized with zero value, i.e., $D = [0,0,0,0,0]^T$. The learning rate λ was taken of value 0.1. The significance of learning rate is that a lower value of learning rate slows down the convergence of cost whereas higher value speeds up the convergence but it may lead to a diverging solution also.

Figure 5.2 (a) and (b) show the convergence of cost and the control variables with respect to iterations, respectively. The relative cost error at 100^{th} iteration is 3×10^{-4}. Figure 5.2 (c) illustrates the control profile at the 100^{th} iteration. This control profile is generated using the expression (141). The nature of this control profile is such that it minimizes the recirculations in the flow field.

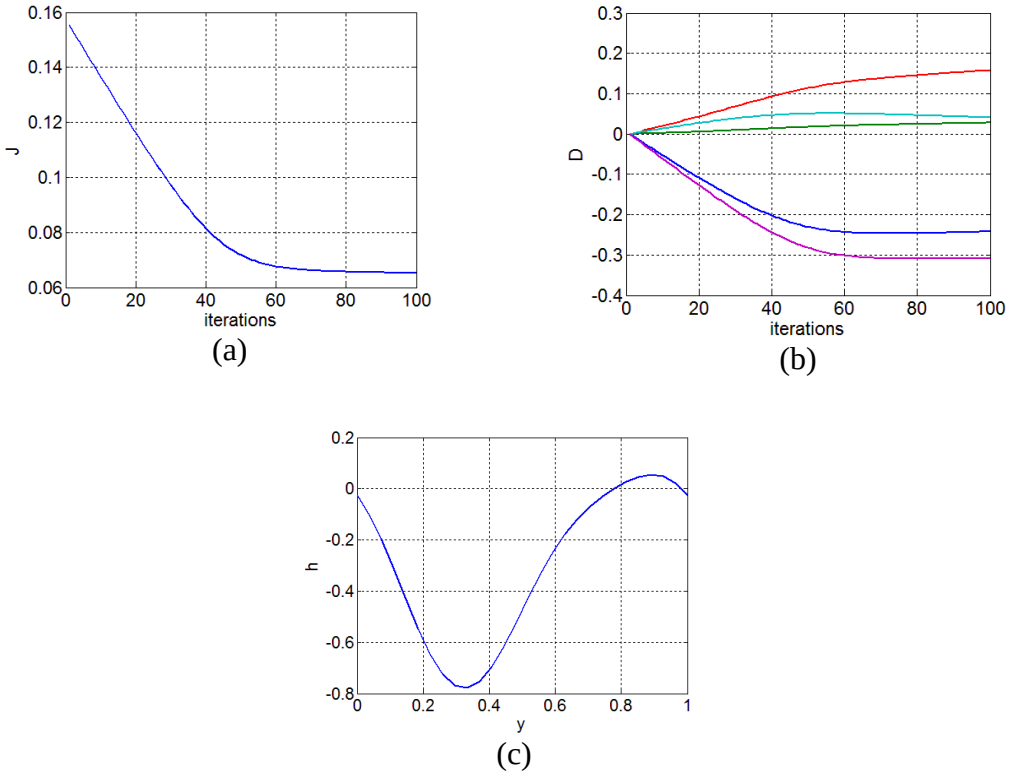

Figure 5.2. (a) Cost with respect to iterations, (b) control variables with respect to iterations, and (c) control profile at the final iteration

Figure 5.3 shows the flow variables at the final iteration. The 3-dimensional plots show the magnitude of each flow variable in the domain. Note that all the flow variables are non-dimensional. The figure illustrates a steady state flow inside the domain where residual is below tolerance limit of value 10^{-5}. The nature of the flow can be understood as follows. The reactant gases are introduced at the inlet in the negative y-direction. The inlet region is shown by negative flow speed in Figure 5.3 (b). The horizontal flow speed is zero at this region as shown in Figure 5.3 (a). Similar interpretation can be made at the outlet. Figure 5.3 (c) shows the temperature profile. The flow is driven by the pressure gradient inside the domain. Figure 5.3 (d) shows the pressure profile. The constant flow speed at the inlet region can be explained by the ramp pressure profile.

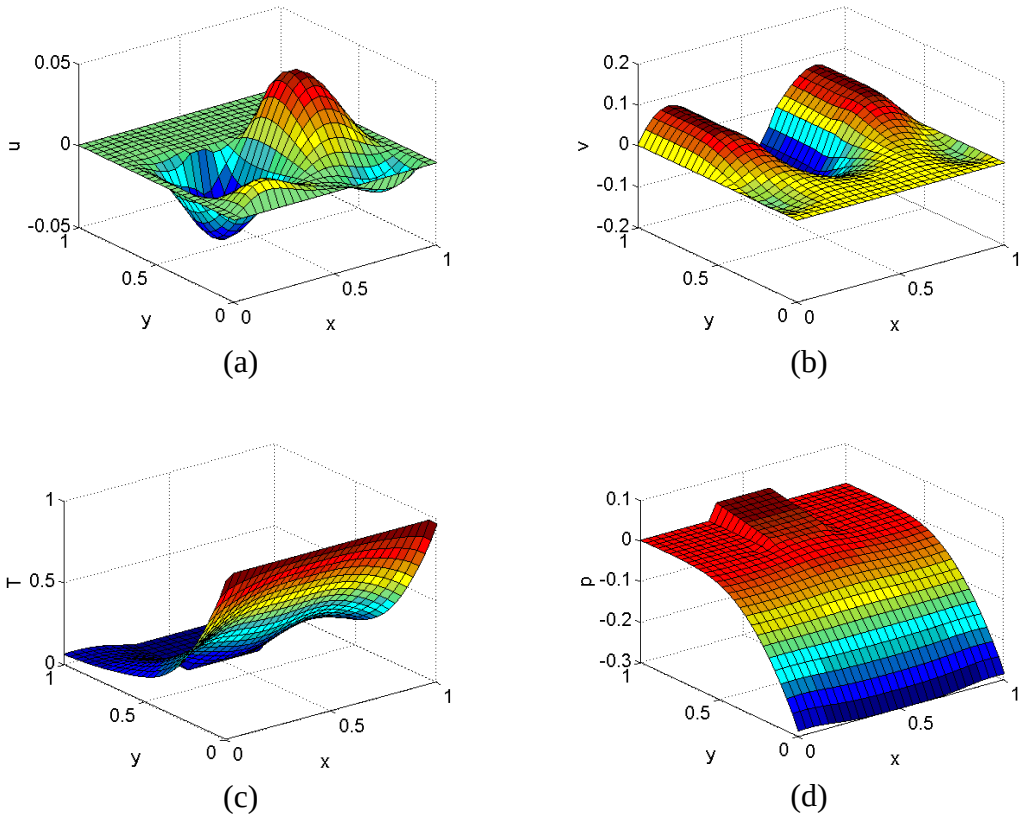

Figure 5.3. (a) Horizontal flow speed, (b) vertical flow speed, (c) temperature, and (d) pressure, at the final iteration

The optimal profile of control, as shown in Figure 5.2 (c), can be explained using the Figure 5.4 that shows the flow with zero control and with the optimal control. A high value of temperature speeds up the flow as shown in Figure 5.4 (a). This action creates the recirculation of high amplitude as shown in Figure 5.5 (a). The control is applied in the form of heat flux at the boundary. A negative value of the heat flux represents that the heat is subtracted from the flow. The subtraction of heat lowers the near temperature and that results into slow fluid flow as shown in Figure 5.4 (b). The resulting vorticity is shown in Figure 5.5 (b).

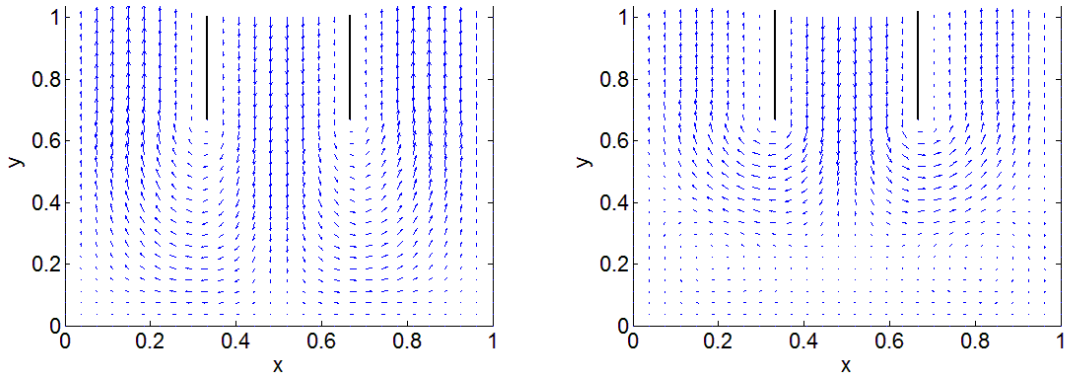

(a) (b)

Figure 5.4. (a) Uncontrolled flow, (b) optimal controlled flow

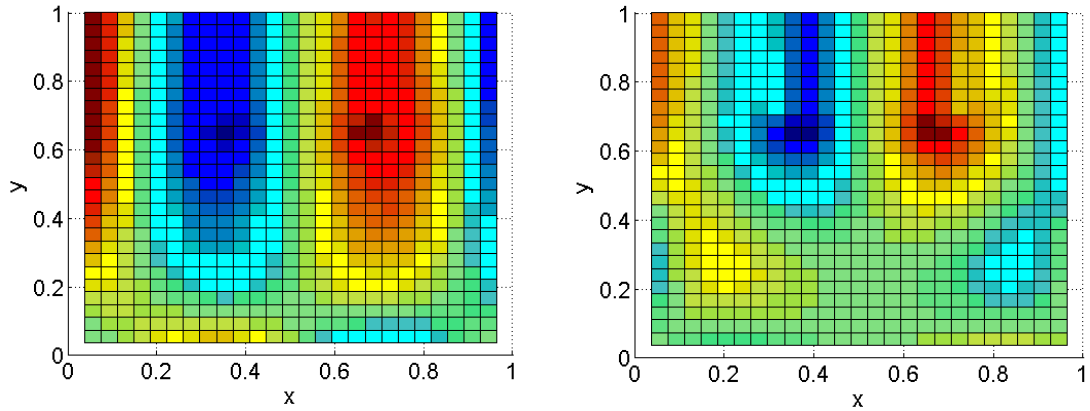

(a) (b)

Figure 5.5. Vorticity plot with (a) zero control, (b) optimal control (blue/red color denotes the region of negative/positive vorticity)

5.3.2.2. Optimization based on reduced order model. The adjoint method was applied on the reduced order model. The key factors, as analyzed towards achieving the computational efficiency and the accuracy of the optimal solution, are: snapshot solutions and grid structure.

Snapshot solutions of the flow variables are needed in order to design POD basis functions. The snapshots should be such that they represent the solutions over the whole domain or at least cover regions of interest. In present study, snapshots are generated by introducing sinusoidal control profiles to the equations (137) - (140).

The number of snapshots is accounted towards the computational efficiency of optimization procedure based on the reduced order modeling.

In the optimization based on actual system, the significant computations are needed in two stages at every iteration. One stage is where the flow is computed at every nodal point, and at the second stage, adjoint equation is solved to find the Lagrange Multiplier $\Psi \in R^{(4\times N_x \times N_y)\times 1}$. As number of unknowns is same at both stages, the computational requirements are also accounted as same. In case of optimization based on a reduced order model, the computational time is taken by three stages: generating snapshot solutions, i.e., computing flow, developing reduced order model, and running optimization procedure on this model. It was observed that the significant time was taken only by the stage of generating snapshot solutions.

The reduced order model was tested using 5, 10, 20, 40 and 100 snapshot solutions. The POD basis functions were designed where 99.999% energy (expression (80)) was captured in each case. The optimization was first carried out using the model developed with 5 snapshot solutions. The optimization procedure did not provide a converging solution. The optimization procedure was run again using the model developed with 10 snapshot solutions.

Figure 5.6 shows the convergence history of the cost and control variables. Note that same parameterization of the control profile is used in both actual system and reduced order modeling. The adjoint method was run with an initial control profile $D = [-0.073, 0.017, 0.1349, 0.0057, -0.2679]$. The criteria of comparing the optimal solution, as obtained using the actual system and the reduced order model, was taken as the relative error. Let, u^* and u' be the optimal solution as obtained using the actual system and the reduced order model, respectively. The relative error

for u was defined as $e_u = (u^* - u')/|u^*|$. Similar errors were obtained for other flow variables.

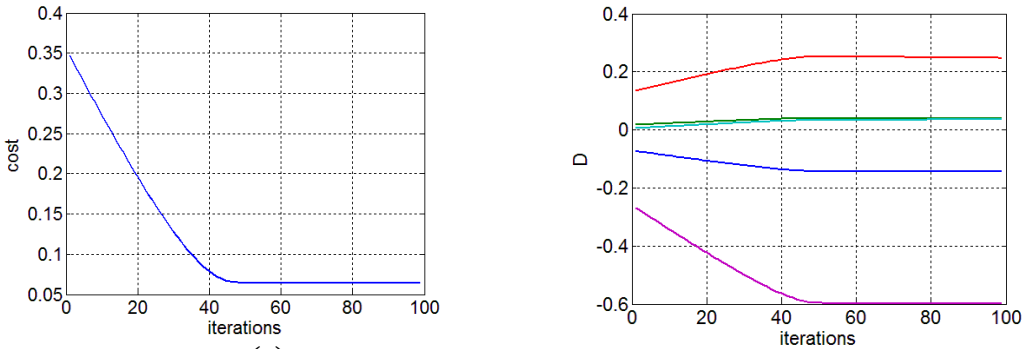

Figure 5.6. (a) Cost, (b) control variables, with respect to iterations

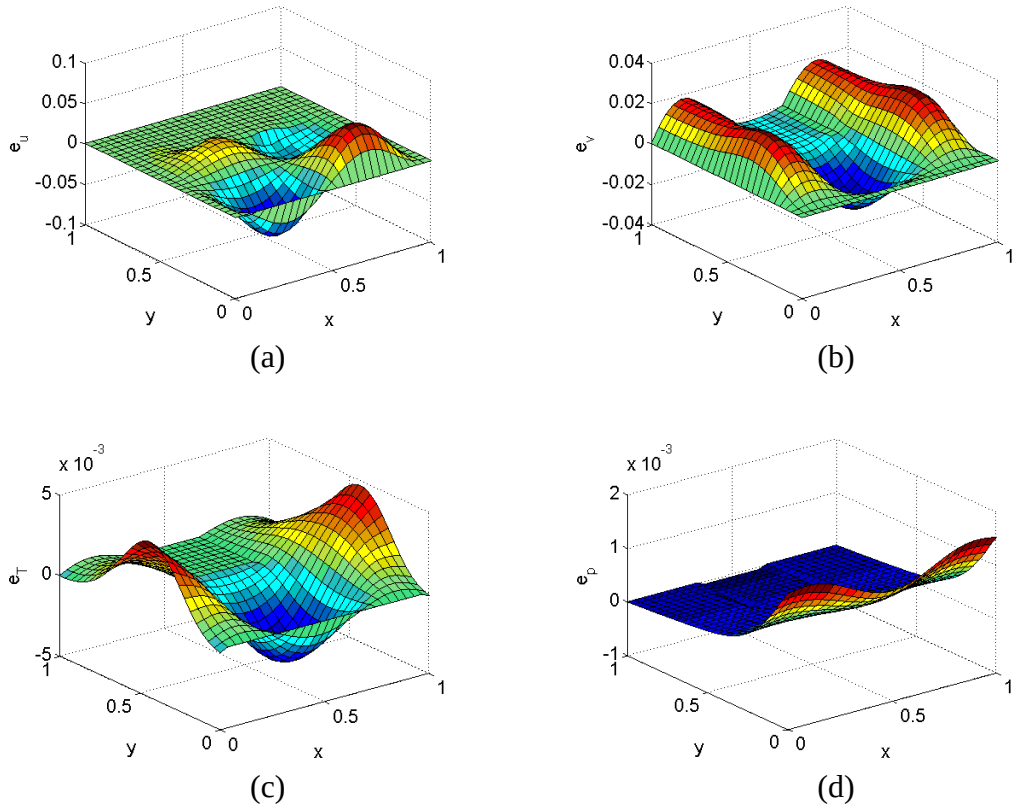

Figure 5.7. Relative errors in the optimal solution of (a) u, (b) v, (c) T, and (d) p, when discretization (28 X 28) is used

Figure 5.7 illustrates the relative error in the flow variables. Large variations in the optimal solution were observed in the flow speed. Similar observation were

made when optimal solution was obtained using reduced order model based on 20, 40 and 100 snapshot solutions. Figure 5.8 shows the norm of relative errors with respect to the model as developed using different snapshots. The trend of error norms with decreasing value can be observed. This trend was expected as a 'good' approximation of the actual system can be obtained by using large number of snapshots that in result gives the near optimal solution.

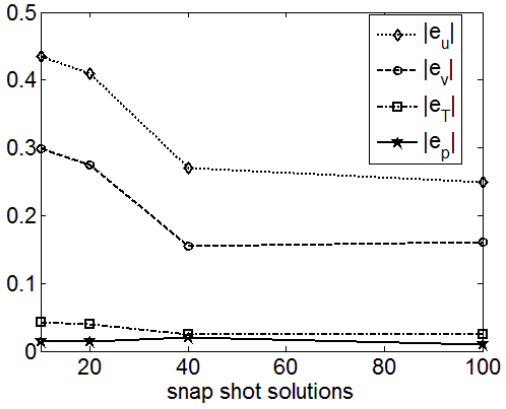

Figure 5.8. Relative error norm of flow variables with respect to reduced order models

Next, the study was carried out for different grid size. The spatial domain was uniformly discretized in x- and y- directions using more number of nodal points. There are two reasons to make this analysis:

1. A steady state solution was obtained for a discretization (e.g., see Figure 5.3). It is not guaranteed that this solution is the actual solution. It was observed that near actual steady state solution can be obtained by taking a finer grid. Consider indexes for flow variables and vorticity as: $u_{index} = \int_{\Omega} u^2 dxdy$, $v_{index} = \int_{\Omega} v^2 dxdy$, $T_{index} = \int_{\Omega} T^2 dxdy$, and $Vorticity_{index} = \int_{\Omega} \left(\frac{\partial v}{\partial x} - \frac{\partial u}{\partial y} \right)^2 dxdy$.

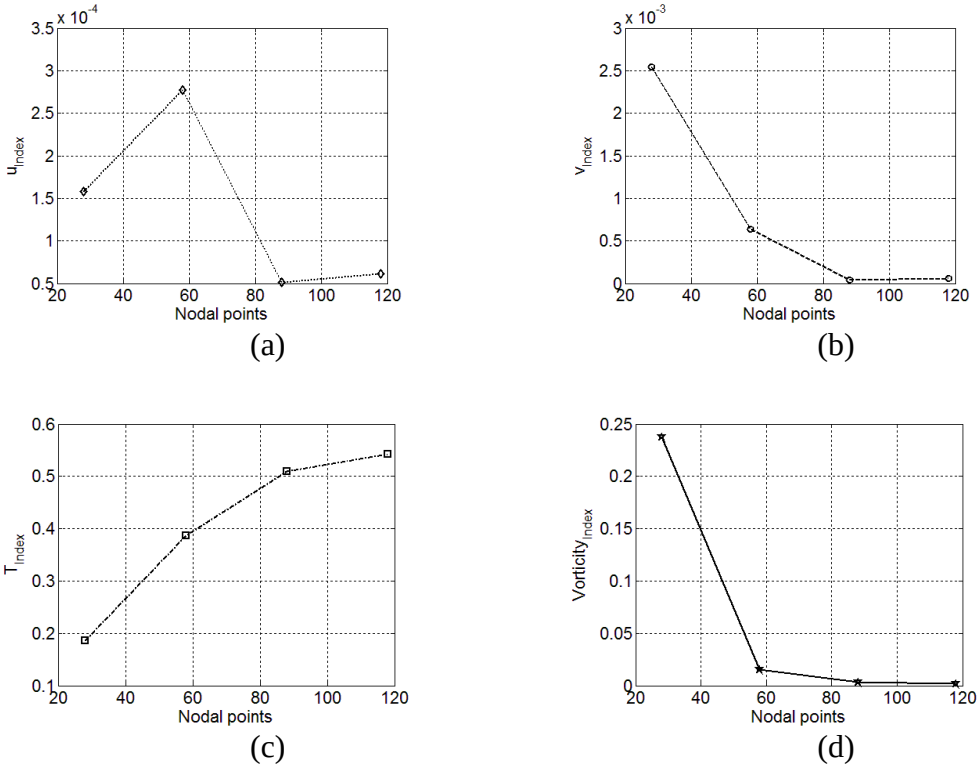

Figure 5.9. Flow variables index with respect to spatial discretization

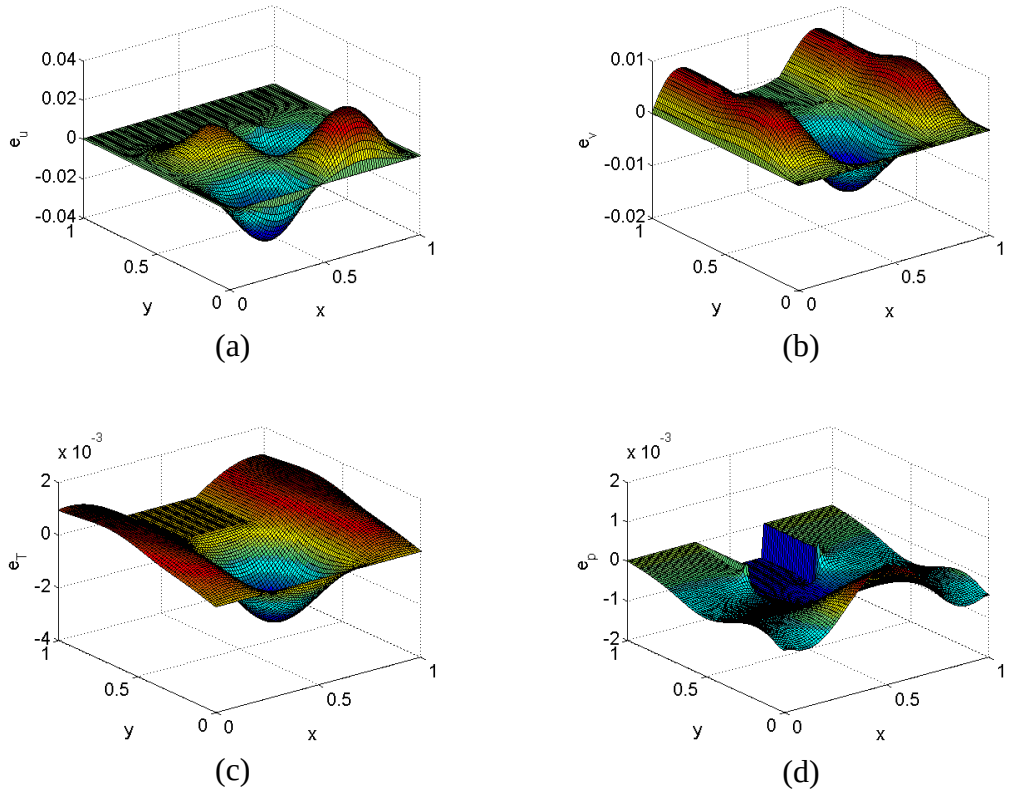

Figure 5.10. Relative errors in the optimal solution of (a) u, (b) v, (c) T, and (d) p, when discretization (88 X 88) is used

Figure 5.9 shows the flow variable index with respect to grid size for a steady state solution. As grid is made finer, each index converges to a value. A grid size can be chosen such that there is not much variation in the indexes after certain refinement of the grid. A discretization (88 X 88) was selected for the reduced order modeling and optimal solution was obtained for this grid. Here reduced order model was developed using 10 snap shot solutions. Figure 5.10 illustrate the relative errors in the flow variables. These plots can be compared with the error profiles as shown in Figure 5.7. These results demonstrate that by taking finer grid, the reduced order model based optimal solution approaches the optimal solution as obtained using the finite difference model.

2. There is always an approximation error in reduced order modeling when Galerkin procedure is used to obtain a weak form [2]. The boundary conditions are satisfied in the weak form. The approximation error can be reduced by taking finer grid. But this action increases the computational time for solving the flow equations. If possible, variable grid size, such as finer grid near the boundary and coarser grid in-domain, should be used. Only uniform grid was examined in this study here.

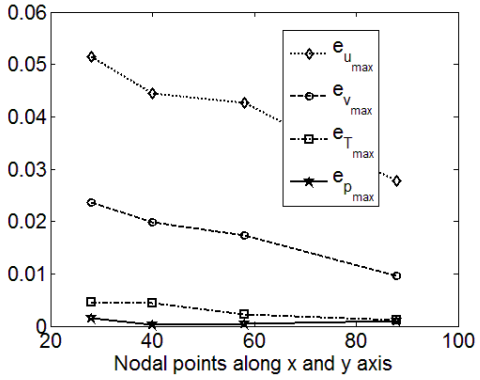

Figure 5.11. Peak values of relative error of flow variables with respect to spatial discretization

Reduced order models were obtained using 10 snap shot solutions for different grids and optimal solution is obtained using these models. Figure 5.11 shows the peak value of relative errors in the flow variables with respect to the change in grid. The plot shows a decreasing trend of the relative errors.

In summary, the steady state solutions were computed using the finite difference scheme from the flow equations (137) - (140). The flow computation takes a significant amount of time. The adjoint method requires solution of the flow equations and the adjoint equation at every iteration, i.e., the computational time is nearly twice as in solving the flow equations. A reduced order model, obtained using few snap shot solutions, can overcome the computational requirements. It is efficient to solve the optimal control problem using a low dimensional model. The accuracy of the solution becomes an issue while achieving the computational efficiency. Two ways, Grid refinement and sufficient snap shot solutions, were proposed in this study to achieve the accuracy as well.

6. CONCLUSION

The first portion of this dissertation presents a control design technique that is based on the principles of dynamic inversion and optimization theory. A controller was formulated for nonlinear systems that are actuated at the boundary. Its formulation is based on the design-then-approximate philosophy. This technique can be useful for a variety of applications due to its relatively general development. The control technique is demonstrated for heat equations and thermal convection loops. An extension of this technique was developed in order to address the issue of parameter uncertainty in a class of systems. Inaccurate values of parameters were used to design an adaptive controller. This controller requires few computations and can be useful for online applications. The third portion of this dissertation includes a discussion on sub-optimal controller for a class of second order systems that are actuated in-domain. A reduced order model was developed to synthesize a computationally efficient controller. This synthesis was based on approximate dynamic programming that provides a comprehensive solution over the system's domain. The generic development and computational efficiency of this feedback controller makes it attractive to use for a class of second order nonlinear systems. A flexible aircraft wing was used to demonstrate the applicability of the developed controller. The last portion of this document includes an attempt to compute optimal control for stationary thermally convected fluid flow while overcoming the computational requirements. Reduced order modeling based optimization was examined. The optimization procedure became computationally efficient when a low dimensional system model was used. Solutions based on finer grid and different snap shots were analyzed to achieve the accurate optimal solution.

BIBLIOGRAPHY

[1]. Houghton, E. L., Carpenter, P. W., Collicott, S. H., and Valentine, D. T., "Aerodynamics for Engineering Students (Sixth Edition)," *Butterworth-Heinemann*, Boston, 2013.

[2]. Reddy, J. N., "An Introduction to the Finite Element Method (Engineering Series)," *McGraw-Hills*, 2005.

[3]. Padhi, R. and Ali, S. F., "An Account of Chronological Developments in Control of Distributed Parameter Systems," *Annual Reviews in Control*, Vol. 33 (1), 2009, pp. 59-68.

[4]. Curtain, R. F. and Zwart, H. J., "An Introduction to Infinite Dimensional Linear System Theory," *Springer-Verlag*, New York, 1995.

[5]. Krstić M. and Smyshlyaev, A., "Boundary Control of PDEs: A Course on Backstepping Design," *Advances in Design and Control, SIAM*, PA, USA, 2008.

[6]. Liu, W., and Krstić M., "Global Boundary Stabilization of the Korteweg-de Vries-Burgers Equation," *Computational and Applied Mathematics*, Vol. 21 (1), 2002, pp. 315 – 354.

[7]. Smyshlyaev, A., and Krstić M., "On Control Design for PDEs with Space-Dependent Diffusivity or Time-Dependent Reactivity," *Automatica*, Vol. 41 (9), Sept. 2005, pp. 1601 – 1608.

[8]. Smyshlyaev, A., and Krstić M., "Lyapunov Adaptive Boundary Control for Parabolic PDEs with Spatially Varying Coefficients," *Proceedings of American Control Conference*, June 2006, pp. 41 – 48.

[9]. Vazquez, R., Cochran, J., Aamo, O. M., and Krstić M., "Control of Channel Flow Turbulence, Vortex Shedding, and Thermal Convection by Backstepping Boundary Control," *Proceedings of American Control Conference*, July 2007, pp. 876 - 881.

[10]. Smyshlyaev, A., Guo, B., and Krstić M., "Arbitrary Decay Rate for Euler-Bernoulli Beam by Backstepping Boundary Feedback," *IEEE Transaction on Automatic Control*, Vol. 54 (5), May 2009, pp. 1134 – 1140.

[11]. Krstić M., and Bresch-Pietri, D., "Delay-Adaptive Full-State Predictor Feedback for Systems with Unknown Long Actuator Delay," *American Control Conference*, June 2009, pp. 4500 – 4505.

[12]. Paranjape, A. A., Guan, J., Chung, S., and Krstić M., "PDE Boundary Control for Flexible Articulated Wings on a Robotic Aircraft," *IEEE Transactions on Robotics*, Vol. 29 (3), June 2013, pp. 625 – 640.

[13]. Padhi, R. and Balakrishnan, S. N., "Optimal Dynamic Inversion Control Design for a Class of Nonlinear Distributed Parameter Systems with Continuous and Discrete Actuators," *IET Control Theory & Applications*, Vol. 1 (6), Nov. 2007, pp. 1662-1671.

[14]. Karhunen, K., "Zur Spektral Theorie Stochasticher Prozesse," *Annales Academiae Scientiarum Fennicae*, Vol. 37, 1946.

[15]. Loeve, M., "Functiona Aleatoire De Second Ordre," *Compte Rend. Acad. Sci., Paris*, 1945.

[16]. Lumley, J. L., "The Structure of Inhomogeneous Turbulence," *Atmospheric Turbulence and Radio Wave Propagation*, 1967, pp. 166-178.

[17]. Sirovich, L., "Turbulence and the Dynamics of Coherent Structures: Part I-III," *Quarterly of Applied Mathematics*, Vol. 45 (3), 1987, pp. 561 - 571, 573 - 590.

[18]. Ravindran, S. S., "Proper Orthogonal Decomposition in Optimal Control of Fluids," *NASA/TM-1999-209113*.

[19]. Singh, S. N., Myatt, J. H., Addington, G. A., Banda, S., and Hall, J. K., "Adaptive Feedback Linearizing Control of Proper Orthogonal Decomposition Nonlinear Flow Models," *Proceedings of American Control Conference, 2001*, Vol.2, pp.1533 – 1538.

[20]. Ravindran, S. S., "Optimal Boundary Feedback Flow Stabilization by Model Reduction," *Computer Methods in Applied Mechanics and Engineering*, Vol. 196 (25–28), May 2007, pp. 2555 – 2569.

[21]. Atwell, J. A., and King, B. B., "Proper Orthogonal Decomposition for Reduced Basis Feedback Controllers for Parabolic Equations," *Mathematical and computer modeling*, Vol. 33, 2001, pp. 1 – 19.

[22]. Yadav, V., Padhi, R. and Balakrishnan, S. N., "Robust/Optimal Temperature Profile Control of a High-Speed Aerospace Vehicle Using Neural Networks," *IEEE Transactions on Neural Networks*, Vol. 18 (4), July 2007, pp. 1115-1128.

[23]. Padhi, R. and Balakrishnan S. N., "Optimal Management of Beaver Population Using a Reduced-Order Distributed Parameter Model and Single Network Adaptive Critics," *IEEE Transaction on Control Systems Technology*, Vol. 14 (4), July 2006.

[24]. Padhi, R. and Balakrishnan, S. N., "Proper Orthogonal Decomposition Based Optimal Neurocontrol Synthesis of a Chemical Reactor Process using Approximate Dynamic Programming," *Neural Networks*, Vol. 16 (5-6), 2003, pp. 719-728.

[25]. Prabhat P., Padhi R., Look Jr D. C. and Balakrishnan S. N., "Proper Orthogonal Decomposition Based Modeling and Experimental Implementation of a Neurocontroller for a Heat Diffusion System," *Proceedings of the American Control Conference*, Denver, Colorado, June 4-6, 2003, pp. 2652-2657.

[26]. Kumar, M., Rajagopal, K., Balakrishnan S. N. and Nguyen N. T., "Proper Orthogonal Decomposition Technique for Near-Optimal Control of Flexible Aircraft Wings," *Guidance, Navigation & Control Conference, AIAA*, DOI: 10.2514/6.2013-4935, Boston, August 2013.

[27]. Kumar, M., and Balakrishnan S. N., "Proper Orthogonal Decomposition Technique for Sub-Optimal Control of Flexible Aircraft Wings using Discrete Actuators," *American Control Conference*, 4 – 6 June, 2014, pp. 2717 – 2722.

[28]. Hidayat, Z., Babuska, R., Schutter, B. D., and Nunez, A., "Observers for Linear Distributed Parameter Systems: A Survey," *IEEE International Symposium on Robotic and Sensors Environments*, Sept. 2011, pp. 166 – 171.

[29]. Antoniades, C., and Christofides, P. D., "Integrating Nonlinear Output Feedback Control and Optimal Actuator/Sensor Placement for Transport-Reaction Processes," *Chemical Engineering Science*, Vol. 56 (15), Aug. 2001, pp. 4517 – 4535.

[30]. Alonso, A. A., Kevrekidis, I. G., Banga, J. R., and Frouzakis, C. E., "Optimal Sensor Location and Reduced Order Observer Design for Distributed Process Systems," *Chemical & Computer Engineering*, Vol. 28 (1-2), Jan. 2004, pp. 27 – 35.

[31]. Liu, W., Hou, Z., and Demetriou, M. A., "A Computational Scheme for the Optimal Sensor/Actuator Placement of Flexible Structures using Spatial H_2 Measures," *Mechanical Systems and Signal Processing*, Vol. 20 (4), May 2006, pp. 881 – 895.

[32]. Zhang, J., He, L., Wang, E., and Gao, R., "A LQR Controller Design for Active Vibration Control of Flexible Structures," *Pacific Asia Workshop on Computational Intelligence and Industrial Application*, Vol. 1, Dec. 2008, pp. 127 – 132.

[33]. Ji, X., and Wang, W., "A Neural Fuzzy System for Vibration Control in Flexible Structures," *Intelligent control and Automation*, Vol. 2 (3), 2011, pp. 258 – 266.

[34]. Kasinathan, D., and Morris, K., "H_∞-Optimal Actuator Location," *IEEE Transaction on Automatic Control*, Vol. 58 (10), Oct. 2013, pp. 2522 – 2535.

[35]. Nestorovic, T., and Trajkov, M., "Optimal Actuator and Sensor Placement based on Balanced Reduced Models," *Mechanical Systems and Signal Processing*, Vol. 36 (2) April 2013, pp. 271 – 289.

[36]. Ali, A., Ghotbi, E., and Dhingra, A. K., "Optimum Placement of Actuators in Structural and Control Design using Stackelberg Games," *Journal of Vibration and Control*, July 2013, DOI: 10.1177/1077546313494113

[37]. Bossens, F., and Preumount, A., "Active Tendon Control of Cable-Stayed Bridges: A Large Scale Demonstration," *Earthquake Engineering and Structural Dynamics*, Vol. 30 (7), 2001, pp. 961 – 979.

[38]. Baudouin, L., Neild, S., Rondepierre, A., and Wagg, D., "Robust Measurement Feedback Control of an Inclined Cable," *1st IFAC Workshop on Control of Systems Goverened by Partial Differential Equations*, Paris, France, 2013, pp. 55 – 60.

[39]. Nguyen N., "Model Predictive Optimal Control of a Time-Delay Distributed Parameter System," *AIAA Guidance, Navigation and Control Conference and Exhibit*, August 2006.

[40]. Xing, H., Zhao, W., and Wang, H, "Feedback Control for Parabolic Distributed Parameter Systems with Time-Delay," *Proceedings of the 7th World Congress on Intelligent Control and Automation*, June 2008, pp. 4604 – 4609.

[41]. Krstić, M., "Delay Compensation for Nonlinear, Adaptive, and PDE Systems," *Systems & Control: Foundations & Applications, Birkhauser*, 2009.

[42]. Bekiaris-Liberis, N., "Nonlinear Control of Delay and PDE Systems," *Ph.D. Dissertation, University of California, San Diego*, 2013, link: http://escholarship.org/uc/item/32t0g9js.

[43]. Zheng, F., Fu, L., and Teng, M., "Exponential Stability of a Linear Distributed Parameter Bioprocess with Input Delay in Boundary Control," *Journal of Function spaces and applications*, Vol. 2013, 2013.

[44]. Vogel, C. R., and Yang, Q., "Modeling, Simulation, and Open-Loop Control of a Continuous Facesheet MEMS Deformable Mirror," *Journal of the Optical Society of America*, Vol. 23 (5), May 2006, pp. 1074 – 1081.

[45]. Ruppel, T., Osten, W., and Sawodny, O., "Model-Based Feedforward Control of Large Deformable Mirrors," *European Journal of Control*, Vol. 17(3), pp. 261 – 272.

[46]. Ruppel, T., Dong, S., Rooms, F., Osten, W., and Sawodny, O., "Feedforward Control of Deformable Membrane Mirrors for Adaptive Optics," *IEEE Transaction of Control System Technologies*, Vol. 21 (3), May 2013, pp. 579 – 589.

[47]. Nguyen, N., Trinh, K., Nguyen, D., and Tuzcu, I., "Nonlinear Aeroelasticity of a Flexible Wing Structure Coupled with Aircraft Flight Dynamics," *53rd AIAA/ASME/SHS/ASC Structure, Structural Dynamics and Material Conference*, April 2012.

[48]. Nguyen, N., and Urnes, J. Sr., "Aeroelastic Modeling of Elastic Shaped Aircraft Concept via Wing Shaping Control for Drag Reduction," *Atmospheric Flight Mechanics Conference, AIAA*, August 2012.

[49]. Yucelen, T., Calise, A. J., Kim, K., and Nguyen, N. T., "Derivative-Free Output Feedback Adaptive Control of an Aeroelastic Generic Transport Model," *Guidance, Navigation and Control Conference, AIAA*, August 2011.

[50]. Gibson, T. E., Annaswamy, A. M., and Lavretsky, E., "Modeling for Control of Very Flexible Aircraft," *Guidance, Navigation and Control Conference, AIAA*, August 2011.

[51]. Quindlen, J., How, J., Chowdhary, G., Nguyen, N., and Yucelen, T., "Concurrent Learning Adaptive Control of the Aeroelastic Generic Transport Model," *Guidance, Navigation, and Control Conference, AIAA*, August 2013.

[52]. Luo, Z., Li, H., Sun, P., An, J., Navon, I. M., "A Reduced-Order Finite Volume Element Formulation based on POD Method and Numerical Simulation for Two-Dimensional Solute Transport Problems," *Mathematics and Computers in Simulation*, Vol. 89, March 2013, Pages 50-68.

[53]. Everson, R., and Sirovich, L., "Karhunen-Loeve Procedure for Gappy Data," *Journal of the Optical Society of America A: Optics, Image Science and Vision*, Vol. 12 (8), Aug. 1995, pp. 1657 – 1664.

[54]. Moore, B. C., "Principal Component Analysis in Linear Systems: Controllability, Observability, and Model Reduction," *IEEE Transaction of Automatic Control*, Vol. 26 (1), Feb. 1981, pp. 17 – 32.

[55]. Willcox, K. E., "Unsteady Flow Sensing and Estimation via the Gappy Proper Orthogonal Decomposition," *AIAA Fluid dynamics conference and exhibit*, 2004.

[56]. Willcox, K., and Peraire, J., "Balanced Model Reduction via the Proper Orthogonal Decomposition," *Journal of AIAA*, Vol. 40 (11), Nov. 2002, pp. 2323 – 2330.

[57]. Varshney, A., Pitchaiah, S., and Armaou, A., "Feedback Control of Dissipative PDE Systems using Adaptive Model Reduction," *American Institute of Chemical Engineers Journal*, Vol. 55 (4) , April, 2009, pp. 906 – 918.

[58]. Pitchaiah, S., and Armaou, A., "Ouput-Feedback Control of Dissipative PDE Systems with Partial Sensor Information based on Adaptive Model Reduction," *American Institute of Chemical Engineers Journal*, Vol. 59 (3), March 2013, pp. 747 – 760.

[59]. Kim, T., "Frequency-Domain Karhunen-Loeve method and its Applications to Linear Dynamic Systems," *Journal of AIAA*, Vol. 36 (11), 1998, pp. 2117 – 2123.

[60]. Liu, W. J., "Boundary Feedback Stabilization of an Unstable Heat Equation," *SIAM Journal of Control and Optimization*, 42 (3), pp. 1033 - 1043.

[61]. Camphouse, R. C., "Boundary Feedback Control Using Proper Orthogonal Decomposition Models," *Journal of Guidance, Control and Dynamics*, Vol. 28 (5), Sept.-Oct., 2005, pp. 931-938.

[62]. Efe, M. Ö., "Issues in the Modeling and Boundary Control of 2D Heat Flow: POD Based Modeling," *IEEE International Conference on Control Applications*, Munich, Germany, 4-6 Oct. 2006, pp. 2486 - 2491.

[63]. Kumar, M., and Balakrishnan, S. N., "Optimal Dynamic Inversion based Boundary Control Design for 2D Heat Equations," *Journal of IET control theory & applications*, Sept. 2014, pp. 2013 - 2025.

[64]. Ou, Y., Xu, C., Schuster, E., Luce, T. C., Ferron, J. R., Walker, M. L. and Humphreys D. A., "Optimal Tracking Control of Current Profile in Tokamaks," *IEEE Transaction on Control System Technology*, March 2011, Vol. 19 (2), pp. 432 – 441.

[65]. Gaye, O., Moulay, E., Bremond, S., Autrique, L., Nouailletas, R., Artaud, J. F. and Orlov, Y., "Robust Stabilization of the Current Profile in Tokamak Plasmas using Sliding Mode Approach in Infinite Dimension," *Control Engineering Practice*, Vol. 21 (10), Oct. 2013, pp. 1350 – 1358.

[66]. Böhm, M., Krstić, M., Kuchler, S. and Sawodny, O., "Modeling and Boundary Control of a Hanging Cable Immersed in Water," *Journal of Dynamic Systems, Measurement, and Control, ASME*, Vol. 136 (1), Jan. 2014, Paper No. DS-12-1193.

[67]. Smyshlyaev, A. and Krstić, M., "Adaptive Control of PDEs," *Annual Reviews of Control*, Vol. 32 (2), 2008, pp. 149 – 160.

[68]. Krstić, M., "Adaptive Boundary Control for Unstable Parabolic PDEs – Part I: Lyapunov design," *IEEE Transaction of Automatic Control*, Vol. 53 (7), Aug. 2008, pp. 1575 - 1591.

[69]. Smyshlyaev, A. and Krstić, M., "Adaptive Boundary Control for Unstable Parabolic PDEs – Part II: Estimation-Based Design," *Automatica*, Vol. 43 (9), Sept. 2007, pp. 1543 – 1556.

[70]. Smyshlyaev, A. and Krstić, M., "Adaptive Boundary Control for Unstable Parabolic PDEs – Part III: Output feedback examples with swapping identifiers," *Automatica*, Vol. 43 (9), Sept. 2007, pp. 1557 – 1564.

[71]. He, W. and Ge, S. S., "Robust Adaptive Boundary Control of a Vibrating String under Unknown Time-Varying Disturbance," *IEEE Transactions on Control Systems Technology*, Vol. 20 (1), Jan. 2012, pp. 48 - 58.

[72]. He, W., Ge, S. S. and Zhang S., "Adaptive Boundary Control of a Flexible Marine Installation System," *Automatica*, Vol. 47 (12), Dec. 2011, pp. 2728 – 2734.

[73]. Banks, H. T., del Rosario, R. C. H., and Tran H. T., "Proper Orthogonal Decomposition based Control of Transverse Beam Vibrations: Experimental Implementation," *IEEE transaction on control system technology*, Vol. 10 (5), Sept. 2002, pp. 717 – 726.

[74]. Enns, D., Bugajski, D., Hendrick, R. and Stein, G., "Dynamic Inversion: An Evolving Methodology for Flight Control Design," *International Journal of Control*, Vol. 59 (1), 1994, pp. 71-91.

[75]. Bryson, A. E. and Ho, Y. C., "Applied Optimal Control: Optimization, Estimation and Control," *Taylor and Francis*, New York, 1975.

[76]. Khalil H. K., "Nonlinear Systems," *Prentice-Hall, Inc*. 2002.

[77]. Lane, S. H. and Stengel, R. F., "Flight Control using Non-Linear Inverse Dynamics," *Automatica*, Vol. 24 (4), 1988, pp. 471-483.

[78]. Kim, B. S. and Calise, A. J., "Nonlinear Flight Control using Neural Networks," *AIAA Journal of Guidance, Control and Dynamics*, Vol. 20 (1), 1997, pp. 26-33.

[79]. Efe, M. Ö., "Low-Dimensional Model-Based Boundary Control of 2D Heat Flow Utilizing Root Locus," *Transaction of the Institute of Measurement and Control*, Vol. 29 (1), March 2007, pp. 53-69.

[80]. Strauss, W. A., "Partial Differential Equations: An Introduction (Second Edition)," *John Wiley & Sons*, Ltd, USA, Dec. 21, 2007.

[81]. Creveling, H. F., De Paz, J. F., Baladi, J. Y. and Schoenhals, R. J., "Stability Characteristics of a Single-Phase Free Convection Loop," *Journal of Fluid Mechanics*, Vol. 67 (1), 1975, pp. 65 - 84.

[82]. Wang, Y., Singer, J. and Bau, H., "Controlling Chaos in a Thermal Convection Loop," *Journal of Fluid Mechanics*, Vol. 237, 1992, pp. 479 – 498.

[83]. Louisos, W. F., Hitt, D. L. and Danforth, C. M., "Chaotic Flow in a 2D Natural Convection Loop with Heat Flux Boundaries," *International Journal of Heat and Mass Transfer*, Vol. 61, June 2013, pp. 565 – 576.

[84]. Burns, J. A., King, B. B. and Rubio, D., "Feedback Control of a Thermal Fluid using State Estimation," *International Journal of Computational Fluid Dynamics*, Vol. 11 (1 – 2), 1998, pp. 93 – 112.

[85]. Bošković, D. M. and Krstić, M., "Nonlinear Stabilization of a Thermal Convection Loop by State Feedback," *Automatica*, Vol. 37, 2001, pp. 2033–2040.

[86]. Vazquez, R. and Krstić, M., "Explicit Integral Operator Feedback for Local Stabilization of Nonlinear Thermal Convection Loop PDEs," *Systems & Control Letters*, Vol. 55, 2006, pp. 624–632.

[87]. Narendra, K. S. and Annaswamy, A. M., "Stable Adaptive Systems," *Dover Publication Inc.*, Mineola, New York. 1995.

[88]. Rajagopal, K., Balakrishnan S. N., Nguyen, N. T. and Krishnakumar, K., 'Time Delay Margin Analysis of Modified State Observer Based Adaptive Controller," *Guidance, Navigation, and Control (GNC) Conference, AIAA*, Aug. 19 – 22, 2013, Boston, MA.

[89]. Werbos P. J., "Neuro Control and Supervised Learning: An Overview and Evaluation, Handbook of Intelligent Control: Neural, Fuzzy and Adaptive Approaches," White D. and Sofge D. (Eds.), *Van Nostrand Reinhold*, 1992.

[90]. Padhi R., Unnikrishnan N., Wang X. and Balakrishnan S. N., "A Single Network Adaptive Critic (SNAC) Architecture for Optimal Control Synthesis for a Class of Nonlinear Systems," *Neural Networks*, Vol. 19, 2006, pp. 1648-1660.

[91]. Padhi, R., "Optimal Control of Distributed Parameter Systems using Adaptive Critic Neural Networks," (Order No. 3034870, University of Missouri – Rolla, 2001). ProQuest Dissertations and Theses, pages 136, retrieved from http://search.proquest.com/docview/287876584?accountid=14594.

[92]. Cloutier, J. R., "State-Dependent Riccati Equation Techniques: An Overview," *Proceedings of the American Control Conference*, Vol.2, *1997*, pp. 932 - 936, DOI: 10.1109/ACC.1997.609663

[93]. Ito, K., and Ravindran, S. S., "Optimal Control of Thermally Convected Fluid Flows," *SIAM Journal on Scientific Computing*, Vol. 19 (6), Jan. 1998, DOI: 10.1137/S1064827596299731.

[94]. Fotiadis, D. I., Keida, S., and Jensen, K. F., "Transport Phenomena in a Vertical Reactors for Metalorganic Vapor Phase Expitaxy," *Journal of Crystal Growth*, Vol. 102, pp. 441 – 470, 1990.

[95]. Jameson, A., "Aerodynamic Design via Control Theory," *Journal of Scientific Computing*, Vol. 3 (3), 1988, pp. 233 – 260.

[96]. Jameson, A., and Martinelli, L., "Aerodynamic Shape Optimization Techniques based on Control Theory," *Computational Mathematics Driven by Industrial Problems Lecture Notes in Mathematics*, Vol. 1739, 2000, pp. 151 – 221.

[97]. LeGresley, P. A., and Alonso, J. J., "Airfoil Design Optimization using Reduced Order Model based on Proper Orthogonal Decomposition," *Fluids Conference and Exhibit, AIAA*, June 2000.

[98]. Bui-Thanh, T., Damodaran, M., and Willcox, K., "Aerodynamic Data Reconstruction and Inverse Design using Proper Orthogonal Decomposition," *AIAA Journal*, Vol. 42 (8), August 2004, pp. 1505 – 1516.

[99]. Oyama, A., Nonomura, T., and Fujii, K., "Data Mining of Pareto-Optimal Transonic Airfoil Shapes using Proper Orthogonal Decomposition," *Journal of Aircraft*, Vol. 47 (5), Sept. – Oct. 2010, pp. 1756 – 1762.

[100]. Nguyen, N., Trinh, K., Reynolds, K., Kless, J., Aftosmis, M., Urnes, J. Sr., and Ippolito, C., "Elastic Shaped Wing Optimization and Aircraft concept for Improved Cruise Efficiency," *51st AIAA Aerospace Sciences meeting Including the new Horizons Forum and Aerospace Exposition*, Jan. 2013.

[101]. Noboru, K., Chung, K. Y., Toshikazu, T., Taylor, J. E., "Adaptive Finite Element Methods for Shape Optimization of Linearly Elastic Structures," *Computer Methods in Applied Mechanics and Engineering*, Vol. 57 (1), Aug. 1986, pp. 67 – 89.

[102]. Morin, P., Nochetto, R. H., Pauletti, M. S., and Verani, M., "Adaptive Finite Element Methods for Shape Optimization," *ESAIM: Control, Optimisation and Calculus of Variations*, Vol. 18 (4), Oct. 2012, pp. 1122 – 1149.

[103]. Nadal, E., Rodenas, J. J., Albelda, J., Tur, M., Tarancon, J. E., and Fuenmayor, F. J., "Efficient Finite Element Methodology based on Cartesian Grids: Application to Structural Shape Optimization," *Abstract and Applied Analysis*, Vol. 2013, 2013,Article ID: 953786.

[104]. Gobal, K., and Grandhi, R. V., "Continuum Sensitivity Analysis for Structural Shape Design Variables Utilizing Finite Volume Method," *AIAA SciTech, 10th AIAA Multidisciplinary Design Optimization Conference*, Jan. 2014.

[105]. Hoffman, J. D., "Numerical Methods for Engineers and Scientists, 4th Ed.," *McGraw–Hill Inc.*, New York, 1992

VITA

Manoj Kumar was born on January 16, 1986, in Haryana, India. He received his Bachelor's and Master's degree in aerospace engineering from Indian Institute of Technology Kanpur, India, in 2010. He started his PhD studies in Aerospace Engineering at Missouri University of Science & Technology in 2010. His research interests include optimization, optimal control, and distributed parameter systems. He received his PhD degree in May 2015.